

Review

Open Access



A review of the energy storage aspects of chemical elements for lithium-ion based batteries

Tariq Bashir¹, Sara Adeeba Ismail¹, Yuheng Song², Rana Muhammad Irfan¹, Shiqi Yang¹, Shaowen Zhou¹, Jianqing Zhao¹, Lijun Gao¹

¹College of Energy, Soochow Institute for Energy and Materials Innovations, Soochow University, Suzhou 215006, Jiangsu, China.
²Materials and Nanosciences, University of Waterloo, Ontario N2L 3G1, Canada.

Correspondence to: Prof./Dr. Jianqing Zhao, College of Energy, Soochow Institute for Energy and Materials Innovations, Soochow University, 1 Shizi Street, Suzhou 215006, Jiangsu, China. E-mail: jqzhao@suda.edu.cn; Prof./Dr. Lijun Gao, College of Energy, Soochow Institute for Energy and Materials Innovations, Soochow University, 1 Shizi Street, Suzhou 215006, Jiangsu, China. E-mail: gaolijun@suda.edu.cn

How to cite this article: Bashir T, Ismail SA, Song Y, Irfan RM, Yang S, Zhou S, Zhao J, Gao L. A review of the energy storage aspects of chemical elements for lithium-ion based batteries. *Energy Mater* 2021;1:100019.
<https://dx.doi.org/10.20517/energymater.2021.20>

Received: 19 Oct 2021 **First Decision:** 24 Nov 2021 **Revised:** 13 Dec 2021 **Accepted:** 17 Dec 2021 **Published:** 31 Dec 2021

Academic Editors: Yuping Wu, Bin Wang **Copy Editor:** Xi-Jun Chen **Production Editor:** Xi-Jun Chen

Abstract

Energy storage devices such as batteries hold great importance for society, owing to their high energy density, environmental benignity and low cost. However, critical issues related to their performance and safety still need to be resolved. The periodic table of elements is pivotal to chemistry, physics, biology and engineering and represents a remarkable scientific breakthrough that sheds light on the fundamental laws of nature. Here, we provide an overview of the role of the most prominent elements, including s-block, p-block, transition and inner-transition metals, as electrode materials for lithium-ion battery systems regarding their perspective applications and fundamental properties. We also outline hybrid materials, such as MXenes, transition metal oxides, alloys and graphene oxide. Finally, the challenges and prospects of each element and their derivatives and hybrids for future battery systems are discussed, which may provide guidance towards green, low-cost, versatile and sustainable energy storage devices.

Keywords: Lithium-ion based batteries, specific capacity, cathode materials, anode materials



© The Author(s) 2021. **Open Access** This article is licensed under a Creative Commons Attribution 4.0 International License (<https://creativecommons.org/licenses/by/4.0/>), which permits unrestricted use, sharing, adaptation, distribution and reproduction in any medium or format, for any purpose, even commercially, as long as you give appropriate credit to the original author(s) and the source, provide a link to the Creative Commons license, and indicate if changes were made.



INTRODUCTION

Energy storage is critical to our everyday lives and is one of the most important solutions for addressing the current energy crisis. It was announced by the general assembly of the United Nations that 2019 would be the international year of the periodic table to highlight its importance as one of the most influential discoveries in modern science. The nature and periodic behavior of microscale matter was extensively investigated and confirmed throughout the 19th and early 20th centuries. This activity led to insights into the predictable periodic behavior of the quantified atomic building blocks, as well as their chemical combinations to produce many stoichiometric molecular structures with many new properties. These efforts proceeded to the acceptance of Mendeleev's periodic table in 1867. Similar periodic behavior was observed at the subatomic level. An extension of this similar periodic paradigm to more complex hierarchical blocks beyond atoms (i.e., the nanoscale) has also been proposed^[1].

The increase in atomic number leads to an increase in atomic radius compression and ionization potential across the periods of the periodic table. Therefore, p-block elements (e.g., B, C and N) play a crucial role in forming strong covalent bonds with most of the strongly electronegative atoms, like O and F. Electrons in the *p* subshell form conjugated π -bonds, in addition to σ -bonds, and this ability leads to a large number of inorganic polymers. Therefore, B, C and N can form a variety of one-dimensional (1D), two-dimensional (2D) and three-dimensional (3D) nanomaterials, including fullerenes, graphene and its BN analogs, nanodiamonds, MXenes and carbon nanotubes. This group is the largest and fastest-growing category of nanomaterials triggered by the nanotechnological revolution and the rapid rise of nanotechnological architecture. Oxygen is also one of the most active oxidants in the surrounding environment and plays a universal role in this group. Oxygen is pivotal to the synthesis of different transition metal oxides (TMOs) and their derived nanoparticles, which can be used as electrode materials in lithium-ion batteries (LIBs). Nanotechnological architectures are used to make supercapacitors, sensors, molecular electronics, fuel cells, batteries and advanced energy devices^[2-7].

To achieve high energy density, batteries should be based on cathode and anode active materials with large potential differences, light atomic or molecular weights and the ability to generate high voltages that result in the transformation of a large number of electrons for each active molecule. The highest known theoretical voltage (6 V) is for Li/F₂, which may be the limiting voltage that an electrochemical cell can reach. At present, the voltage of commercial LIBs has reached more than 4 V (i.e., Li-LiMn₂O₄^[8] and Li-LiCoO₂ batteries^[9]), while the voltage of some LIBs under development (such as Li-LiNi_{0.5}Mn_{1.5}O₄ batteries^[10]) may exceed 5 V. Therefore, increasing the voltage of a battery can be one of the measures to increase its energy density. The energy density of a battery material can be determined as follows:

$$ED = \frac{nFE^0}{\sum M_i} \quad (1)$$

where *ED* represents the energy density, *n* is the number of electrons transferred, *F* is the Faraday constant, *E*⁰ is the electromotive force and $\sum M_i$ represents the summation of the formula masses of the active substances.

In addition, most current battery systems are based on various transition metals and their oxides^[11]; however, their energy density is very low due to their high mass. Therefore, electroactive materials composed of light elements and their derivatives, as well as hybrid materials, can be chosen to achieve greater energy density^[12]. The properties of the coating materials may match the lithium energy in the

electrolyte by providing different energy ranges for different lithium sites. Thus, changing the potential of the Li surface can enhance the adsorption of Li from the electrolyte. The nanosized particles of a material undoubtedly contribute to its high discharge rate capability and its rate performance is significantly better than similar^[13] or smaller-sized nanoparticles, as reported in the literature^[14], which shows that the rate capability can be improved by coating^[15-17].

Furthermore, Stevens *et al.*^[18] recently discovered that hard carbon intercalated with Na has a higher reactivity with non-aqueous electrolytes than Li_xC_6 , which has sparked new interest in the stability of electrolytes. The rate capacity can be masked by the limited electron transport across electrodes^[19,20]. A large amount of carbon decreases the volumetric energy density of the electrode and therefore the highest rates (e.g., 200 and 400 C) can only be tested with a high amount of carbon to enhance the electronic conductivity of the active material. It should be noted that the volumetric energy density is more significant than the gravimetric energy density for many applications, particularly for portable electronic devices and vehicles. In this case, a similar procedure should be applied to balance the performance of the electrodes in asymmetric batteries. Volume capacitance and electrode volume can be used instead of weight capacitance and mass. Volumetric and gravimetric performances are linked by the density of the electrode and are mostly defined by the electrode design and porosity^[21,22]. It is possible to specify structural characteristics, such as a fine distribution of pore straightness, pore connectivity, availability of redox-active sites and excellent balancing of ion and pore sizes, which are needed for optimum efficiency. A comparison of the energy density for various battery prototypes is presented in [Figure 1a](#). LIBs have higher volumetric energy density than potassium ion batteries, sodium ion batteries, Ni-MH, Ni-Cd and lead-acid batteries, as shown in [Figure 1b](#)^[21].

2D materials, like MXenes^[11], graphene^[23,24], carbides^[25], sulfides (e.g., MoS_2)^[26] and other dichalcogenides^[27], are promising for energy storage applications. The theoretical capacities of Li, Na, Ca and K calculated for $\text{Ti}_3\text{C}_2\text{Tx}$ MXenes are 447.8, 351.8, 319.8 and 191.8 mAh g⁻¹, respectively, which are far beyond that of graphite^[28]. Therefore, 2D materials are potentially excellent electrode materials for battery applications. An important factor for battery charge and discharge is the diffusion barrier, which allows the battery to discharge and charge at a specific rate. Researchers have calculated the diffusion barriers of Li, Na, K and Ca in Ti_3C_2 monolayers using the nudged elastic band method applied in the Vienna Ab initio Simulation Package to evaluate 2D Ti_3C_2 as a promising high rate performance electrode material^[29,30].

In this review, we briefly discuss the types of LIBs, their mechanisms and the electrochemical properties of their electrode materials, such as specific capacity, rate performance, cycling performance and energy density, from the perspective of chemical elements. The mechanisms and long-term cycling stability of LIBs for s-, p-, d- and f-block elements, different transition metals and their oxides are studied in detail to provide appropriate treatment methods and creative remedial measures for energy storage devices with enhanced performance. We also discuss hybrid 2D materials (e.g., MXenes and graphene) and alloys for battery applications. Finally, this review provides insights into the challenges and future prospects of next-generation LIBs.

TYPES OF LI-ION BATTERIES

Li-sulfur batteries

Sulfur is a potential cathode material for future battery technologies, with an order of magnitude higher theoretical capacity (1675 mA h g⁻¹) than existing transition metal oxides. It has a larger abundance in the Earth's crust than nickel and cobalt and is also low cost^[31,32]. [Figure 2](#) depicts the working principle diagram of a lithium-sulfur battery^[33]. Despite these considerable benefits, sulfur cathodes face a number of

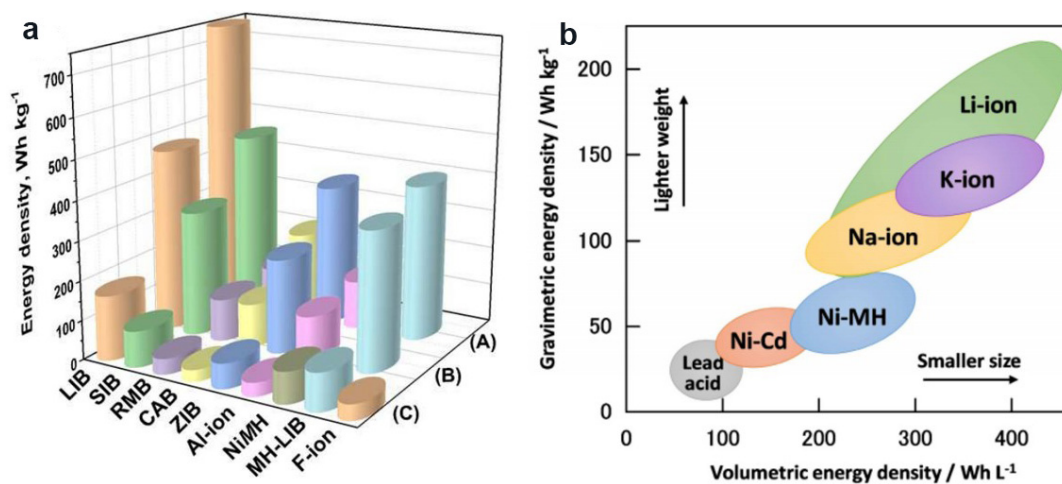


Figure 1. (a) Comparison of energy density for various battery prototypes. Average values are calculated using the available data, where (A) represents cathode, (B) represents both electrodes and (C) represents full cells (LIB normalized). (b) Volumetric and gravimetric energy densities of commercial batteries (LIBs, KIBs, SIBs, Ni-MH, Ni-Cd and lead-acid). Reproduced with permission from Ref.^[21] (Copyright 2020, Journal of Alloys and Compounds, Elsevier). LIBs: Lithium-ion batteries; KIBs: potassium ion batteries; SIBs: sodium ion batteries.

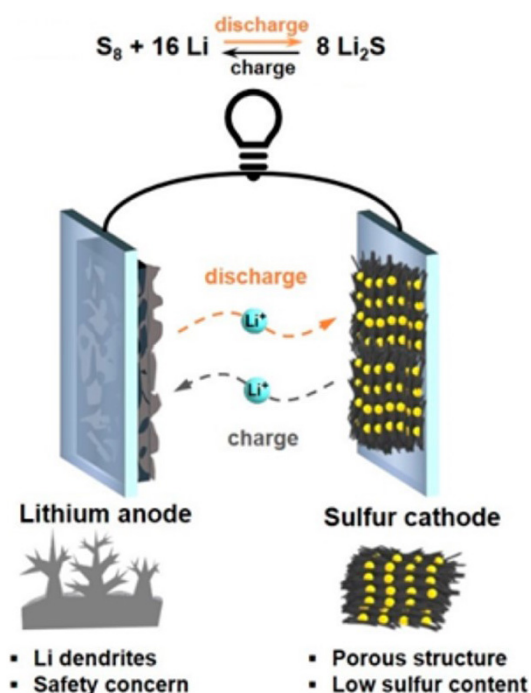


Figure 2. Schematic of the working principles of a Li-S battery. Reproduced with permission from Ref.^[33] (Copyright 2020, ACS Energy Letters).

technological challenges that limit their usage. They have a lower conductivity and electrochemical potential vs. Li/Li^+ . The volume expansion rate of sulfur, like many other conversion electrodes, can reach up to 80%, causing a drop off in the electrode conductivity, pulverization and cracking^[34]. Furthermore, the evaporation temperature of sulfur-based cathodes is low, resulting in the loss of pure sulfur during vacuum electrode drying^[35]. Moreover, the intermediate reaction product produced during the charging/discharging process

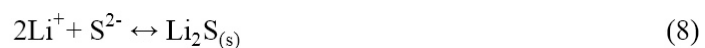
(Li₂S_n polysulfides) can dissolve in the electrolyte, leading to capacity loss due to the shuttle effect^[36,37]. The polysulfides dissolved in the electrolyte move back to the anode where they are converted to low-order polysulfides, which then migrate back to the cathode, causing reoxidation. Insoluble compounds, like Li₂S and Li₂S₂, are produced via the shuttle effect^[38]. Cañas *et al.*^[39] investigated this mechanism using ex-situ spectroscopic techniques and high-performance liquid chromatography and proposed complex steps for the discharge in a bis(trifluoromethanesulfonyl)imide and tetraethylene glycol dimethyl ether electrolyte system, as described in the below Equations (2-8):



(30% initially dissolves)



(70% of S₈ is consumed as the concentration in the solution decreases)



(at a 60% depth of discharge, solid Li₂S is observed)

The lithium anode is corroded by this polysulfide shuttle, which leads to self-discharge and low Coulombic efficiency^[38]. Many studies have been conducted in an attempt to overcome these challenges facing Li-S batteries^[40]. According to Luo *et al.*^[41], oxygen stabilized sulfur in a carbon matrix of Li-S batteries has excellent reversible capacity and long cycling stability. The suppression of polysulfide intermediates caused by sulfur interception in the carbon matrix explains the increase in Li-S battery performance. Another study found that carbonized mesoporous wood fiber may be utilized as the primary material for intercalated sulfur, resulting in a Li-S battery with better cycling stability^[41].

Li-air batteries

The operating concept of a Li-O₂ battery can be explained by the redox reaction between oxygen and Li metal. Abraham *et al.*^[42] used an organic electrolyte for the first time in 1996 for a lithium-air battery. The lithium-air battery has received significant interest as an alternative to LIBs because of its high theoretical energy density (3500 Wh kg⁻¹)^[43,44]. In Li-O₂ batteries, the cathode is usually a carbon matrix containing a catalyst, while the anode is generally Li metal. Their energy density can be as high as 1700 Wh kg⁻¹. These

batteries can be classified into four distinct types based on the type of electrolyte used: (1) Li-O₂ water batteries; (2) Li-O₂ aprotic batteries; (3) Li-O₂ all-solid-state batteries; and (4) Li-O₂ hybrid batteries. The aprotic structure of Li-O₂ batteries has received particular attention, since it forms a barrier between the anode and the electrolyte, protecting the lithium metal from the redox interaction with the electrolyte during the charge/discharge process. The Li-O₂ battery has the following redox reactions:



Li is converted into Li₂O₂ during discharge. The electromotive force of the battery when configured with a lithium metal anode is 2.9 V with a high theoretical specific energy density of 3500 Wh kg⁻¹[45,46]. In terms of formal capacity per mass and volume, Li₂O₂ is an excellent charge storage medium; however, it is a poor medium for the basic charge storage process. Unlike other Li⁺ storage materials, Li⁺ and e⁻ do not need insertion and extraction through the bulk of Li₂O₂ because dissolution and growth occurs on the surface of Li₂O₂. This distinct property of Li₂O₂ results in significant cycling stability and rate capability. The slow charge transport in these batteries is due to the several orders of magnitude slower ion diffusivity compared to liquids, which results in extremely fast charging transfer^[47].

It is possible to synthesize high-power Li-O₂ batteries by bypassing Li₂O₂ for the transmission of ions and electrons across the phase, both of which are simple to execute, where only Li₂O₂ stores charge, while liquid electrolytes provide facile ion transportation. In contrast, electron transport through liquids is difficult. The second electron transfer can be carried out by the second electron disproportionation or reduction, whether the solution or surface pathway is dominant [Figure 3A]. O₂/Li₂O₂ has a standard potential of 2.96 V, O₂/O₂⁻ has a standard potential of ~2.65 V and O₂⁻/Li₂O₂ has a standard potential of ~3.3 V^[48]. The other is a redox mediator, which is reduced or oxidized and then goes through the electrolyte to oxidize Li₂O₂ or reduce O₂ in order to restore itself, as shown in Figure 3B. Furthermore, the cost of lithium-oxygen batteries is reduced compared to LIBs due to the simplicity of the active material composites. Aqueous or non-aqueous electrolytes can be used in lithium-air batteries.

The production of LiOH in aqueous conditions can help avoid air cathode obstruction and protect it from over voltage during discharge. However, because LiOH cannot be entirely dissolved during charging, it precipitates, resulting in inefficient cycling and lower energy density^[32,45]. To avoid direct contact between H₂O and the surface of lithium metal, aqueous batteries require a surface protective barrier or a Li superionic conductive layer (LISICON glass with the composition Li_(1+x+y)Al_xTi_{2-x}Si_yP_(3-y)O₁₂)^[32]. However, the duration of these surface coating treatments is inadequate for preventing lithium dendrite formation^[45]. To overcome this problem, not only must the breakdown rate of Li₂O₂ be enhanced, but also the side reactions of lithium metal must be reduced. Furthermore, using ambient air in the presence of H₂O vapor, N₂ and CO₂ may result in a variety of side reactions, as well as poor cycling^[32]. Although organic electrolyte research has been conducted for several years on current LIB technology, the electrolytes of LIBs cannot be utilized directly in lithium-oxygen batteries due to electrode stability issues. The aprotic electrolyte of a lithium-oxygen battery must be able to stably withstand the active redox process, resulting in reducing oxygen species. To increase the rate of mass transfer towards the cathode, high O₂ diffusivity and solubility are required, as well as a high boiling point and low volatility to reduce cathode solvent evaporation^[49]. Initially, carbonate-based liquid electrolytes, including dimethyl carbonate, vinyl carbonate (EC) and propylene carbonate, were commonly employed in Li-O₂ batteries, although the cycling performance was clearly

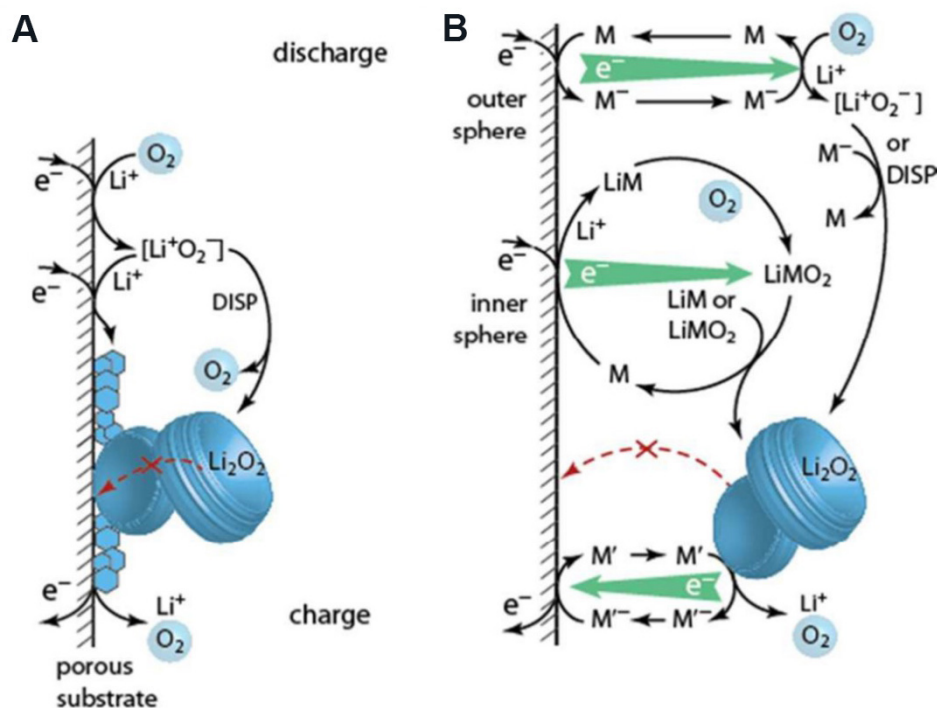


Figure 3. (A) Schematic diagram of reactions in a Li-O₂ cathode ($O_2 + 2Li^+ + 2e^- \leftrightarrow Li_2O_2$) during charge/discharge process in a typical electrolyte. Li₂O₂, an insulating and insoluble discharge product, develops on the surface of the conducting porous substrate and suppresses the electron transport. (B) The mediators M and M' mediate electron/hole transport. In an inner sphere process, the reduction mediator M can transfer electrons to O₂ via an O₂-binding transition state or in an outer sphere process via an O₂-binding transition state. Reproduced with permission from Ref.^[48] (Copyright 2017, Royal Society of Chemistry).

inadequate^[50,51]. In Li-O₂ batteries, sulfur-based solvents, such as ether-based electrolytes, sulfolane and dimethyl sulfoxide (DMSO), are also commonly employed. DMSO has low acidity, a high boiling point (189 °C) and a high oxidation potential (4.8 V)^[52]. Lithium-air batteries with ether electrolytes and DMSO are thought to be extremely reversible in performance.

Organic electrode batteries

Organic materials have been proposed as electrodes for LIBs in recent decades, although they have received less attention than metal-based electrodes^[53]. Organic electrode batteries benefit from good sustainability, eco-friendly features, flexibility in materials design, lightweight elements (e.g., C, H, N and O) and abundant resources^[53,54]. In the last two decades, many studies have been carried out for various types of organic materials, carbonyl compounds and organic free radicals (or free radical polymers), particularly organic sulfur and imino groups (C=N)^[55]. Because of their strong redox potential and activity and abundance, carbonyl compounds have received significant interest. When carbonyl group conjugation is added, the redox activity with reversible electron transfer can be expanded to a multiple electron reaction, resulting in the synthesis of multivalent anions. Liang *et al.*^[54] described the use of quinone compounds as battery cathodes for secondary batteries in 1972. Another organic material, chloroaniline, showed a capacity retention rate of 95% at 0.5 C over 50 cycles^[56].

Nevertheless, organic electrode batteries have a number of drawbacks, including solubility in the electrolyte, low energy density, poor conductivity and slow reaction kinetics^[53,54,57]. Adjusting the electrode level, adding conductive materials (such as carbon) and modifying the structure with conductive materials (such as graphene, carbon nanotubes and nanofibers and super-P) are all typical strategies for overcoming these

issues. Luo *et al.*^[55] demonstrated that azo (N=N) functional groups can be used as alternate organic electrode materials (OEMs) for addressing these issues. More than two functional groups are required for imino or carbonyl groups, whereas azo electrodes only require one functional group, thereby simplifying the chemical structure. Azo-based batteries offer high rate performance and strong cycling stability^[55]. Another approach that can potentially overcome the fundamental issues of organic electrodes in LIBs is utilizing self-assembled organic nanowires using $C_5Na_2O_5$ (croconic acid disodium salt)^[57,58]. Two benzo-dipteridine derivatives, BF-H₂ and BF-Me₂, were reported as high-capacity electrodes for LIBs by Cariello *et al.*^[59]. These portions enable each molecule to bind numerous lithium ions and maintain low solubility in the supporting electrolyte, which is often an exclusion issue for organic electrodes. As indicated in Figure 4A-D, BF-H₂ and BF-Me₂ have Coulombic efficiencies of ~100% and ~96%, respectively, over 100 cycles at a 0.1 C rate. Different reaction processes involve a variety of structural approaches. Carbonyl molecules have a number of challenges, one of which is their high solubility in organic electrolytes, which can be reduced by salt formation.

In OEMs, two or more carboxylic acid groups are linked to conjugated structures (i.e., benzene rings). The two -C=O in the lithium terephthalate carboxyl group react reversibly with two Li⁺ and two e⁻ during the lithiation and delithiation process [Figure 5A]. The air-stabilized lithium cathode material, which is based on the main chain of 1,4-benzenedisulfonate, contains two sulfonate groups, which improves the reaction potential to 3.25 V and maintains a reversible capacity of 100 mAh g⁻¹ over 50 cycles at C/20 [Figure 5B]^[60,61]. The anthracene-based organic disulfide cathode material can reversibly react with six Li⁺ and six e⁻, resulting in the regeneration and dissociation of disulfide bonds. However, its low conductivity and high solubility are still challenging [Figure 5C]. The electrochemically active center in the OEMs of LIBs was found to be the azo group^[62]. The double bond in the azo group of aromatic azo compounds is transformed to a single bond in the process of lithiation and then converted back to a double bond in the delithiation process. Each N atom reacts with one Li⁺ and one e⁻ in the lithiation and delithiation reaction [Figure 5D].

In the imine group (C=N), there is a reversible electrochemical reaction between Li⁺ and nitrogen atoms. Peng *et al.*^[63] reported that π -conjugated heteroaromatic quinoxaline molecules (3Q) represent an example of an imine-based organic cathode material. The reaction can be divided into two steps, as shown in Figure 5E. One Li⁺ reacts with two N atoms in the imine group in the first step. In the second step, each Li⁺ further reacts with two N atoms, resulting in a N-Li-N structure. In 3Q, each of the six imine groups reacts with six e⁻ and six Li⁺ to yield a reversible capacity of 395 mAh g⁻¹ over 10000 cycles. The super-lithiation reaction is based on the conjugated hydrocarbon, such as in polyacetylene, where the carbon-carbon bond in the unsaturated hydrocarbons is converted to a saturated carbon-carbon bond during discharge^[64]. During the discharge process, the unsaturated carbon bond in the OEMs is transferred to a saturated carbon bond and each carbon atom receives one e⁻ and one Li⁺. The reaction process of the unsaturated carbon-based organic anodes and carbonyl is shown in Figure 5F. The carbonyl group in naphthalenetetracarboxylic dianhydride first reacts with Li⁺ and e⁻ and then the unsaturated carbon-carbon bond combines with Li⁺ and e⁻ at a low reaction potential, resulting in an ultra-high capacity of 1000 mAh g⁻¹.

Solid-state batteries

In the development of solid-state batteries, the solid electrolyte is a critical component. Thin-film solid electrolytes and solid polymer electrolytes are the two main types of solid electrolytes. Inorganic solid electrolytes, such as garnets (e.g., Li₇La₃Zr₂O₁₂)^[65], NASICONs [e.g., LiZr₂(PO₄)₃, LiGe₂(PO₄)₃ and LiTi₂(PO₄)₃], sulfides (e.g., Li₂S-SiS₂ and Li₂S-P₂S₅ based)^[66] and perovskites (Li_{3x}La_{2/3-x}TiO₃)^[67,68], are the most widely studied inorganic solid electrolytes. Oxide materials, such as NASICONs, garnets and perovskites, have drawn much interest, since they provide many benefits for all-solid-state batteries, such as mechanical

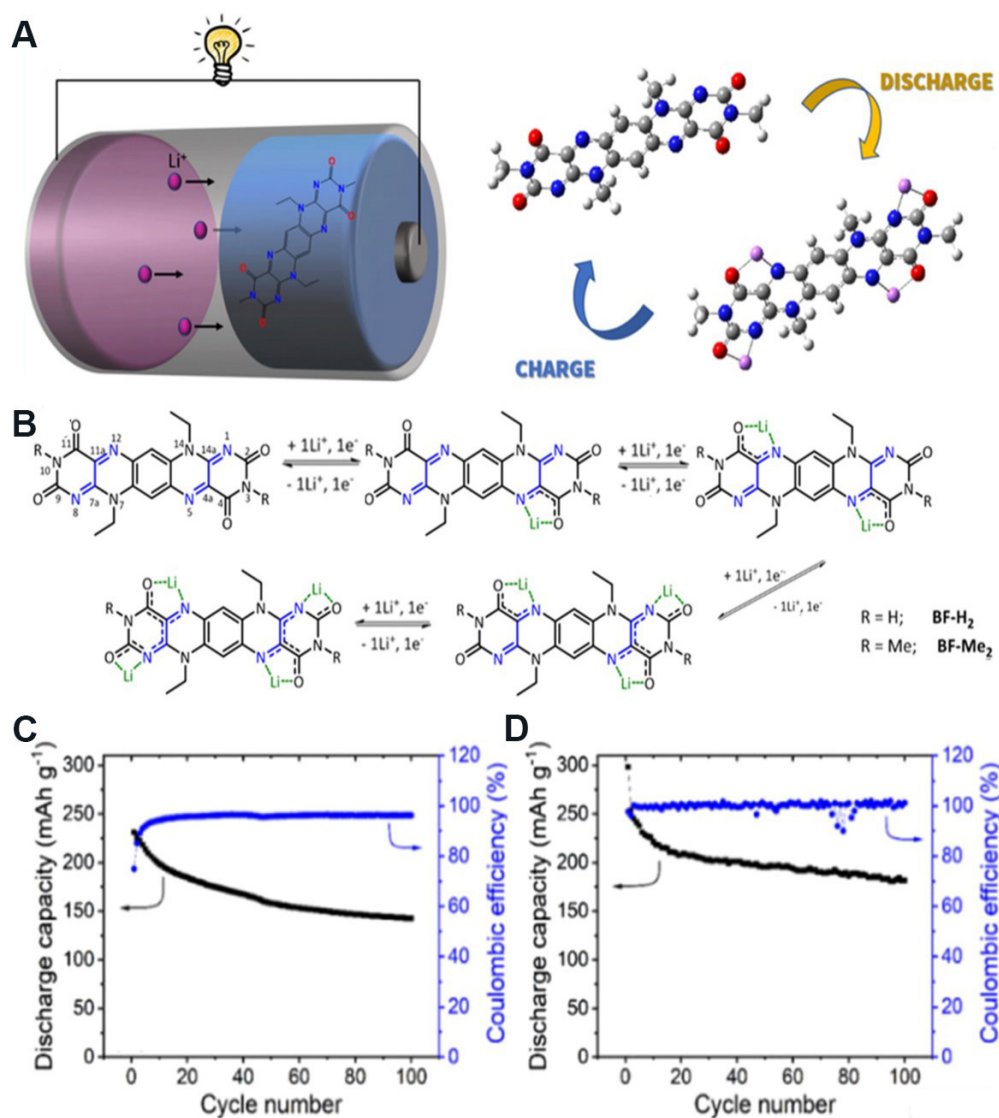


Figure 4. (A) Schematic illustration of organic electrode. (B) Potential reaction procedure and structure of benzo-dipiperidine derivatives BF-H₂ and BF-Me₂ with lithium. Cycling and Coulombic efficiency of (C) BF-Me₂ and (D) BF-H₂ at a 0.1 C rate in an ether-based electrolyte. Reproduced with permission from Ref.^[59] (Copyright 2020, American Chemical Society).

characteristics, chemical stability, conductivity (10^{-4} to 10^{-3} S cm⁻¹) and safety. In contrast, sulfide solid electrolyte have high conductivity (10^{-2} S cm⁻¹), low grain boundary resistance, excellent flexibility and high mechanical characteristics^[69]. However, sulfide solid electrolytes are limited by their high reactivity with metal oxides and their instability when exposed to moisture, which can result in H₂S gas evolution^[69,70].

Another potential solid electrolyte type for solid-state batteries is the solid polymer electrolyte. Poly(methyl methacrylate)^[71], polyethylene oxide (PEO)^[72], poly(acrylonitrile)^[73] and polyvinylidene fluoride^[71,74] are commonly used as polymer host materials in composite polymer electrolytes. However, these materials have considerable drawbacks, such as reduced electrode compatibility and oxidation stability. Therefore, improving the conductivity of solid electrolytes over a long period remains a major challenge and there still remains the question of whether amorphous or crystalline structures boost ionic conductivity. With lithium metal, polymers have the benefits of high stability, low shear modulus and superior flexibility, but they also

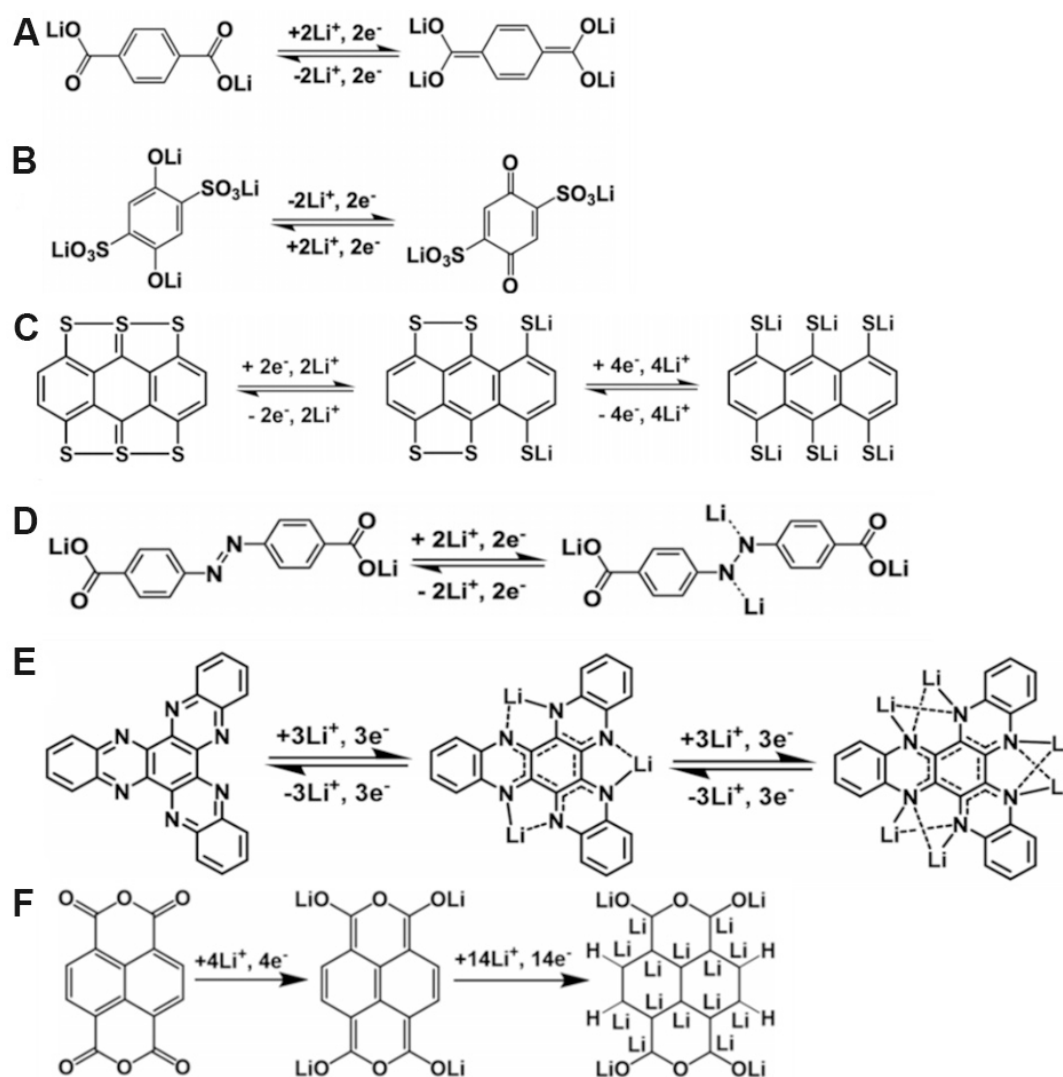


Figure 5. Reaction mechanisms of (A) a carboxylate-based organic anode, (B) an air stable quinone-based organic cathode, (C) an organodisulfide cathode material based on anthracene, (D) an azo compound, azobenzene-4,4'-dicarboxylic acid lithium salt, (E) lithiated structures of π -conjugated quinoxaline-based heteroaromatic molecules (3Q) during the discharge process and (F) a carbonyl- and unsaturated carbon-carbon group-based organic anode with carbon-carbon bonds in naphthalenetetracarboxylic dianhydride. Reproduced with permission from Ref.^[61] (Copyright 2020, American Chemical Society).

have low oxidation chemical potential, ionic conductivity and thermal stability. The practical use of solid polymer electrolytes is significantly hampered by these issues.

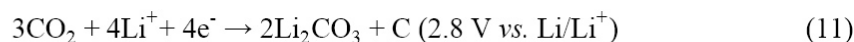
Thin-film solid electrolytes have also piqued interest, owing to their greater flexibility in design applications and high energy density compared to standard LIBs. In the early 1980s, a $\text{Li}/\text{Li}_{3.6}\text{Si}_{0.6}\text{P}_{0.4}\text{O}_4/\text{TiS}_2$ composite was the first thin-film solid electrolyte to be used for secondary LIBs^[75]. There are a variety of thin-film deposition techniques, including chemical vapor deposition^[76], radio frequency sputtering^[77], pulsed-laser deposition^[78] and atomic layer deposition^[79]. The lithium phosphorus nitrogen oxide glass (LiPON) battery is one of the most studied thin-film batteries. Bates *et al.*^[80] first reported its use in 1992 and a team from Oak Ridge National Laboratory (ORNL, USA) then investigated it further. The stability window of LiPON compared to a Li metal electrode is reported to be between 0 and 5.5 V^[81]. The thermal stability and hardness of LiPON have further advantages^[82]. As a result, the thin-film LiPON battery ($\text{LiNi}_{0.5}\text{Mn}_{1.5}\text{O}_4$

/LiPON/Li) shows a cycle life of 10000 cycles, a 90% capacity retention rate and a voltage of up to 5 V^[83]. Although LiPON has recently become a common solid electrolyte for all-solid-state thin-film batteries, its low conductivity in comparison to oxide materials must be overcome to build high-capacity thin-film batteries. Solid-state LIB chemistries operated with solid electrolytes and their performance metrics (i.e., power density, cycle life, energy density and other relevant parameters) at the current stage of development are summarized in [Table 1](#).

Ion transport in solids is a complicated process that is influenced by a variety of parameters and is still in the early stages of development at the moment. Liquids have a distinct wetting effect compared to inorganic solids^[88]. When in contact with solid electrodes, they disintegrate quickly and generate undesired phases, which obstruct ion transport and lower the total ionic conductivity^[89]. It is anticipated that it will become possible to alter key parameters and eliminate related issues during the manufacturing process in order to obtain appropriate products in future years.

Li-CO₂ batteries

Lithium-carbon dioxide batteries have gained significant interest from the battery industry in recent years. This battery system can store energy by removing carbon dioxide from the atmosphere. Takechi *et al.*^[90] reported that a novel form of gas battery, Li/CO₂-O₂, has a high irreversible discharge capacity, which is three times that of a lithium-air battery. Lim *et al.*^[91] later developed a reversible Li/CO₂-O₂ battery utilizing DMSO, which resulted in the reversible production of Li₂CO₃. In response to the earlier O₂ and CO₂ mixed gas battery, Xu *et al.*^[92] developed a main Li-CO₂ battery that achieves charging capacity by employing pure CO₂ gas as the working electrode. Liu *et al.*^[93] demonstrated a 100% reversible Li-CO₂ battery by utilizing LiCF₃SO₃ (1:4 mol) as an electrolyte a year later. The following electrochemical reaction can be used to increase the charging capacity of lithium-carbon dioxide batteries. In Li-CO₂ batteries, there is a disproportionation process based on the ultimate discharge products of C and Li₂CO₃. Equations (11-15) show that CO₂ undergoes a single electron reduction to C₂O₄²⁻ (Equation 12), resulting in an open circuit potential of 3 V. The intermediate, C₂O₄²⁻, is further disproportionated (Equations 14 and 15) to synthesize stable crystalline Li₂CO₃^[94,95]:



The main component in determining the reversibility of the application of these batteries is Li₂CO₃. Although Li₂CO₃ is an insulator, its oxidation requires a large overpotential while charging. Qiao *et al.*^[96] employed ruthenium as a cathode catalyst in a recent study to successfully minimize the excessive overpotential and increase the reversibility of lithium-carbon dioxide batteries. Li-CO₂ batteries are undoubtedly an attractive technology as they can simultaneously help to address both energy and

Table 1. Summary of performance metrics of various solid-electrolyte battery systems

Battery system	Solid electrolyte	Energy density (Wh kg ⁻¹)	Power density (mW cm ⁻²)	Cycle life (number of cycles)	Cell voltage (V)	Refs.
All-solid-state LIBs	Oxide (NASICON, LISICON and garnet)	300-600	10-50 (temperature dependent)	300	3.5-5.0	[84,85]
	Sulfide (Li ₂ S-P ₂ S ₅ -MS _x)		10-60 (temperature dependent)	1000	4.5-5.0	[86]
	Thin-film LiPON		5-50 (cathode dependent)	10000	3.0-4.0	[83]
	Polymer (PEO)		10-100 (elevated temperatures)	400	3.3-3.7	[87]

LIBs: Lithium-ion batteries; LiPON: lithium phosphorus nitrogen oxide glass; PEO: polyethylene oxide

environmental issues. However, in practice, the major issues to be addressed for their widespread application are excessive overpotential and low Coulombic efficiency.

PERIODIC CLASSIFICATION OF ELEMENTS FOR LIBS

S-block elements

Hydrogen is one of the most abundant chemical substance in the universe, accounting for ~75% of all baryonic matter. On this basis, studies have shown that storing renewable energy in the form of hydrogen through an electrolytic process is considered the most promising option. Hydrogen storage offers several benefits and hydrogen and fuel cells have the potential to contribute to future sustainable development in terms of energy demand and environmental sustainability^[97]. For decades, hydrogen fuel cells have been investigated as clean alternatives to internal combustion engines. In the past decade, a widespread search for alternative fuels has resulted from a lack of safe and effective hydrogen supply and storage. Among the different anodic fuels studied, borohydride has been reported to a good choice due to its rapid anodic kinetics, high energy density, high stability and easy storage, transport, usage and disposal. It is also free of hazards and pollutant emissions. The eight-electron oxidation process of borohydride results in high-density energy storage. According to the complete oxidation reaction of the eight electrons, the theoretical specific capacity of NaBH₄-based anodes is up to 5700 mAh g⁻¹. The equilibrium voltage of a NaBH₄/O₂ fuel cell with an oxygen cathode was 1.64 V and its energy density was 9.3 kWh kg⁻¹, while a gaseous ammonia fuel cell gave 5.5 kWh Kg⁻¹ and a pure methanol fuel cell gave 6.2 kWh kg⁻¹^[12].

Lithium has attracted attention because of its high voltage capacity and energy density. LIBs are widely used in portable devices, wearable electronics and electric vehicles due to their small size and superior performance^[98]. Graphite is the most prevalent anode material used in LIBs^[99]. Unfortunately, the Li storage capacity of graphite (372 mAh g⁻¹) is limited and further higher capacity materials are therefore needed for modern appliances. Ideal anode materials have high adsorption capacity and easily diffusion of Li⁺ on their surface. Single-walled carbon nanotubes can adsorb lithium internally and comparatively show a high reversible capacity (500 mAh g⁻¹)^[100]. Furthermore, chemical etching and ball milling techniques offer the potential to synthesize Li_{2.7}C₆ CNTs, which give higher Li capacity (1000 mAh g⁻¹). High mechanical strength, electrical conductivity, surface area and thermal conductivity and wide electrochemical applications make graphene a potential alternative anode material for LIBs^[101]. Unfortunately, graphene still has some problems as an anode

material. Regardless of the concentration of Li^+ on graphene, lithium atoms can form clusters and dendrites, which may reduce the battery charge and discharge capacity^[102]. The adsorption energy of Li^+ on graphene is weaker than that of Li-Li, which is the prominent reason for the synthesis of Li clusters.

To solve this problem, the adsorption energy of Li^+ on graphene must be higher than their cohesive energy. The most studied dopants for graphene are N and B, adjacent to the C atom in the periodic table. In graphene, N is electron doped (n-type) and B is hole doped (p-type). These dopants can change the electronic structure of graphene by increasing (N) or decreasing (B) the Fermi levels in the valence and conduction bands. There is a wealth of information regarding the nitrogen substitution concentration of graphene and its applications in oxygen reduction reactions and fuel cell materials^[103]. Lowering the mobility of the counter anions bis(trifluoromethanesulfonyl)imide with the help of amine-functionalized boron nitride nanosheets can improve Li^+ transport in ionic gels. Boron nitride nanosheets (BNNS) exhibit acidic properties and interact with bases. The activation of BNNS with amine functional groups increases Li^+ mobility and anion migration, thus improving the ionic conductivity^[104,105]. Reportedly, the formation energy of N-substituted graphene changes with the N doping concentration, indicating the maximum possible content of N in graphene.

The formation of B dopants in graphene can interfere with cluster formation. Therefore, B-doped graphene can be considered as an excellent long-term material for battery applications. Reportedly, B-doped graphene delivers a very high reversible capacity (1549 mAh g^{-1}) at 50 mA g^{-1} . Wang *et al.*^[106] stated that the theoretical capacity of Li for Li_6BC_5 (B-doped graphene) was calculated using density functional theory (DFT), which was higher than 2271 mAh g^{-1} . It was reported that B-doped graphene is more efficient than N-doped graphene in terms of Li adsorption. This is because B can transfer most of its valence charge to graphene, leaving graphene as a p-type dopant and Li as an electronic dopant for graphene. The high theoretical capacity of B-doped graphene for Li^+ storage makes it one of the most attractive alternatives to graphite.

Some materials (e.g., Si and Sn with theoretical capacities of 4200 and 994 mAh g^{-1} , respectively) are capable of storing multiple Li^+ on a single atom through an alloying reaction, thus delivering high energy. However, these alloying reactions show a rapid capacity decay as they are primarily associated with large volume changes during cycling^[107]. Several methods have been proposed to solve the problem of large volume changes. One method involves making electrodes based on nanostructures, such as nanotubes, nanowires, nanoparticles or porous nanostructures^[57,108]. Another method is to dope inactive elements to reduce the volume changes. The third method involves the preparation of nanocomposites containing an inert matrix and an active substance. In nanocomposites, an inert matrix is used as a mechanical buffer for various active substances, which results in better cycling performance than the pristine material^[109].

The electrode material determines the electrochemical performance of LIBs. $\text{LiMn}_{1-x}\text{M}_x\text{O}_2$, $\text{LiMn}_{2-x}\text{M}_x\text{O}_4$, LiCoO_2 and LiMPO_4 ($\text{M} = \text{Ni, Co or Fe}$) are all lithium metal oxides with high positive redox potentials and are commonly used as LIB cathodes. At high current rates of 1-10 C, they can deliver capacities of $100\text{-}200 \text{ mAh g}^{-1}$. LIB anodes are usually made of low-cost carbonaceous materials with a storage capacity of less than 372 mAh g^{-1} . Large-scale applications place a premium on lithium safety. Well-known LIB anode materials, such as Si, Sn, Al and their alloys have very high capacities ($1000\text{-}4000 \text{ mAh g}^{-1}$). However, their capacities are prone to fading rapidly even at low current rates (0.05-0.20 C), meaning their actual performance is far below that expected due to their rapid volume expansion ($> 300\%$) during cycling. This causes the electrode to disintegrate and shatter, thereby losing electrical contact between adjacent particles^[110].

Due to their high capacity, rich abundance and safety, metal oxides are considered as promising next-generation anode materials for LIBs. Metal oxides form a Li_2O buffer matrix or crystalline structure (such as TiO_2) when compared to Al, Sn and Si electrodes. This facilitates the insertion of Li^+ in the electrochemical reaction and significantly extends the Li^+ cycle life. Many metal oxides can be used as anodes at high rates of 0.5 to 1 C by their redox reaction with Li and have a high capacity of 500-800 mAh g^{-1} . In addition, the charge/discharge process for TiO_2 electrodes may be faster despite their low storage capacity (100-170 mAh g^{-1}) at different rates^[111,112]. Low charge/ion conductivity and long-term cycling stability are currently limiting the use of metal oxides as anodes in LIBs. Preparing a hollow-structured material with a short diffusion path and a large surface area is one of the most efficient methods to solve this problem. Metal oxides have large surface areas, which provide more space to store more Li ions. Furthermore, there is a large contact area between the electrolyte and electrode, resulting in higher Li^+ flux passing through the interface. The transparent thin shell provides a very simplified pathway for the diffusion of Li^+ and electrons, thereby increasing the rate capacity^[113]. The hollow interior provides additional free space, reduces structural distortions and accommodates large volume changes due to repeated Li^+ ion insertion/extraction processes, thereby improving the cycling stability. Due to the significant reduction of electrode pulverization and polarization, the excellent electrochemical properties of hollow metal oxide structures are highly anticipated^[114].

In Li_2O_2 batteries, the morphologies of the byproducts of Li_2O_2 have been well documented. At low current density, toroid-shaped nuclei are formed, while at high current density, stratified growth occurs^[115]. Li_2S is also a promising cathode material that is being developed for use in emerging energy storage fields. Li_2S and S cathodes require effective encapsulation to reduce the dissolution of lithium polysulfide (Li_2Sn) in the electrolyte. The Li_2S cathode is coated with a 2D layered transition metal disulfide, which has high conductivity and strong binding to $\text{Li}_2\text{S}/\text{Li}_2\text{S}_n$. In particular, titanium disulfide (Ti_2S) is used as the packaging material and demonstrates a high specific capacity of 503 mAh g^{-1} at 4 C and a high area capacity of 3.0 mAh cm^{-2} at high mass loading (5.3-25.3 $\text{mg}_{\text{Li}_2\text{S}} \text{cm}^{-2}$). This opens up new possibilities by using transition metal disulfides instead of conventional carbon-based materials to effectively enhance the capacity of electrode materials^[116]. The anode of a Li-ion batteries is made of lithium compounds that are reversibly inserted by Li^+ , while the cathode is made of carbon or graphite, which holds the Li^+ in a solid state. Non-aqueous electrolytes, such as propylene carbonate, and a suitable lithium solution are used to avoid the violent reaction of Li with water. The separator is a microporous plastic film that can be coated with ceramic particles to improve the safety of the battery.

The safety of Li^+ cells should be carefully considered. Thermal runaway is a crucial problem facing LIBs; therefore, selected materials, battery design, organic electrolyte and charging systems should be carefully identified to minimize the risk. A schematic diagram for the thermal runaway of different materials is given in Figure 6^[117]. Battery safety systems with thermal sensors, voltage and current measurements and fuses are used for safe operation^[118]. The following are the main criteria to improve LIBs.

Energy capacity

The energy accumulated in LIBs corresponds to the amount of Li^+ ions that can be neutralized and absorbed in the battery electrodes during the charge/discharge phase. The effectiveness of Li^+ neutralization and the way they can be reversibly evacuated and absorbed or desorbed should be considered. Compounds with low Li binding energy should be used for all battery parts. For example, in the case of cathode materials, LiFePO_4 , LiCoO_2 , Li in graphite electrodes and some aprotic polymer electrolytes represent ideal candidates^[119]. The following Equation (16) is used to determine the storage capacity of LIBs:

$$C = \frac{(nF)}{M} \times \frac{1000}{3600} \quad (16)$$

where n shows the number of charges (Li^+), F is the Faraday constant, M is the molar mass of the electrode material and to convert from Coulombs to mAh, $1000/3600$ is used^[120].

Power and loading time

The cathode materials must be capable of repeatedly accepting and releasing Li^+ at high current rates. This depends on the Li^+ flux and how fast they can move in the electrolyte and can absorb on the electrode surface. The latter aspect requires a low work function, where incoming Li^+ ions can be neutralized more easily, and high surface mobility and mass diffusion, by which the neutralized Li atoms can be released.

Number of cycles and Li^+ loss

The reduction in the number of charge/discharge cycles is mainly because of chemical modification of the electrode and electrolyte surfaces. However, this also depends on the release of Li^+ with different mechanisms that affect the reversibility of Li^+ neutralization and absorption, which should be avoided or limited. Some of the stable compounds with impurities and degraded electrolyte compounds may recombine with Li^+ ; therefore, electrolytes should be selected appropriately. The neutralized Li^+ may diffuse further into the body of the electrode material and may recombine into a larger low-diffusivity compound or rearrange into a solid Li cluster, meaning that specific methods must be adopted. These strategies limit the overall diffusion of Li atoms with an appropriate stable diffusion barrier and hinder the formation of Li clusters in the electrode bulk material. The synthesis of a passivation layer on the electrode surface and any rearrangement of atoms, which is beneficial to dielectric materials, should also be avoided. This particularly affects the electrical conductivity of electrode materials containing graphene^[119].

It has been reported that a simple and effective method of synthesizing Li anodes is by rationally designing 3D current collectors with optimized surface and skeleton characteristics from a metal foam wrapped in porous carbon nanostructures with N-doped carbon nanosheets (designated as M/NPCN, $M = \text{Cu}$ or Ni). This potentially enables the placement of a large amount of Li and ensures uniform nucleation/growth of Li [Figure 7A]. The synthesized M/NPCN can enhance the stability of the Li anode and the cycle life of high sulfur loading in lithium-sulfur anodes. Figure 7B and C show that NPCN has a highly porous surface area. A Li/Cu foil|C/S cell showed a capacity of 129 mAh g^{-1} with an 84.9% CE after 92 cycles (capacity retention of 16.6%), while a Li/Cu foam|C/S cell gave a capacity of 280 mAh g^{-1} with a 95.0% CE of over 300 cycles (34.2% capacity retention) [Figure 7D]. A Li/Cu/NPCN|C/S cell gave a high capacity (816 mAh g^{-1}) and very stable CE ($\sim 99.9\%$) after 300 cycles, as shown in Figure 7D. Therefore, the prominent reason for the poor cycling stability of the Li/Cu foil|C/S and Li/Cu foam|C/S is the instability of the anode, which shows that the Li anode limits the practical application of the sulfur in the cathodes. In order to observe the Li anode intuitively, the battery cell was disassembled after the cycling test. Many Li dendrites were found, which are also known as “dead Li”, as noted in both Li foil and Li/Cu anodes. In contrast, the surface of Li/Cu/NPCN was smooth without clear Li dendrites^[121].

Graphene becomes an electron-deficient system when doped with Be. DFT simulations were used to model the adsorption of Li^+ on Be-doped graphene. The adsorption energy of Li^+ on Be-doped graphene can be increased to -2.53 eV/Li , which is 2.24 times that of Li on undoped graphene^[122]. Li^+ can be stored on the hexagon centered and also on the nearest hexagon of graphene, which can easily interact with 12 Li^+ for single vacancies of Be on the hexagon and provide 16 Li^+ for vacancies around each Be center hexagon of graphene. This shows that graphene can be doped with a small amount of dopant to store more Li^+ , thereby

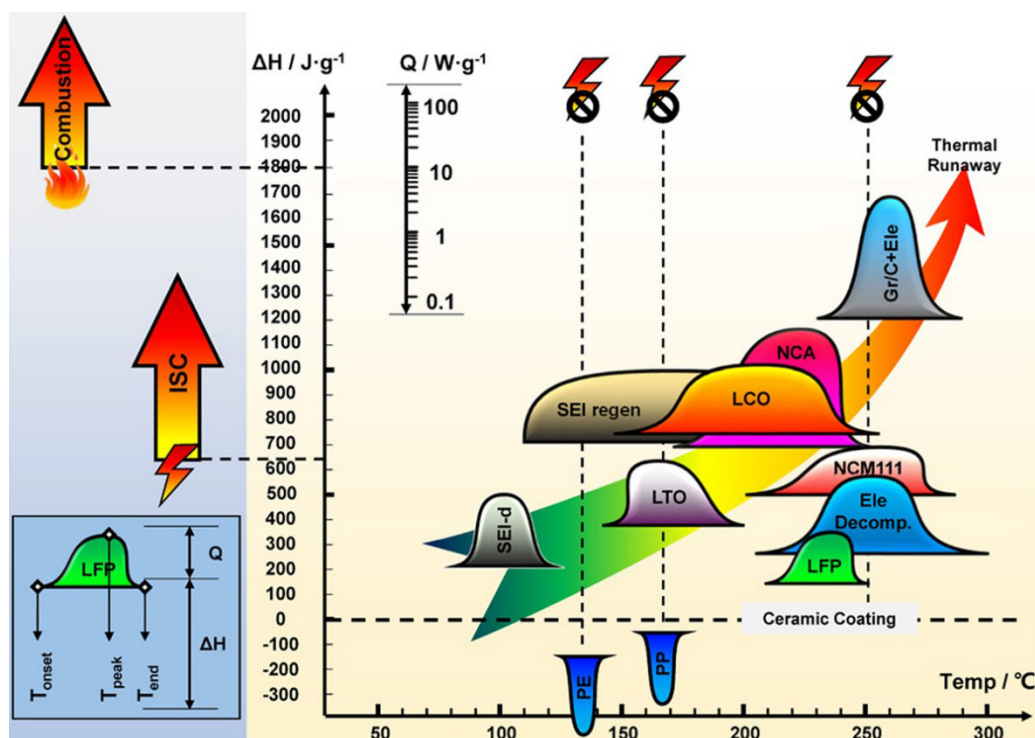


Figure 6. Energy release diagram for a LIB with an NCM/graphite electrode used to analyze the thermal runaway mechanism. Reproduced with permission from Ref. [117] (Copyright 2015, Energy Storage Materials, Elsevier). LIB: Lithium-ion battery; SEI: solid electrolyte interface; LTO: $\text{Li}_4\text{Ti}_5\text{O}_{12}$; LCO: LiCoO_2 ; LFP: lithium Iron Phosphate (LiFePO_4/C); ISC: internal short circuit; NCA: lithium nickel-cobalt-aluminum oxide ($\text{Li}[\text{Ni}_x\text{Co}_y\text{Al}_z]\text{O}_2$); PE: polyethylene; PP: polypropylene.

retaining the extraordinary properties of graphene to a large extent and increasing its Li storage capacity up to $2303.2 \text{ mAh g}^{-1}$. This is because Be doping produces Li_8BeC_7 with a reasonable adsorption energy of -1.47 eV/Li . The reported capacity value is 6.19 times that of graphite. This surprising result represents a breakthrough for using Be-doped graphene as a LIB anode material [120]. It is important to consider the capacity of Be-doped graphene and bare graphene compared with other anode materials. The theoretical specific capacities of $\text{Li}_{16}\text{BeC}_{48}$, $\text{Li}_{12}\text{BeC}_{48}$ and $\text{Li}_{12}\text{BeC}_{49}$ were found to be 73.355, 549.266 and $538.226 \text{ mAh g}^{-1}$, respectively, which are greater than that of $\text{Li}_{6.84}\text{B}_2\text{C}_{70}$ (212.6 mAh g^{-1}). These specific capacity values are also higher than those of phosphorus (433 mAh g^{-1}), graphite (372 mAh g^{-1}), Ti_3C_2 (320 mAh g^{-1}) and even Mo_2C (526 mAh g^{-1}).

When six Li^+ (three up and three down) are adsorbed in this system, Li_6BeC_7 is formed. The measured adsorption energy is -1.59 eV/Li , which is slightly lower than that of $\text{Li}_8\text{BeC}_{49}$ (-1.68 eV/Li). Curiously, the theoretical lithium capacity calculated by Li_6BeC_7 is very high ($1727.47 \text{ mAh g}^{-1}$). The calculated adsorption energy (Li_6BeC_7) of a given eight Li^+ is as high as -1.475 eV/Li , with a theoretical efficiency of $2303.29 \text{ mAh g}^{-1}$. This storage capacity is far more than the experimental (1549 mAh g^{-1}) and theoretical capacity (2271 mAh g^{-1}) of B-doped graphene used as an anode material for LIBs. The following formula can be used to calculate the lithium potential (V_{Li}) of an anode material for LIBs:

$$V_{\text{Li}} = -\frac{E_{\text{tot}} - E_{\text{sheet}} - nE_{\text{Li}}}{nzF} \quad (17)$$

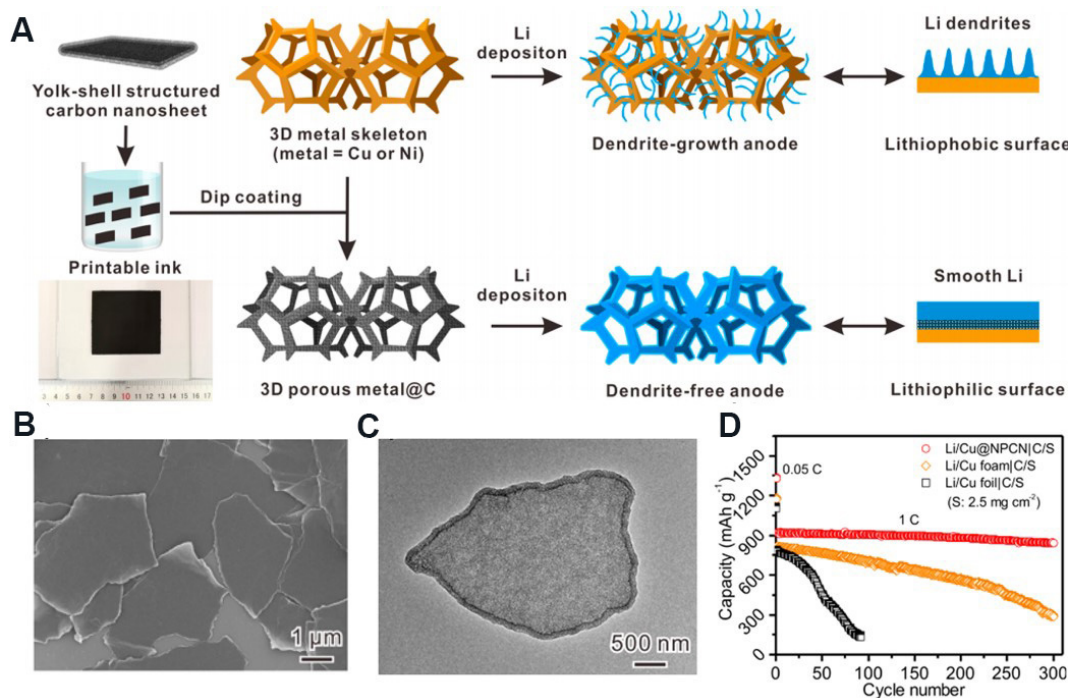


Figure 7. (A) Schematic representation of dendrite-free Li anode (inset: NPCN ink screen printed onto polyethylene terephthalate substrate) by designing NPCN-wrapped 3D metal foam. (B) SEM and (C) TEM images of NPCN. (D) Cycling performance of Li/Cu/NPCN|C/S, Li/Cu foam|C/S and Li/Cu foil|C/S full cells of sulfur at 1 C. Reproduced with permission from Ref. [121] (Copyright 2019, American Chemical Society). NPCN: N-doped porous carbon nanosheets; SEM: scanning electron microscope; TEM: transmission electron microscope.

where E_{tot} corresponds to the formation and total energy, n is the number of charges (Li^+) adsorbed, F is the Faraday constant and z is the charge of the lithium ions in the electrolyte ($z = 1$). An increase in Li concentration leads to a decrease in V_{Li} . When the Li concentration in one vacancy (doping) increases from one to 12 atoms in a single vacancy (doped), the V_{Li} decreases from 2.53 to 1.33 V and when the Li concentration in a double vacancy (doping) increases from one to 16 atoms, the V_{Li} value is reduced from 2.38 to 1.33 [120].

Strontium (Sr) doping can effectively increase the rate performance of $\text{Li}_4\text{Ti}_5\text{O}_{12}$. Sr^{2+} has a much larger ionic radius (0.118 nm) than Li^+ (0.076 nm) and Ti^{4+} (0.0605 nm), which makes it difficult to form $\text{Li}_4\text{Ti}_5\text{O}_{12}\text{Sr}$. Nevertheless, if Sr^{2+} can enter the $\text{Li}_4\text{Ti}_5\text{O}_{12}$ network, it expands the Li^+ intercalation and deintercalation channels and thus improve the $\text{Li}_4\text{Ti}_5\text{O}_{12}$ performance. This high performance can be attributed to a decrease in particle size and charge transfer resistance and an increase in network parameters due to the introduction of Sr into the lattice of $\text{Li}_4\text{Ti}_5\text{O}_{12}$. Sr-doped $\text{Li}_4\text{Ti}_5\text{O}_{12}$ has a specific discharge capacity that is 1.62 times greater than undoped $\text{Li}_4\text{Ti}_5\text{O}_{12}$ at 5 C. The Sr content has a significant effect on the performance of Sr-doped $\text{Li}_4\text{Ti}_5\text{O}_{12}$ and the optimum Sr content was found to be 0.02 at an atomic ratio of Sr to Ti. A small amount of $\text{SrLi}_2\text{Ti}_6\text{O}_{14}$ was formed in the Sr-doped $\text{Li}_4\text{Ti}_5\text{O}_{12}$, which has a positive effect on the charge/discharge specific capacity of the doped $\text{Li}_4\text{Ti}_5\text{O}_{12}$ because Li^+ can intercalate/deintercalate within $\text{SrLi}_2\text{Ti}_6\text{O}_{14}$ at lower charge/discharge potentials than $\text{Li}_4\text{Ti}_5\text{O}_{12}$ [123].

The chemical preparation processes for barium and potassium ferrate for alkaline electrochemical energy storage are now described. Synthetic salts have been used to show the structure of different super-iron (zinc anode) alkaline AAA batteries using Fe(V) salts at high capacity. The results show that the synthesized

K_2FeO_4 is completely stable over 500 cycles. The synthetic route is introduced, which can produce 80-100 g of 96.5%-99.5% pure K_2FeO_4 and BaFeO_4 . These synthetic products have been proven to give high energy discharge in various AAA alkaline batteries. Super-iron alkaline AAA batteries like BaFeO_4 can provide more than 0.8 Wh of electricity during 2.8 Ω of discharge, which is more than 200% of the capacity of traditional alkaline batteries. The studied barium super-iron battery configuration gives a greater capacity than the studied configuration of potassium super-iron alkaline batteries^[124].

Adding witherite (BaPbO_3) to the anode of lead-acid batteries can increase the efficiency and current acceptance of deep discharge batteries. At room temperature, the half-life of BaPbO_3 in the battery acid determined from the decomposition rate constant is ~ 4 years. However, the rate of decomposition of BaPbO_3 increases with increasing temperature, applied potential and acid concentration. It is estimated that the threshold of BaSO_4 content detriment to the cycle life of a lead-acid battery is $\sim 0.3\%$. With 1% BaPbO_3 , an appreciable improvement of the formation can be attained. At this level, the decomposition of BaPbO_3 into BaSO_4 is not detrimental to the life of the battery^[125]. Mn-doped BaPbO_3 showed improved rate and capacity compared to typical MnO_3 , with a first cycle capacity of $\sim 360 \text{ mAh g}^{-1}$, as well as better recharge capacity even after a deep discharge. Further investigation is required to determine the load storage mechanism and its specific crystalline and amorphous phases synthesized during the process. The high capacity performance of Mn/ BaPbO_3 suggests that these materials may be potential electrode materials^[126]. The high impedance characteristics and power discharge performance of cathodes of K_2FeO_4 and BaFeO_4 in dry alkaline Zn cells show that ferrate materials are bonded to maximize the surface area of the cathode and they can offer superior performance over electrolytic MnO_2 at running voltages of $> 1.6 \text{ V}$ and currents of up to 100 mA g^{-1} of the active material^[124].

P-block elements

The anode performance of B-doped graphite was studied by electrochemical measurements. In the galvanostatic measurements, a discharge capacity of $\sim 315 \text{ mAh g}^{-1}$ was achieved for B-doped pitch coke-derived graphite. Due to the graphitization of B, the discharge capacity of B-doped graphite was enhanced compared to B-free graphite^[127]. It is reported that the doping of B with boric acid, boron oxide and boron carbide enhances the discharge capacity and Coulombic efficiency. It is also noted that the B-doped mesophase pitch-based carbon fiber exhibits a prominent phenomenon of B doping in carbon, which is effective for battery performance. Co-B and Fe-B alloy powders affect the electrochemical performance when used in aqueous alkaline solutions as anodic materials. The discharge capacities of Co-B and Fe-B electrodes were 1100 and 1200 mAh g^{-1} at a high rate of 100 mA g^{-1} , respectively, which are much higher than that of Zn (820 mAh g^{-1}). The activated B maintains the electrode potential in the negative range, thereby preventing passivation of the transition metal^[128,129].

Carbon remains a highly promising material for electrochemical devices. Li^+ can easily disperse between the hexagonal graphite planes of the cathode in lithium-metal/graphite batteries (LiCoO_2 batteries), where the anode content is made of graphite as opposed to the previously cited design. In the case of LiFePO_4 batteries, black carbon is used as a cathode material to improve its porosity for ionic conductivity and reversible Li^+ absorption. The graphene-plated anode of LIBs improves the energy storage capacity and charging speed of the battery, although it does not provide the desired results in other areas. Furthermore, most results have been obtained on a semi-empirical basis, so further research into higher performance and reliability is needed. For example, dendritic growth may cause short circuit, attract unwanted compounds of basic electrochemical elements or may redeposit and cover the surface of the electrode, eventually resulting in electrical and material leakage, and the release of combustible compounds, which may be the result of manufacturing failures. Graphite is the utmost common material used for LIBs. However, its limited Li storage capacity (372 mAh g^{-1}) restricts LIB performance.

A suitable anode material is one with high adsorption capacity for Li^+ and facile diffusion on the anode material. Carbon nanotubes (CNTs) have the potential to adsorb Li, either internally or externally. Therefore, experimentally studied single-walled CNTs have been found to be better than graphite and give a reversible capacity of 500 mAh g^{-1} . In addition, ball milling techniques and chemical etching offer the possibility of synthesizing $\text{Li}_{2.7}\text{C}_6$ CNTs, which show even higher Li capacities of up to 1000 mAh g^{-1} . Graphene is a potential and alternative material for LIBs anode due to its special properties, such as a large surface area, high mechanical strength, high thermal and electrical conductivity^[121]. In 2015, multilayer Ti_3C_2 /carbon nanofiber (CNF) particles were used as LIB anode materials and their electrochemical performance was successfully improved by growing conductive “CNF bridges” within each $\text{Ti}_3\text{C}_2\text{T}_x$ flake. The rate performance of the Ti_3C_2 /CNFs was improved, while their specific capacity was still maintained at 320 mAh g^{-1} over 295 cycles at 1 C. More notably, the capacity of the Ti_3C_2 /CNF hybrid at a super-high rate of 100 C is only slightly lower than that of pure $\text{Ti}_3\text{C}_2\text{T}_x$ particles at 1 C. It was also reported that a delaminated Nb_2CT_x /CNT composite, when used as an anode material, shows an excellent capacity of 400 mAh g^{-1} at 0.5 C^[130]. However, the maximum specific capacity for carbon cathodes to date is $\sim 120 \text{ mAh g}^{-1}$ for graphene nanoribbons directly developed on extremely porous 3D graphene structures. Despite their high performance, most reported graphene and graphite-based cathodes exhibit low Coulombic performance at low rates^[131].

Graphene was discovered more than a decade ago. Carbon materials with sp^2 bonding have a variety of structure forms with different dimensions, including 0D, 1D, 2D and 3D structures, fullerenes, nanotubes, graphene and graphite. Graphene is composed of a single honeycomb lattice with covalently bonded carbon atoms and fully conjugated π electrons, giving it excellent electronic, mechanical, thermal and chemical properties. It is a semiconductor and can withstand a high current density exceeding 109 A cm^{-2} . Graphene is also an excellent energy storage material due to its high surface area ($2630 \text{ m}^2 \text{ g}^{-1}$) and is conductive and easy to functionalize with other molecules. Graphene family include double- and few- (three to nine) layer graphene and graphene resembling large polyaromatic molecule called graphene nanoribbon (single-, double-, few- or multilayer; multilayer graphene nanoribbons are also called stacked graphite nanofibers or graphene nanofibers)^[132]. Graphene oxide, represented as a monolayer of graphite oxide, is the most important chemically-derived form of graphite and is typically synthesized by its exfoliation, long-time stirring of graphite oxide/water mixtures or simple sonication^[130].

In recent decades, the insertion of lithium ions in the graphite lattice has been studied in detail for electrochemical energy storage applications. Graphite carbon forms the structure of LiC_6 and as a result has a low Li^+ storage capacity of only 372 mAh g^{-1} . Single graphene sheets can store Li on either side to form LiC_3 with a capacity limit of 744 mAh g^{-1} . Graphite-based electrode materials suffer from the large size of lateral graphite and long Li-ion diffusion paths into the material. In order to enhance the diffusion of Li^+ into the interlayer space of the substrate and to increase the reversibility, a solution that decreases the lateral dimensions (x-y axes) is used. Stacked graphene nanofibers represent such a solution and have a length of several micrometers and lateral dimensions of tens of nanometers. Graphite shows high electrochemical performance because of its high surface area, edge-like structure and interlayer spacing, although its base planes only have space at the ends of nanofibers. These nanosized lateral dimensions provide a better energy storage capacity of more than 461 mAh g^{-1} . Nanosized stacked graphene nanofibers have high energy storage capacity. Additionally, electrodes made of graphene sheets have been used to boost the basic potential of LIBs, resulting in a capacity of 540 mAh g^{-1} . However, to prevent graphene nanosheets from restacking, CNTs were used as spacers and the reported storage capacity for LIBs was enhanced to $730\text{-}784 \text{ mAh g}^{-1}$ ^[133].

In other work, Li and graphene were used as anode and cathode materials, respectively, and the observed discharge capacity was 582 mAh g⁻¹. The high discharge capacity of this anode is due to the nanoholes in the sheets of graphene. This is a significant discovery for the further development of Li⁺ graphene-based batteries because graphene nanoholes can be used to support the passage of selective ions. However, due to the comparatively strong bonds formed with defects during the charge process, the discharge of Li necessitates high voltages and, as a result, a large voltage hysteresis. Tangled graphene has a high reversible capacity of 794-1054 mAh g⁻¹. These high volumes are very similar to the Li₂ covalent model. Although graphene batteries initially had poor performance, current devices show outstanding cycling performance (90%-95%). It is noteworthy that studies have shown that the solid electrolyte interface between graphene with a high specific surface area and electrolyte morphology has a high capacity of reversibility^[134].

With the aim of synthesizing metal/graphene nanocomposites, DFT and volumetric experiments proved that the capacity of LIB composites of Sn/graphene show an improvement in storage capacity of the cathode material and can store up to 994 mAh g⁻¹. Li⁺ interacts with Sn to form Li_{4,4}Sn but pure Sn can induce accumulation and clustering of Sn nanoparticles; therefore, repeated cycles may cause a loss in capacity of such electrode materials. Graphene plays a double role in supporting Sn atoms for the adsorption of Li⁺ and avoiding their aggregation. For Sn/graphene nanocomposites, a capacity of up to 795 mAh g⁻¹ has been observed. Another option is to use metal oxides (especially transition metal oxides) as components of graphene nanocomposites. To separate their adjacent flakes, Co₃O₄ nanoparticles (10-30 nm) can be homogeneously dispersed on graphene sheets. Over 30 cycles, the recycling efficiency of the material was 98% and the capacity was maintained at 935 mAh g⁻¹. TiO₂ nanoparticle/graphene nanocomposites were constructed similarly with a recycling efficiency of over 98%^[135]. Si and graphene nanosized composites have an average Coulombic efficiency of 93% and a high capacity of 1168 mAh g⁻¹ over 30 cycles. Graphene can also act as a conductive source for batteries with olivine-based LiFePO₄, with minimal capacity fade even after several hundreds of cycles^[136]. Graphene sheets with a single-fold layer material have the highest capacity of 1175 mAh g⁻¹, while threefold and fivefold layer materials have capacities of 1007 and 842 mAh g⁻¹, respectively. It is evident from these capacity values that graphene sheets with high edge sites, increased defects and reduced size are very beneficial for Li storage.

The performance of LIBs can be efficiently increased by heteroatomic doping, which effectually increase the surface chemical properties and electronic band structure. For example, B- or N-doped graphene has a very high reversible capacity of over 1040 mAh g⁻¹ at a very low rate of 50 mA g⁻¹^[133]. More significantly, it has a high rate and superb long-term cycling capabilities and can charge and discharge easily in a short period of 1 h to tens of seconds. Heteroatomic defects, disordered surface morphologies and the unique 2D structure of the material increase the inter-sheet distance and electrical conductivity, which are helpful for increasing the absorption of Li⁺ at the surface and providing high Li⁺ diffusion. Doped materials generally outperform pristine carbonaceous materials. Porous graphene has rich porosity and an extraordinary specific surface area (SSA), which are advantageous for the faster diffusion of electrolytes and the transportation of electrons in energy storage. For instance, well-ordered mesoporous graphene sheets with a large pore volume (1.8 cm³ g⁻¹) and high SSA (1000 m² g⁻¹) have a capacity of 520 mAh g⁻¹ at 300 mA g⁻¹ over 400 cycles. However, their practical use in LIBs is limited because of the resulting significant irreparable capacity^[137]. A quasi-1D form of graphene, graphene nanoribbons (GNRs), has rich edges, which are advantageous for Li⁺ storage. A low capacity (250 mAh g⁻¹) over 50 cycles was delivered by pure GNRs. Taking advantage of N doping and the edge effect, N-doped GNRs have a stable capacity of 714 mAh g⁻¹ after 100 cycles at 3 A g⁻¹. An N-doped GNR-based 3D aerogel structure exhibited an improved Li⁺ storage capacity and consequently gave 910 mAh g⁻¹ at 0.5 A g⁻¹^[133,138].

Nanomaterials, such as Si and Ge, have short ion diffusion pathways, which are appropriate for the insertion of Li^+ , enhance the energy efficiency and cycling performance and minimize the internal strain for LIBs. Si, Ge and their alloys are used as elemental anodes and can provide high capacities but have greater volumetric expansion during charging. Therefore, for phase change cathodes, a complex 3D architecture should be used for better cycling and rate performance^[139]. Si is an excellent anode material for LIBs because it has a low discharge potential, high theoretical capacity (4200 mAh g^{-1}) and is ten times more efficient than graphite and much higher than various oxide and nitride materials. However, due to drastic volume changes ($> 300\%$) upon extraction and insertion of Li^+ , its usage results in capacity fade and pulverization^[140]. Results illustrate that Si nanowires have better capacity than other types of Si. Even at a higher 1 C rate, they give a capacity of 2100 mAh g^{-1} , which is five times higher than that of graphite. Despite their improved performance, due to the interfacial phase of the solid electrolyte, Si nanowire anodes lose irreversible capacity through the initial cycling^[139]. The performance of gold-plated porous Si is superior to that of non-gold-plated porous Si, which has a discharge capacity of 500 mAh g^{-1} at the initial cycle but quickly decreases over the 10th cycle to only 76 mAh g^{-1} .

The composition of the gold coating and internal pores shows excellent long-term cycling stability and high performance for LIB anodes^[141]. The maximum possible specific capacity of Si (3579 mAh g^{-1}) is much higher than the theoretical capacity of graphite (372 mAh g^{-1}). Nevertheless, the increase in volume ($\sim 300\%$) of Si during cycling causes cracking of the Si electrode and results in short circuit and rapid capacity loss^[142]. It is known that at low potentials, Au reacts with Li and has a capacity of 451 mAh g^{-1} for $\text{Li}_{15}\text{Au}_4$. Lee *et al.*^[143] observed that a 50 nm Au film causes an initial charge capacity of 47 mAh g^{-1} at 20 C; however, by increasing the number of cycles, the charge/discharge capacity decreases rapidly. The low discharge potential ($< 0.5 \text{ V}$ compared to Li/Li^+) and increased capacity of Si make it a good choice as a cathode material in high-energy LIBs. Despite their huge volume changes, Si and Si-based alloys are considered to be possible substitutes for graphite-based cathodes in current commercial LIBs^[141].

The electrochemical performance of a Si- Cu_3Si -CNT/G electrode was shown to be good but it has not yet reached current commercial goals (a reversible capacity of 1000 mAh g^{-1} , an 80% capacity retention over 100 cycles and a Coulombic efficiency of $> 85\%$). To enhance the performance of Si- Cu_3Si -CNT/G, a known pyrolytic carbon coating method has been used. A schematic of the three-step manufacturing process of Si- Cu_3Si -CNT/G-C is given in [Figure 8A](#). Under full discharge conditions (100% SOC at 0 V), the expansion of the Si- Cu_3Si -CNT/G and Si- Cu_3Si -CNT/G-C electrodes was 39.5% and 48.0%, respectively, much lower than that of Si- Cu_3Si (110.3%) and bulk Si (140.4%). When fully charged (0% SOC at 2 V), the expansion rates of the Si- Cu_3Si -CNT/G and Si- Cu_3Si -CNT/G-C electrodes are 9.5% and 8.3%, respectively. In [Figure 8B](#), the cycling performance of Si- Cu_3Si -CNT/G-C, commercial graphite and bulk Si is compared at 200 mA g^{-1} in a voltage range of 0-2 V. Due to the formation of $\text{Li}_{3.75}\text{Si}$, the volume of Si changes significantly, resulting in mechanical cracking and destruction, decreasing the ICE and fading the cycling performance and the stability of bulk Si. Si- Cu_3Si -CNT/G-C shows a high CE of over 99% and a stable cycling performance at 100 cycles, while the capacity retention rate was 94.9% and 88.0% of IRC after 50 and 100 cycles, respectively^[143]. A uniform distribution of nanosized Li-active Si nanocrystals prevents agglomeration of Si nanocrystals during cycling and buffering effects on bulk Si nanocrystals of a multi-carbon matrix, providing excellent ICE, IRC and retention of capacity and volume changes.

[Figure 8C](#) shows the rate performance of commercial graphite and Si- Cu_3Si -CNT/G-C at 1 C and 1200 mA g^{-1} . [Figure 8D](#) summarizes the capacity retention and ICE of Si, Si- Cu_3Si (1st step), Si- Cu_3Si -CNT/G (2nd step) and Si- Cu_3Si -CNT/G-C (3rd step). The CV peaks of Si- Cu_3Si -CNT/G-C agree well with Si- Cu_3Si , but by using a multi-carbon substrate, the CV peak is smoothed. In addition, Si- Cu_3Si -CNT/G-C

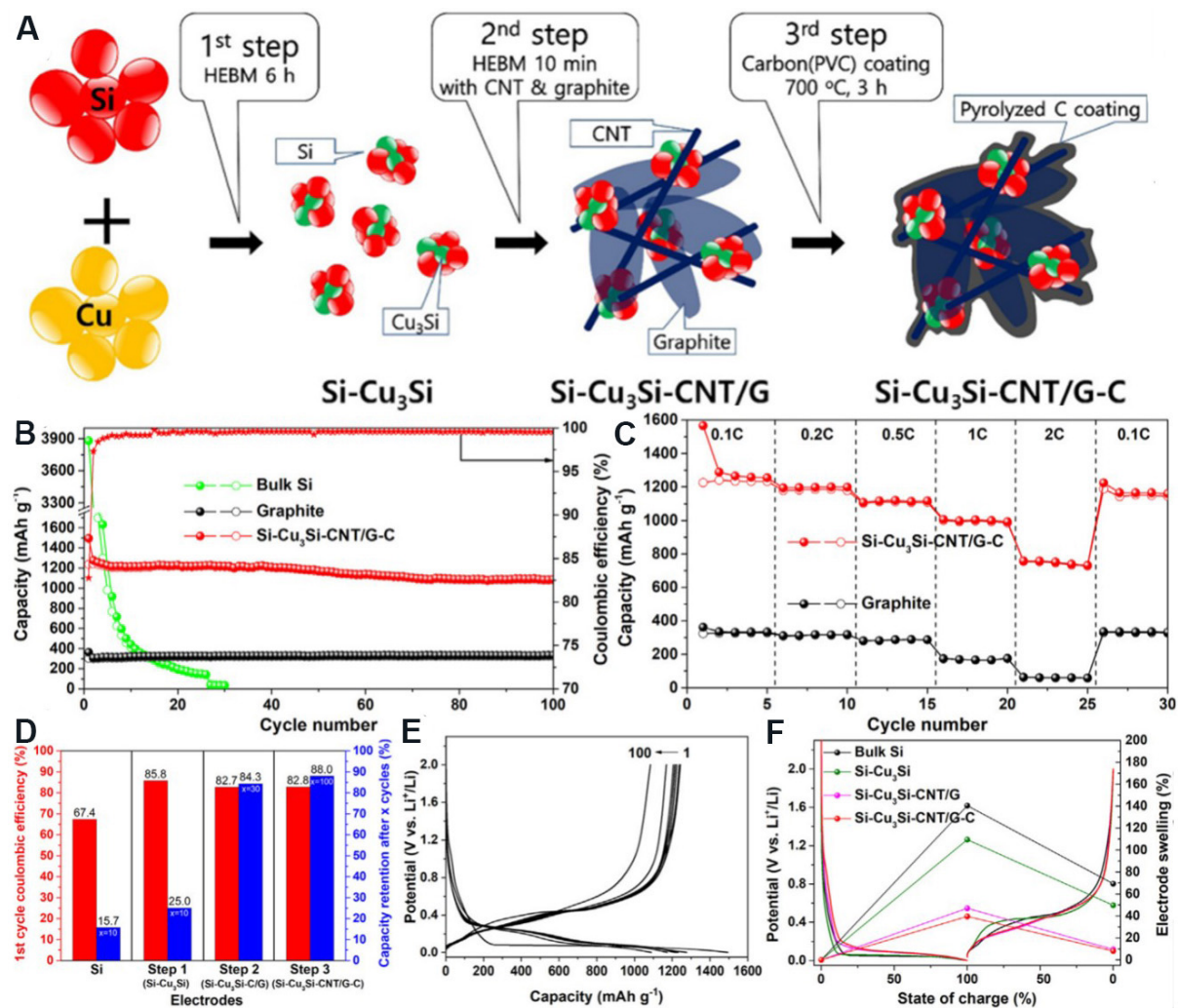


Figure 8. (A) Schematic representation of Si-Cu₃Si-CNT/G-C synthesis. (B) Cycling behavior of graphite, bulk Si and Si-Cu₃Si-CNT/G-C. (C) Rate capabilities of graphite and Si-Cu₃Si-CNT/G-C. (D) ICE and capacity retention for bulk Si, Si-Cu₃Si, Si-Cu₃Si-CNT/G and Si-Cu₃Si-CNT/G-C electrodes. (E) Voltage profiles from 1st to 100th cycle for Si-Cu₃Si-CNT/G-C. (F) Changes to the thickness of bulk Si, Si-Cu₃Si, Si-Cu₃Si-CNT/G and Si-Cu₃Si-CNT/G-C electrodes according to the SOC. Reproduced with permission from Ref.^[143] (Copyright 2020, Chemical Engineering, Elsevier). CNT: Carbon nanotube; HEBM: heat treatment and ball milling; SOC: state of charge.

has better capacity retention [Figure 8D-F]. Figure 8D summarizes bulk Si, Si-Cu₃Si (first preparatory stage), Si-Cu₃Si-CNT/G (second preparatory stage) and Si-Cu₃Si-CNT/G-C (third preparatory stage). After 100 cycles, the ICE of Si-Cu₃Si-CNT/G-C is as high as 82.8%, the value of IRC is 1237 mAh g⁻¹ and the stable capacity retention rate is 88%. All these electrochemical parameters (capacity retention, ICE and IRC) have reached a certain goal of commercialization for high capacity Si-based anodes for LIBs. Figure 8F shows changes in thickness for the Si, Si-Cu₃Si-CNT/G, Si-Cu₃Si and Si-Cu₃Si-CNT/G-C electrodes during the charge/discharge process^[143].

SnO₂ is an excellent semiconductor with high acid/alkali resistance and stability. The capacity of a SnSb nanocomposite was almost twice that of a carbon-based cathode material^[18]. SnO₂ has a high theoretical capacity but its volume expansion and rapid capacity fade during cycling render it unsuitable for LIBs. It has been reported that rGO and fluorine-doped tin oxide nanocomposites (FTO) are ideal anode materials with high rate performance and good capacity and show better structural stability throughout the process of

lithiation and delithiation. Through conductive FTO nanocrystals, a stable and thin solid electrolyte interfacial film can be formed, which has a discharge capacity of 1439 mAh g⁻¹ after 200 cycles at 100 mA g⁻¹^[144].

Plante invented the lead-acid battery in 1859 and it has been extensively used ever since. Lead-acid batteries are a simple technology with low production costs, but they have a limited number of charge/discharge cycles, charge slowly and cannot be completely discharged due to their low energy to weight and volume ratios. A passive layer of lead sulfate is synthesized through the charge/discharge process on the positive electrode surface:



The lead sulfate layer, near the electrode surface, acts as a selective membrane for the diffusion of ions and can pass only ions, such as H⁺ and Pb²⁺. The growth of lead dioxide (PbO₂) is determined by the flux of Pb²⁺ ions. Pb²⁺ ions move by surface diffusion, besides the surface of PbSO₄ crystals to the PbO₂ phase and oxidized there. The electrochemical properties of carbon-based electrode materials can be improved by the modification of their surface with non-carbon-based elements, such as B and N. The presence of non-carbon-based heteroatom functional groups on the carbon surface can increase Li⁺ storage capacity, conductivity and reactivity. N-doped CNFs have an excellent rate capability and high capacity (943 mAh g⁻¹) at 2 A g⁻¹ over 600 cycles^[145].

Despite their widespread usage in mobile and portable electronic devices as a result of their high specific capacity and power density, LIBs can be ignited, especially under extreme conditions, such as crushing, overheating and charging. In order to improve the thermal stability of LIBs, electrochemists have considered the development of nonflammable electrolytes. An effective approach is to add flame retardants directly into standard electrolytes. Phosphite and phosphate are used as flame retardants and show outstanding nonflammability. Among these additives, the compounds of phosphorous(III), such as trimethyl phosphite and tris(2,2,2-trifluoroethyl) phosphite, have more efficient nonflammability and can enhance the electrochemical performance of LIBs compared to subsequent phosphorous(V) compounds^[146].

For the protection of Li anodes, LiPON films represent excellent protective layers for Li secondary batteries. A LiPON layer may be adsorbed on a Li electrode surface using radio frequency sputtering as an amorphous phase. This layer has excellent characteristics as a lithium ionic conductor and electric insulator for protecting the electrode surface from electrolytic decay. Such films are also predicted to be outstanding passive layers to protect the anode surfaces of LIBs. The deposition of a LiPON layer synthesizes a stable solid electrolyte on the lithium anode surface, which effectively decreases the reaction between lithium and the electrolyte (1:1 w/w EC + DEC + 1.0 M LiPF₆). Impedance measurements show that the LiPON layer is a fast ionic conductor compared to the film formed by electrolyte decay^[147]. Triphenylphosphite is also used as a phosphorous additive for LIBs. It can improve the thermal stability of electrolytes (1 M LiPF₆/ethylene carbonate, dimethyl carbonate and diethyl carbonate, 1:1:1 by weight) and provide overcharge safety for LIBs. Recently, it has been suggested that metal phosphides can be used as anode materials for LIBs. Zhao *et al.*^[148] prepared a CuP₂/C composite material with a capacity of 430 mAh g⁻¹ after 30 cycles at 150 mA g⁻¹. Li *et al.*^[149] reported yolk-shell Sn₄P₃/C nanospheres with an excellent capacity of 790 mAh g⁻¹ at 100 mA g⁻¹.

In LIBs, arsenic (As) is the most promising anode material substitute for graphite. A theoretical and experimental approach was used to investigate the electrochemical performance of As/carbon nanocomposite materials for LIBs. The LIBs provided good cycling performance with a promising capacity of 1306 mAh g⁻¹ (over 100 cycles), which is higher than that of Li₃As (1072 mAh g⁻¹)^[150].

Microsized antimony (Sb) can be successfully applied as an electrode material for LIBs and provides a high capacity of 600 mAh g⁻¹ over 160 cycles and a CE of 99%. It delivers 310 mAh g⁻¹ of discharge capacity at a very high current rate of 30 C for LIBs^[151,152]. A SnSb/C nanocomposite material based on a Na alloy electrode can provide a very high capacity (544 mAh g⁻¹, about double that of intercalated carbon materials) and recyclability of Na⁺ storage (80% capacity over 50 cycles)^[153]. However, the poor rate capability and low capacity of existing anodes are major hindrances to future development. The homogenous coating of antimony sulfide (stibnite) on a graphene surface has also been reported, which provides a capacity of 730 mAh g⁻¹ at 50 mA g⁻¹. It also provides a model site for the anchoring of nanoparticles. A study has also shown that a battery made of a stibnite-graphene composite material does not contain Na metal and its energy density is 80 Wh kg⁻¹. This energy density can be optimized over some LIBs^[154].

Bismuth is a promising anode material for LIBs and the theoretical capacity of bismuth oxide (Bi₂O₃) is 690 mAh g⁻¹. Surprisingly, little attention has been paid to Bi₂O₃, Bi₂O₃ nanoparticles with a particle size of ~5 nm were uniformly dispersed on rGO sheets. The nanocomposite Bi₂O₃/rGO enhances cycling stability and electrochemical reversibility compared to agglomerated bare Bi₂O₃ nanoparticles. This Bi₂O₃/rGO anode material can provide an excellent rate capability of 270 mAh g⁻¹ at a high current rate of 10 C and an initial capacity of 900 mAh g⁻¹ at 0.1 C [Figure 9A]. Over 100 cycles at 1 C, the capacity of the Bi₂O₃/rGO anode material is maintained at 347.3 mAh g⁻¹ and its capacity retention rate is 79% [Figure 9B]. The diffusion coefficient of Li⁺ is ~10⁻¹⁵-10⁻¹⁶ cm² S⁻¹ during the lithiation/delithiation of Bi₂O₃/rGO nanocomposites^[23].

The specific initial charge/discharge capacity of bare Bi₂S₃ is 598 and 921 mAh g⁻¹, respectively. The charge/discharge capacity of a Bi₂S₃/rGO composite at 100 mA g⁻¹ is 685 and 1004 mAh g⁻¹, which is 14.5% and 9.0% higher than that of Bi₂S₃, respectively. The retention rate of the capacity of Bi₂S₃ is only 0.4% (4 mAh g⁻¹) after 50 cycles, far less than that of Bi₂S₃/rGO [11.9%, (110 mAh g⁻¹)]. These results show that graphene not only increases the electrochemical activity of the whole electrode but also greatly improves the conductivity of Bi₂S₃ during cycling^[155]. The layered structure of Bi₂S₃ also provides host sites for the insertion of Na ions. CNTs play a role in promoting the high conductivity network of electron transport in Bi₂S₃/CNT nanocomposites. The results exhibit that Bi₂S₃/CNT nanocomposites have a stable capacity in the range of 0.01-3.0 V (vs. Na/Na⁺), particularly better than bare Bi₂S₃ materials^[156]. Bismuth directly developed on nickel foam (p-Bi₂O₃/Ni) has excellent electrochemical properties compared with Bi₂O₃ powder (p-Bi₂O₃) prepared by a polymer-assisted solution and commercial Bi₂O₃ (c-Bi₂O₃). The capacity of p-Bi₂O₃/Ni was maintained at 782 mAh g⁻¹ over 40 cycles at 800 mA g⁻¹^[157].

Of the chalcogens, S as a cathode material for lithium-sulfur batteries has been widely studied because of its low cost and high theoretical gravimetric energy density of 2570 Wh kg⁻¹. By the one-electron transfer method, synthesizing LiO₂ by absorbing oxygen on the surface of Li was proposed to reduce the oxygen content of Li and then one electron reduction to form Li₂O₂ (solid). It is also proposed that LiO₂ can chemically decompose to Li₂O₂ and O₂. Furthermore, Li₂O₂ is reduced to LiO₂ in the discharge potential range of Li-O₂ batteries (2.8-2.0 V Li). The specific capacities of Li-air batteries are dominated due to the electrode porosity required for the storage of Li₂O_x and by the diffusion of oxygen through the pores of flooded electrolytes. Therefore, using electrolytes with high oxygen solubility and oxygen pressure enhances

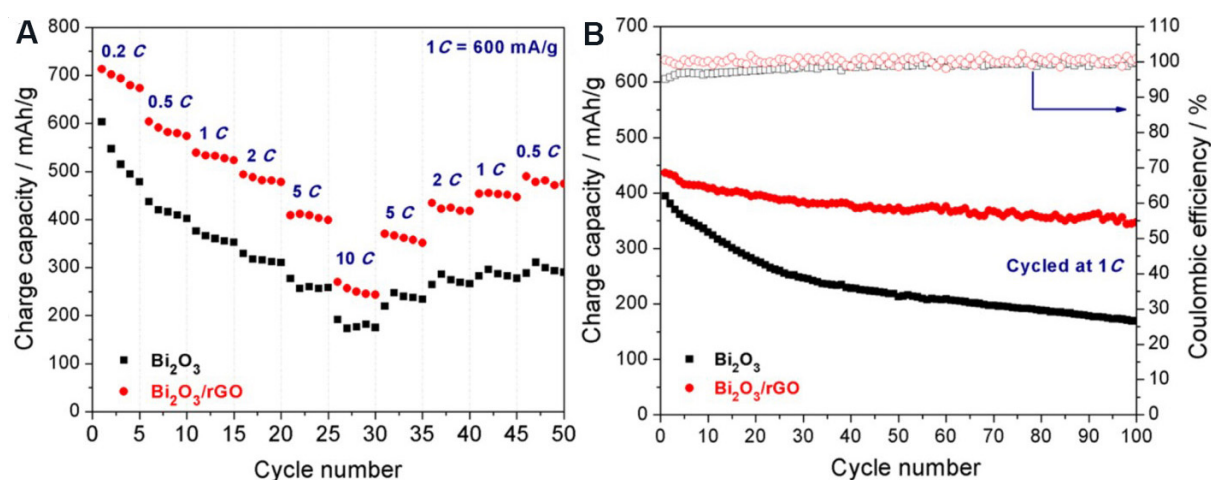


Figure 9. (A) Rate and (B) cycling performance of Bi₂O₃ and Bi₂O₃/rGO anode materials at 0.01-3.0 V vs. Li/Li⁺. Reproduced with permission from Ref. [23] (Copyright 2017, American Chemical Society).

the specific activity. Usually, the reported specific capacities for carbon-based Li-air cathodes are 2500-5000 mAh g⁻¹. Pt/C is a useful catalyst for the charging of LiO₂ batteries and it provides one of the lowest charging voltages (3.8 V Li at 250 mA g⁻¹)^[158].

Li-S batteries are extremely promising for future two-electron reaction energy storage systems. Li-S has a capacity of 1675 mAh g⁻¹, which is much greater than typical LIBs (387 Wh kg⁻¹). Furthermore, elemental sulfur has other advantages, such as its abundance in nature and low environmental pollution and cost. However, there are many barriers to improving Li-S batteries, including the dissolution of polysulfides in the liquid electrolyte and reaction of intermediates with the Li anode in the electrolyte, leading to the migration of low-order polysulfides towards the cathode and the “shuttle effect”. The slow decay of active S from the cathode into the electrolytic solution and onto the Li metal anode also results in “shuttle reactions”, severe degradation of cycle life, low Coulombic efficiency, low utilization of the cathode, self-discharge, poor conductivity of S and a large expansion in volume (80%) from S to Li₂S after lithiation, resulting in rapid capacity decay and instability of the cathode.

Extensive research attempts have been devoted to resolving these challenges. Chen *et al.*^[159] successfully anchored S nanoparticles on the surface of multiwalled CNTs to improve the sulfur cycling performance. The capacities of the S/C nanocomposites were increased up to 1000 mAh g⁻¹, depending on the content of S in the composite material. Ji *et al.*^[160] noted that mesoporous carbon/sulfur nanofillers had a specific capacity of up to 1300 mAh g⁻¹. Carbon enhances the electrical contact between the carbon matrix and insulating sulfur particles and decreases the solubility of the polysulfides by anchoring the sulfur particles on some supports. However, the manufacturing procedure of these composite materials is complicated. Xiao *et al.*^[161] stated that MoS₂ may reduce to Li₂S and Mo at 0.01 V (vs. Li⁺/Li).

However, it has been experimentally clarified that the Li storage process of a fully discharged MoS₂/Li cell estimates the feasibility of applying Li₂S as a cathode active material with carbonate-based electrolytes in Li-S batteries^[162]. Therefore, Li-S batteries undergo rapid capacity decay and low Coulombic efficiency, thereby hindering the commercialization of S cathodes. The polar oxygen-containing functional groups in graphene oxide nanosheets are eliminated by microwave irradiation. S₂O₃²⁻ ions are reduced to nanostructures by HCl treatment after adding Na₂S₂O₃ into the suspension of irradiated GO. The mixture of GOF/nano-S is evenly

dispersed in a VC-Na solution and heated for 3 h at 95 °C to obtain the mixture of rGOF/nano-S, as given in Figure 10A. When the specific capacity of rGOF/nano-S hybrids ($\sim 886 \text{ mAh g}^{-1}$) is compared with rGO/nano-S (612 mAh g^{-1}), it is again proved that the sulfur utilization ratio of the rGOF/nano-S hybrid structure at 0.1 C is better than that of the rGO/nano-S structure. In addition, the rate performance [Figure 10B] shows that when the discharge rate is raised from 0.1 to 2.0 C, the discharge capacity of the rGO/nano-S hybrid material is still greater than 531 mAh g^{-1} (61%). Figure 10C compares the cycling performance of the rGOF/nano-S and rGO/nano-S hybrid cathodes. The initial specific capacity of the rGO/nano-S cathode is 598 mAh g^{-1} and it remains 408 mAh g^{-1} (68.3%) over 800 cycles, showing that the capacity of each cycle decreases by 0.04%. In contrast, despite the high initial capacity (590 mAh g^{-1}) of the rGO/nano-S hybrids, their capacity is rapidly reduced to 181 mAh g^{-1} over 800 cycles and the capacity of each cycle is decreased by 0.09%. This capacity decay is equivalent to the reported values in the literature^[163].

Like sulfur, selenium is also a chalcogen and may become a candidate material for cathodes in the future. The theoretical gravimetric capacity of Se is 675 mAh g^{-1} , which is lower than S (1675 mAh g^{-1}), but its high density (2.5 times that of S) contributes to a higher theoretical capacity density (3253 mAh cm^{-3}), which is almost equal to S (3467 mAh cm^{-3}). Li-Se batteries have better output voltage and volumetric energy density. Volumetric energy is far most significant than gravimetric energy in portable devices due to its limited battery packaging space. Furthermore, the conductivity of Se (1103 S m^{-1}) is better than S (51028 S m^{-1}), which indicates that Se has good electrochemical activity, a high utilization rate and fast electrochemical reaction with Li. Therefore, Se is believed to be a promising material for the manufacturing of high-energy batteries for transportation and household appliances. Cui *et al.*^[164] recently used Se as a cathode material and noted that the consumption of active substances in bulk Se is 20.45%. This phenomenon is generally not observed in Li-S batteries. Se has higher electrochemical activity and a weak shuttle effect compared to S. However, the synthesis of polyselenide during charge and discharge, weakens the interaction between the conductive substrate and Se, which leads to the shuttle effect and fades the cycling performance of the cathode and as a result, the full theoretical capacity of bulk Se cannot be achieved. This problem can be solved by using a porous conductive carbon matrix.

A Se composite containing only mesoporous carbon cyclic Se_8 molecules (CMK-3) has been synthesized. XRD and Raman spectroscopic analysis show that it is because of the conversion of cyclic Se_8 into Se_n on the carbon channel. Due to the strong attraction between carbon mesopores and Se_n , Se_n has high electrochemical performance. As a result, the cathode of Se gives a better capacity, close to the theoretical capacity of Se and maintains cycling stability^[165]. The Se/CMK-3 cathode provides an excellent reversible discharge capacity ($\sim 600 \text{ mAh g}^{-1}$) over 50 cycles. The unique arrangement of Se molecules restrained in a matrix of mesoporous carbon decreases the shuttle effect and gives excellent cycling performance, high volumetric energy density and better conductivity for LIBs^[165]. It gives a reversible capacity of 516 and 306 mAh g^{-1} for LIBs over 900 cycles at 0.5 and 4 A g^{-1} , respectively.

A flexible Se/porous carbon nanofiber composite material (Se/PCNFs) was synthesized by infiltrating Se into the pores of CNFs and gave a reversible capacity of 516 mAh g^{-1} at 0.05 A g^{-1} over 900 cycles and 306 mAh g^{-1} at 4 A g^{-1} . The uniform distribution of Se in the three-dimensional PCNF framework reduces the shuttle effect of polyselenide in the cycling process and gives excellent conductivity, a better rate capability, high capacity and good cycling stability^[166]. Se has higher electrical conductivity ($1 \times 10^{-3} \text{ Sm}^{-1}$) than S ($5 \times 10^{-28} \text{ S m}^{-1}$), which has led to Li-Se batteries receiving significant attention in recent years. It should be emphasized that Se is the neighbor of S in the periodic table, which makes them very similar in many properties. Thus, the general problems of Li-S batteries also exist for Li-Se batteries, but the Se advantages can make this kind of rechargeable batteries more useful. Nevertheless, the key focus remains on

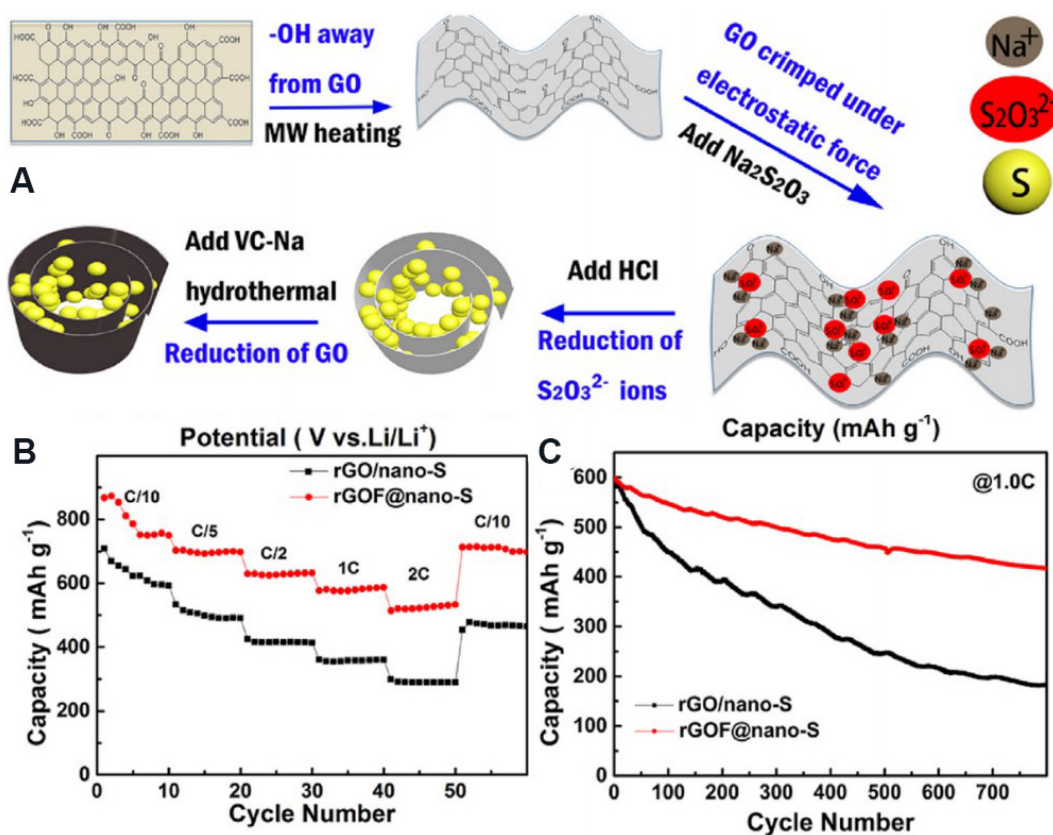


Figure 10. (A) Schematic representation of the synthesis of rGOF/nano-S hybrids. (B) Rate capabilities and (C) cycling performance of rGOF/nano-S and rGO/nano-S. Reproduced with permission from Ref.^[163] (Copyright 2019, Electrochimica Acta, Elsevier).

Li-S batteries. There are some unique properties of Li-Se batteries that require special attention. Se is much more expensive than S and its specific energy is less, but its invaluable advantages make it an attractive option compared to S^[167].

Te is in the same group as O, S and Se. A Te/C composite was prepared by injecting liquid Te into the pores of porous carbon at 600 °C. The Te/C electrode material can provide 1400 mAh cm⁻³ (224 mAh g⁻¹), a high reversible capacity at 312 mAh cm⁻³ and maintain 87% capacity over 1000 cycles. If the current is enhanced by 12,480 mA cm⁻³ (2000 A g⁻¹), the electrode can provide 500 mAh cm⁻³ capacity. Te/C is a promising electrode material for LIBs^[168]. rGO has excellent flexibility, can be used to construct highly conductive 3D skeletons and can be used in binder-free self-supporting lithium tellurium (Li-Te) batteries with excellent electrochemical performance to obtain rich porous cathode materials. The initial capacity of a 0.2 C Li-Te cathode material was 2611 mAh cm⁻³ and the retention rate over 200 cycles was as high as 88%, with a rate capacity at 10 C of 1083 mAh cm⁻³. After 500 cycles, the 3D aerogel cathode maintained a capacity of 1685 mAh cm⁻³ at 1 C and exhibited long-cycling performance at high current density. Because of these useful properties, the stated 3D rGO/Te nanowire aerogel has potential applications and can be utilized as a high-performance cathode for Li-Te batteries^[169].

Since it is complicated to use F₂ gas as a cathode material, various fluorides, chlorides, sulfides and oxides have been examined. Subsequently, it was found that graphite fluoride is the most excellent cathode material for a primary LIB. The first Li/(CF)_n battery was commercialized by Matsushita Battery Co., Ltd. in

1973 in Japan. It was noticed in 1980 that fluorine is absorbed into graphite at room temperature and a fluorine-graphite intercalation compound was synthesized as a result. This material is an electric conductor and is significantly different from graphite fluoride, which was applied to a new graphite anode material using KF_2HF for the electrolytic production of F_2 gas^[170]. The wettability of KF_2HF melt with carbon anode is therefore reduced with increasing CF film having a low surface energy, which result in abrupt decrease in electrolytic current and simultaneously increase in cell potential. This phenomenon is known as the “anode effect”. As a result of the “anodic effect”, a spark or arc is observed between the cathode and anode and electrolysis cannot be sustained. Carbon materials react with F_2 gas giving several different side products (CF , C_2F , CF_4 and C_2F_6) depending on the crystalline nature of the raw carbon materials and reaction temperature^[170].

We can also use graphite oxide for smooth discharge but it is difficult due to the reaction products, such as LiOH and Li_2O , which are not as stable as LiF . It gives a low discharge capacity because the diffusion of Li^+ ions in graphite oxide is slow. However, the discharge properties can be modified by the fluorination of graphite oxide at low temperatures between 100-150 °C. The discharge capacity of fluorinated graphite oxides is similar to those of $(\text{CF})_n$ samples. C_xF synthesized at room temperature contains C-F covalent bonds and works as a cathode material in primary LIBs. It gives a higher discharge potential capacity but the current is reduced^[170]. $\text{Li}/(\text{CF})_n$ batteries have a long life and high stability because graphite fluoride cathode materials are stable compounds under extreme conditions. Organofluorine compounds have much higher stability against the reactions with Li and electrochemical oxidation, effectively enhancing the safety of LIBs^[170]. F- SnO_2 nanoparticles were anchored uniformly on the sheets of rGO by a hydrothermal process. The load of F- SnO_2 in the composite (F- SnO_2 /rGO) was high (~90%). The diffusion and conductivity of Li^+ in the electrode are improved by doping F with rGO, which enhances the rate performance, long-term cycling stability and reversible capacity of the composite material. The electrode provides a reversible capacity of 860 and 770 mAh g^{-1} at 1 and 2 A g^{-1} , respectively, over 150 cycles. Furthermore, over 250 cycles at 500 mA g^{-1} , the electrode can maintain a high reversible capacity of 733 mAh g^{-1} . The composite has excellent electrochemical properties and can be used as a high-energy LIB anode material^[171].

Tin oxide (SnO_2) has a high theoretical capacity; however, its fast fading capability during cycling causes volume expansion, which prohibits its practical application in LIBs. However, if a FTO nanocomposite is used with rGO as an anode active material, it gives a high stability, rate capability and capacity. The composite material (FTO/rGO) has high structural stability through the processes of lithiation and delithiation. The nanocrystals of FTO are conductive and conducive to the synthesis of a stable and solid film of electrolytes. The FTO/rGO composite at a current density of 100 mA g^{-1} provides a discharge capacity of 1439 mAh g^{-1} and at a current density of 1000 mA g^{-1} , provides a rate capacity of 1148 mAh g^{-1} after 200 cycles^[144]. Polyvinylidene fluoride and polyvinyl alcohol were also examined as potential binding materials for the Li, Na, K, Zn, Al and Ag_2O electrodes.

Like F, Cl is also a gas and cannot be used directly. It is instead used in the form of compounds. Polyaniline can be prepared by a usual chemical oxidation method and then the hydrogen atom on the six-membered ring was replaced by HCl. As a result, polyaniline chloride was produced for high-energy secondary LIBs as a cathode material. A button-type battery was prepared and examined through a charge/discharge test, which shows an excellent initial discharge capacity of ~980 mAh g^{-1} ^[172].

D-block elements (transition metals)

Transition metal oxides with different oxidation states are promising energy storage materials for supercapacitors and batteries. Fast surface redox storage (pseudocapacitive) techniques can allow devices to

store far more energy than electrical double-layer capacitors (EDLCs). However, due to their low inherent electrical and ionic conductivity, only a few pseudocapacitive transition metal oxides can deliver significant power.

Scandium (Sc) is the first member of the first transition series. Alloys comprising Sc and Mg have showed a very promising storage capacity of 1500 mAh g⁻¹, which is four times that of metal-based materials. Palladium-capped thin films of Mg_xSc_(1-x) with different concentrations (x = 0.50-0.90) enhance the hydrogen storage capacity by 5%-20% compared to their bulk materials, even using higher discharge rates^[173]. Li₃Sc₂(PO₄)₃ is a promising electrolyte for Li rechargeable micro-batteries due to its resistance to dielectric breakdown, ease of preparation and stability in air. The formation of Li₃(Sc_{2-x}M_x)(PO₄)₃ (M = Y³⁺ or Al³⁺) resulted in a considerable improvement in ionic conductivity, greater sinterability and a decrease of porosity. Li₃Sc₂(PO₄)₃ is yielded by the electron beam evaporation of amorphous thin films of Li_{4.8}Sc_{1.4}(PO₄)₃ with high ionic conductivity (5 × 10⁻⁵ S cm⁻¹)^[174].

Among all anode materials, TiO₂ has the advantages of a comparatively high working voltage (1.5 V vs. Li⁺/Li) and extremely small volume change (< 4%), making it a promising electrode material. The small volume change, high working voltage and excellent long-term cycling stability avoid the synthesis of the solid electrolyte interface layer (SEI) and a lower irreversible capacity. The anatase form of TiO₂ has a theoretical capacity of 335 mAh g⁻¹; however, its poor ionic and electronic conductivity fade its rate performance and cycling stability. The use of specific facets, namely, (001), (101) or (010), for Ti³⁺ carbon coupling and doping (reduction or hydrogenation by Mg) is a useful method for overcoming the above obstacles because these methods can provide greater electronic conductivity and shorter ion diffusion pathways.

In particular, a number of excellent studies have been carried out on TiO₂/MXene, TiO₂/graphene and TiO₂/C^[175]. The typical charge/discharge curves of graphene/Si, TiO₂/graphene/Si, TiO₂/graphene/SiNW, TiO₂/graphene/Ag/SiNW and TiO₂/N-graphene/Ag/SiNW nanocomposites show discharge capacities of 333.5, 525.9, 693.1, 836.7 and 966.1 mAh g⁻¹, respectively, as presented in **Figure 11A**. The high Li storage capacity of TiO₂/N-graphene/Ag/SiNWs is due to the high specific surface area of the SiNWs and the high conductivity of graphene. The rate capabilities of the graphene/Si, TiO₂/graphene/Si, TiO₂/graphene/SiNW, TiO₂/graphene/Ag/SiNW and TiO₂/N-graphene/Ag/SiNW nanocomposites at different current rates are given in **Figure 11B**. As the current rate increased to 5 A g⁻¹, the specific capacity of the TiO₂/N-graphene/Ag/SiNW electrode decreased slowly, showing the highest specific capacity. The TiO₂/N-graphene/Ag/SiNW electrode had a high specific surface area, conductivity and mesoporosity. **Figure 11C** shows that all the EIS curves include semicircles in the range of high-frequency lines to the low-frequency range, which are fixed at a constant angle to the actual axis. The semicircle diameter of the TiO₂/N-graphene/Ag/SiNWs is much smaller than that of other semicircles, indicating that the TiO₂/N-graphene/Ag/SiNWs have interfacial and charge transfer resistance between the three electrodes. This is because N-graphene/Ag substantially increases the electronic transport and its hollow structure enhances the ionic conductivity^[176].

Vanadium pentoxide (V₂O₅) is a potential cathode material with the advantages of rich reserves, high energy density, low costs and easy preparation. The theoretical capacity of V₂O₅ at 2-4 V is ~294 mAh g⁻¹, which is superior to the conventional cathode materials LiFePO₄ (176 mAh g⁻¹) and LiMn₂O₄ (148 mAh g⁻¹). Regardless of these advantages, the electrochemical performance of V₂O₅ is restricted by its sluggish diffusion of Li ions (~10-12 cm² S⁻¹) and its poor electrical conductivity (10⁻³ to 10⁻² S cm⁻¹). Moreover, the phase transitions of Li_xV₂O₅ during the charge/discharge process regularly cause structural instability and can decrease its cycling performance. These shortcomings have limited the practical application of V₂O₅ in

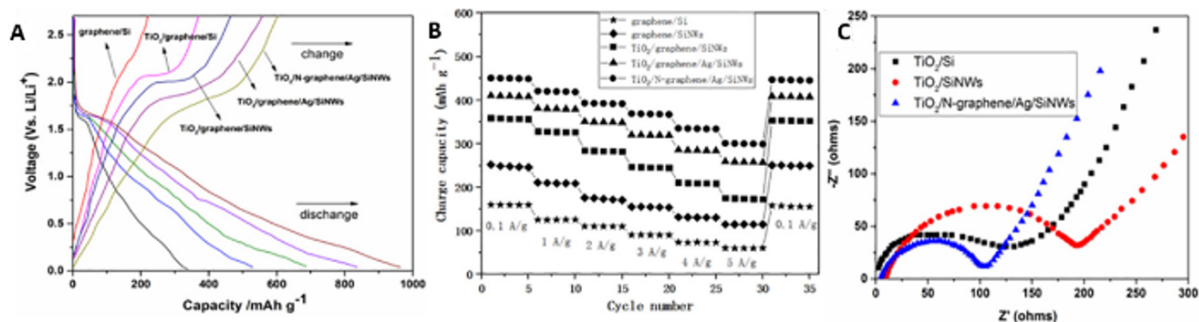


Figure 11. (A) Charge/discharge profiles, (B) comparison of rate capability and (C) EIS analysis of graphene/Si, TiO₂/graphene/Si, TiO₂/graphene/SiNW, TiO₂/graphene/Ag/SiNW and TiO₂/N-graphene/Ag/SiNW electrodes. Reproduced with permission from Ref. [176] (Copyright 2019, Materials Letters, Elsevier).

commercial LIBs^[177]. Ag_xV₂O₅ shows higher discharge capacities, which seem to be credited to the higher diffusion of Li⁺ in Ag-doped V₂O₅ compared to bare V₂O₅ thin-film cathode materials. The poor discharge capacity of Ag_{1.8}V₂O₅ films seems to be due to the cauliflower-like structure of the films. All thin-film solid-state batteries showed excellent reversibility up to 200 cycles. The energy density of the material is relatively low at ~40 Wh kg⁻¹; however, recent research showed that a modified electrolyte solution produces a 70% enhancement in energy density^[178].

The most important benefit of vanadium redox batteries (VRBs) is that it can be charged only by changing the electrolyte and can provide unlimited capacity by using a large storage tank. If the electrolyte is accidentally mixed, the battery will not be permanently damaged and it can be left uncharged for long periods without any effects. The disadvantage of VRBs is that compared with standard batteries, they are complex and their energy volume ratio is relatively low^[178]. Ti₃C₂ MXenes provide a capacity of 410 mAh g⁻¹ for LIBs. Interestingly, the capacity of MXenes can be as high as 800 mAh g⁻¹ after intercalation with different cations, such as Sn⁴⁺, NH₄⁺ and Al³⁺. Compared with the Ti₃C₂ MXene, the V₂C MXene with a smaller molecular weight can obtain a higher theoretical LIB capacity of 940 mAh g⁻¹. Unfortunately, the experimental capacity of V₂C MXene is 260 mAh g⁻¹ at 1 C, which is very far from the theoretical value. Recently, it has been found that the V₂C MXene with Co ion intercalation can provide a 1100 mAh g⁻¹ Li⁺ storage capacity and better cycling stability^[179].

The Ragone diagram in Figure 12A gives the relationship between the density of power and energy for vanadium oxide with different Na, Ca, Zn and H₂O interlayer ions and molecules, as well as materials other than vanadium oxide, such as Na₂V₂(PO)₂F₃/C, VS₂ and Z_nHCF. Compared with Zn_{0.25}V₂O₅ in the low power range and Ca_{0.25}V₂O₅ in the high power range, VONTs provide balanced power and energy density with superior performance in ZIBs. VONTs have a wider working voltage, high discharge capacity and better stability against over-discharge. In addition, the cathode also provides a relatively high discharge capacity between the comparative materials. These cathodes at different current densities of 0.3 A g⁻¹ (1 C), 0.6 A g⁻¹ (2.1 C), 1.2 A g⁻¹ (4.7 C), 2.4 A g⁻¹ (11 C), 4.8 A g⁻¹ (30.5 C), 7.2 A g⁻¹ (60 C) and 9.6 A g⁻¹ (109 C) retain specific capacities of 94.5%, 89.2%, 81.7%, 69.1%, 50%, 38% and 27.9%, respectively, as shown in Figure 12B. The battery was tested at 0.3 and 0.1 A g⁻¹ and the discharge capacity recovered to 296 and 309 mAh g⁻¹, respectively. As presented in Figure 12D, the cathode is activated for the first four cycles at 0.1 A g⁻¹ to obtain the CV data. In this process, the CE slowly increased to 99.8% (the sixth cycle). The capacity retention rate of the cathode is 80.5% after 950 cycles at 2.4 A g⁻¹, while the CE is close to 100% in all cycles, which shows that a minimal decrease in capacity produces outstanding durability under strong current fluctuation, as shown in Figure 12C. The reduction peaks shifted to a higher voltage and then stabilized at

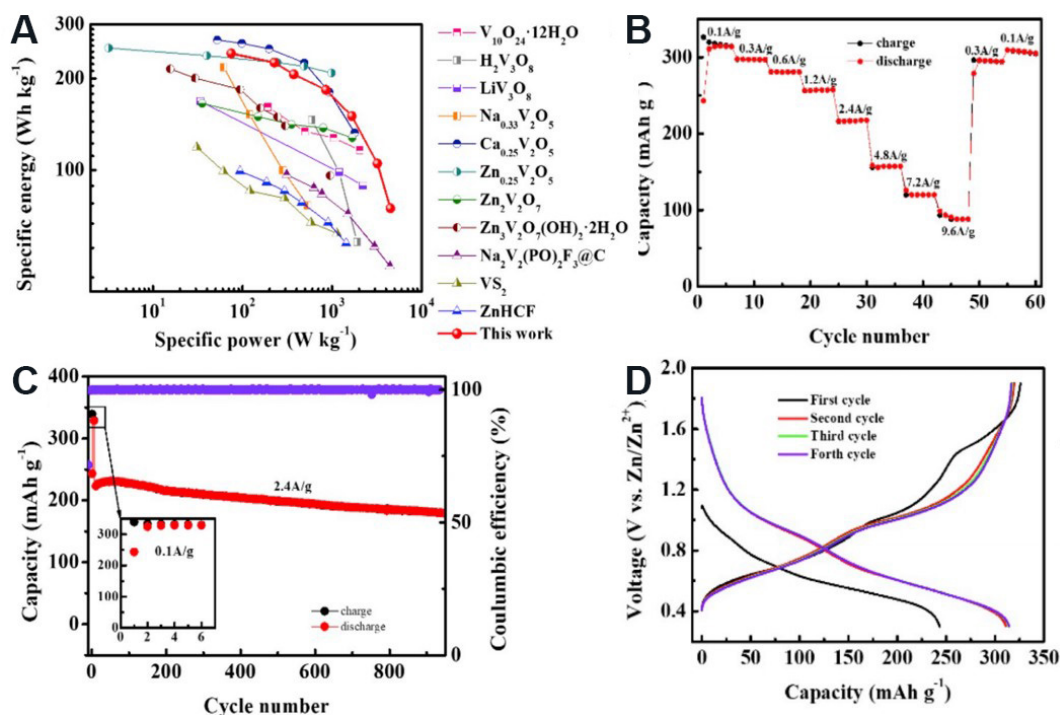


Figure 12. Electrochemical performance of coin cells with VONTs as cathode and Zn as anode in the range of 0.3–1.9 V vs. Zn/Zn²⁺: (A) Ragone plot of different materials; (B) rate performance at current densities from 0.1 to 9.6 A g⁻¹; (C) charge/discharge curves; (D) cycling performance at a current density of 2.4 A g⁻¹. Reproduced with permission from Ref.^[180] (Copyright 2019, Journal of Power Sources, Elsevier). VONTs: Vanadium oxide nanotubes.

0.419 and 0.815 V, while the two oxidation peaks moved to the lower position and then stabilized at 0.736 and 1.1 V, which proves that the change of peak value decreases with increasing cycling. The curve of the fourth cycle almost coincides with the curve of the third period. These phenomena show that the decrease of overpotential and enhancement of cycling stability are highly consistent with the curves of galvanostatic charge/discharge, as given in Figure 12D^[180].

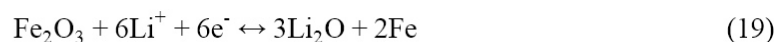
A comprehensive comparison, including cycle and charge/discharge tests and capital cost analyses, was provided for vanadium redox flow batteries (VRFBs) and iron-chromium redox flow batteries (ICRFBs). ICRFBs show similar energy efficiency with VRFBs at high current densities. Energy efficiencies of 78.4% and 80.3% can be achieved for ICRFBs and VRFBs at 120 mA cm², respectively. Through the cycle test, the efficiencies of both RFBs were stable^[181].

Manganese (Mn) can be reduced from Mn(IV) to Mn(II), which allows for full lithiation and gives Li₂MnSiO₄, which may allow two Li-ion insertions/extractions for each transition metal and provides a theoretical capacity of 330 mAh g⁻¹^[19]. It is reported that the capacity of a Na_{0.85}Li_{0.17}Ni_{0.21}Mn_{0.64}O₂ cathode material is 95 mAh g⁻¹ and it has better withholding capacity over 50 cycles. A single-crystal Na₄Mn₉O₁₈ (orthogonal lattice structure) nanowire material with a capacity of 128 mAh g⁻¹ and a cycling stability of more than 1000 times was also reported^[182].

Iron batteries have sufficient capabilities for commercial use in low-power projects and devices. The internal resistance of iron cells is high and therefore their discharge rate is limited. Poor transfer charge rates from the electrode of carbon to the Fe³⁺ in the cathode is because of the poor electrical conductivity of

the electrolyte, poor ionic conductivity of the membrane and poor electrical contact among the components are several probable reasons for high resistance^[183]. Iron batteries can oxidize Fe(II) to Fe(III) at the cathode and store energy by reducing Fe(II) to Fe(0) at the anode. Iron cells are non-toxic, efficient, highly stable and safe. Iron batteries have lower specific energy than commercial batteries but give the opportunity for safe handling and low-cost raw materials. Metal hydrides and Li are flammable, toxic, react strongly with water and oxidize in air. Iron is relatively non-toxic and is only marginally reactive with air and water (i.e., rust formation). Iron with sulfate solution is reliable and represents stable salt chemistry for all-iron batteries. As saturated potassium sulfate solution is mixed with iron chloride and the pH was adjusted to obtain the anodic electrolyte (iron(II) chloride), which is used as a cathode electrolyte^[184]. Although iron(IV) can be easily synthesized, the safety concerns related to the high oxidation state, which prohibit its use. Other iron salt solutions were also examined, including solutions containing fructose, sucrose, ferric cyanide and EDTA. In solution, these unconventional systems exhibit similar behavior but the sulfate precursor exhibits the best Coulombic capacity. While using sulfate solution, less amount of iron is lost from the bulk of the metallic iron electrode over the charge/discharge process. During the reaction, the iron anode is oxidized, liberating electrons at the cathode^[185].

Iron oxides, especially Fe₃O₄ and Fe₂O₃, have attracted significant attention because of their high abundance, low processing costs, excellent theoretical capacity (~1000 mAh g⁻¹), strong corrosion resistance, non-toxicity and other advantages. High Li insertion potential and the good safety protection of non-flammability in large-scale applications are further advantages of iron oxide-based anode materials. The storage mechanism of iron oxide for Li depends on the redox reaction, i.e., the reduction of Fe₂O₃ to metal nanoclusters dispersed in the Li₂O matrix and then the reduction to the initial oxidation state in the process of delithiation. The reaction mechanism of Fe₂O₃ with Li⁺ is given by:



The oxidation of Fe⁰ to Fe³⁺ gives three electrons, resulting in a high theoretical capacity for Li storage and is thermodynamically possible as shown in the above forward reaction. However, it seems that it is not feasible in thermodynamics to extract Li⁺ from the Li₂O matrix. In addition, the cyclability of iron oxides is poor because of the drastic volume decrease during cycling and has low conductivity, especially at high current density^[186]. A 3DG/Fe₂O₃ free-standing mechanical press was used to study the LIBs. The results show that the press has an excellent performance of 1129 mAh g⁻¹ 2022/1/11at 0.2 A g⁻¹ and excellent cycling stability over 130 cycles, while the capacity retention is 98% over 1200 cycles at 5 A g⁻¹^[187]. The direct anchoring of continuous MIO nanofilms on the surface of graphene nanosheets (GNSs) as LIB anode materials via an *in situ* thermal decomposition method was examined and the shrinking effect of the GNSs on the change of volume of MIO at the molecular level was reported. The MIO/GNS nanocomposite has an outstanding specific capacity of ~1000 mAh g⁻¹ at 100 mA g⁻¹ and there is no capacity attenuation even over 400 cycles at 1000 mA g⁻¹. This outstanding cycling performance is credited to the superior strain hosting capability of the MIO/GNS nanocomposite^[188].

From a comparison of the cycling properties of Fe₃O₄-NP/G and Fe₃O₄-NS/G composites at 0.2 C for 160 cycles, the reversible capacity of the Fe₃O₄-NS/G composite was maintained at 1025 mAh g⁻¹ for 50 cycles and then decreased to 920 mAh g⁻¹ for 100 cycles. It then began to increase, reaching 1070 mAh g⁻¹ again after 160 cycles. In contrast, the reversible capacity of the Fe₃O₄-NP/G composite rapidly decreased to 460 mAh g⁻¹ after 50 cycles and then increased to 860 mAh g⁻¹ after 160 cycles. For different nanostructured metal oxide electrodes, the capacity increased over a long cycle and it is believed that the irreversible partial reactivation of Li₂O synthesized in the early cycle is due to the electrochemical grinding effect^[189,190].

Spherical Fe/AuNPs were uniformly dispersed on the surface of rGO sheets. It was proved that the Fe/AuNPs-AETrGO composite has a high specific gravity of 1500 mAh g⁻¹ and a high long-term cycling stability. The improved electrochemical performance of the Fe/AgNPs-AETrGO composite material is credited to the small size and uniform distribution of Fe/AgNPs on rGO sheets^[191]. Co-B and Fe-B alloys examined as anode materials give a reversible capacity of 1100 and 1200 mAh g⁻¹, respectively, at 100 mA g⁻¹. The outstanding high capacities of Co-B and Fe-B anodes are due to the activation of B atoms inside the matrix of transition metal atoms and the negative electrode potential of B prevents the transition metals from passivation^[128]. The charge/discharge capacity of Fe₃O₄/rGO (849.6 mAh g⁻¹) is greater than pristine Fe₃O₄ and rGO, which may be due to the crystalline nature of Fe₃O₄ after calcination and the high conductivity of GO. The capacity of the Fe₃O₄/rGO battery decreased sharply during initial cycles and then increased gradually. This was attributed to the reversible formation of polymer gel films, which have the additional reversible capacity for the first few cycles, as shown in [Figure 13A](#) and [B](#). The rate performance of Fe₃O₄/rGO was measured at various current densities, i.e., 0.05, 0.1, 0.2, 0.5, 1.0, 2.0 and 5.0 A g⁻¹, and gave specific discharge capacities of 1188, 1086, 1011, 903, 811, 718 and 593 mAh g⁻¹, as shown in [Figure 13C](#). [Figure 13D](#) shows the charge/discharge curves of the Fe₃O₄/rGO anodes examined at various current densities. The insertion/extraction of Li⁺ is reversible due to the approximate symmetric shape of the curves^[190].

Today, cobalt (Co) is a very popular metal in the field of energy storage and materials science and is used in most commercial LIBs but it comes at a high price. LiCoO₂ is the most effective commercial cathode material. In the literature, several examples of N-doped carbon coating composites of Co₃O₄ have been reported^[192]. Co has received much attention in the field of energy storage because of its high energy density and thermal stability. Cathodes made with Co cannot catch fire on overheating, which is the main safety issue. Co used in ultrafine amorphous alloy powders (Co-B and Fe-B) as an anodic material show better electrochemical performance than pristine elements when used as an aqueous alkaline solutions for anodic materials. The discharge capacities of Co-B and Fe-B electrodes are 1100 and 1200 mAh g⁻¹ at 100 mA g⁻¹, respectively. It has been noted that the outstanding capacities of these alloys are because of the activation of B atoms in the extremely dispersed transition atoms. The B atoms hold the electrode potential to a negative side to avoid the transition atoms from passivation^[128]. It is particularly attractive in several different cathode materials of rich nickel (LiNi_xCo_yMn_zO₂), which provide a capacity of 195 mAh g⁻¹ with high capacity retention, making them ideal material for electric vehicles, although some problems limit the performance of the materials with increasing Ni content^[193].

Metal-organic frameworks and coordination polymers have high porosity, excellent composite properties, rich network topologies and broad application prospects as electrode materials in LIBs and supercapacitors. Three different phosphonates, C₃₀H₅₀N₆Ni_{2.67}Co_{1.33}O₂₇P₂ (PNC), C₁₅H₃₂Co₂N₃O₁₆P (PC1) and C₃₀H₅₀N₆Ni_{2.67}Co_{1.33}O₂₇P₂ (PNC), have the same structure. Ni and Co have similar oxidation states, the same coordination behavior and similar ionic radii (Ni²⁺ = 0.700 Å and Co²⁺ = 0.745 Å). Therefore, in the same crystallographic position, Ni²⁺ and Co²⁺ can be partially replaced easily, but the rate of occupancy of both ions is not the same. The chains are interconnected by H-bonding, which is provided by four free and five coordinated water molecules, forming a large number of hydrogen bonds between chains, resulting in a complex 3D hybrid framework, as shown in [Figure 14A](#) and [B](#). The specific capacity of PC1 for the first 20 cycles decreases and then increases slowly from the 21st cycle at 50 mA g⁻¹. This may be because of the electrolyte immersion in the anode and the irreversible change of the state of the active substance caused by the current influence, as shown in [Figure 14C](#). The charge/discharge curves of PNC, PC1 and PN1 in the cycle tests are shown in [Figure 14D](#). PC1 has the most stable cycling performance and highest cycle-specific capacity among the three phosphonates^[194].

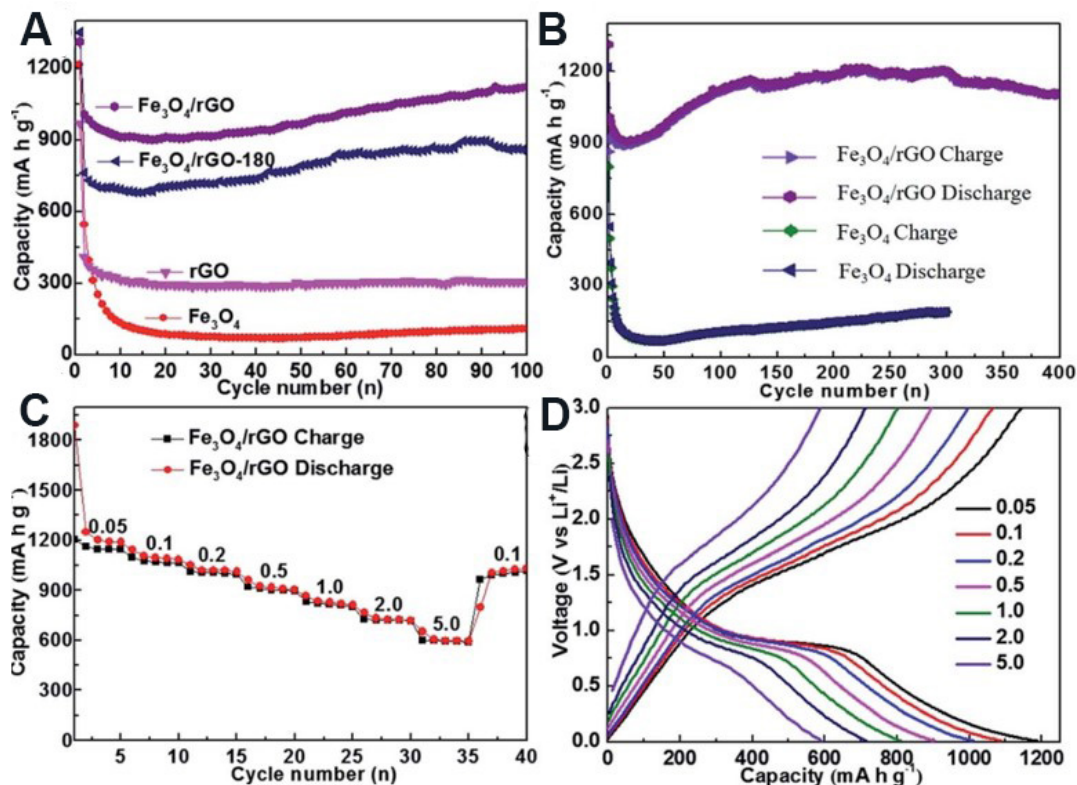


Figure 13. (A) Cycling performance of Fe₃O₄/rGO, Fe₃O₄/rGO-180, rGO and Fe₃O₄ at 0.5 A g⁻¹. (B) Long-term cycling of Fe₃O₄/rGO and Fe₃O₄. (C) Rate performance of Fe₃O₄/rGO electrode at 0.05–5 A g⁻¹. (D) Charge/discharge curves of Fe₃O₄/rGO. Reproduced with permission from Ref.^[190] (Copyright 2017, Royal Society of Chemistry).

a-Ni(OH)₂ is an excellent energy utilization material due to its high specific capacity and discharge potential. If the cation radius to be replaced is larger than Ni³⁺ (0.56 Å) in the state of charge, then the discharge level of a-Ni(OH)₂ will be enhanced due to the change in Madelung energy at the Fermi level point of the nickel hydroxide electrode. Mn³⁺ ions are continuously oxidized to Mn⁴⁺ due to their incorporation into the sites of a-Ni(OH)₂, which enhances the discharge capacity. The results show that the continuous oxidation of Mn³⁺ cations in the interlayer gives poor cycling stability due to the lack of protons in the structural layer, while the number of large anions (like SO₄²⁻, NO₃⁻ and CO₃²⁻) introduced as charge compensating species is limited due to the steric effect^[12].

NiS₂/NG-S is another promising electrode material and can be prepared by the partial etching of nickel in a graphene nanoshell, followed by sulfidation of the nickel and sulfur loading, as shown in Figure 15A. It is noted that the long-term cycling of NG/S and NiS₂/NG-S electrodes at a current density of 0.5 C shows excellent stability and the attenuation is stable and slow from the first cycle. The specific capacity of the NiS₂/NG-S electrode is slightly higher than that of the NG/S electrode, while NiS₂/S has poor cycling performance, low specific capacity and its capacity attenuation is fast. The initial specific capacities of the NiS₂/S, NG/S and NiS₂/NG-S electrodes at a current density of 0.5 C are 894, 973 and 1074 mAh g⁻¹, giving capacity retentions of 67.45%, 80.45% and 78.12% with specific capacities of 603, 783 and 839 mAh g⁻¹, respectively, over 100 charge/discharge cycles, as shown in Figure 15B. The NiS₂/NG-S electrode shows superior electrochemical performance and stable charge/discharge curves at 1 C for the first, 100th and 200th cycles, as presented in Figure 15C, while the NiS₂/S cathode can be attributed to low conductivity, a lack of buffer space due to the absence of graphene and the slow diffusion rate of Li ions. The existence of

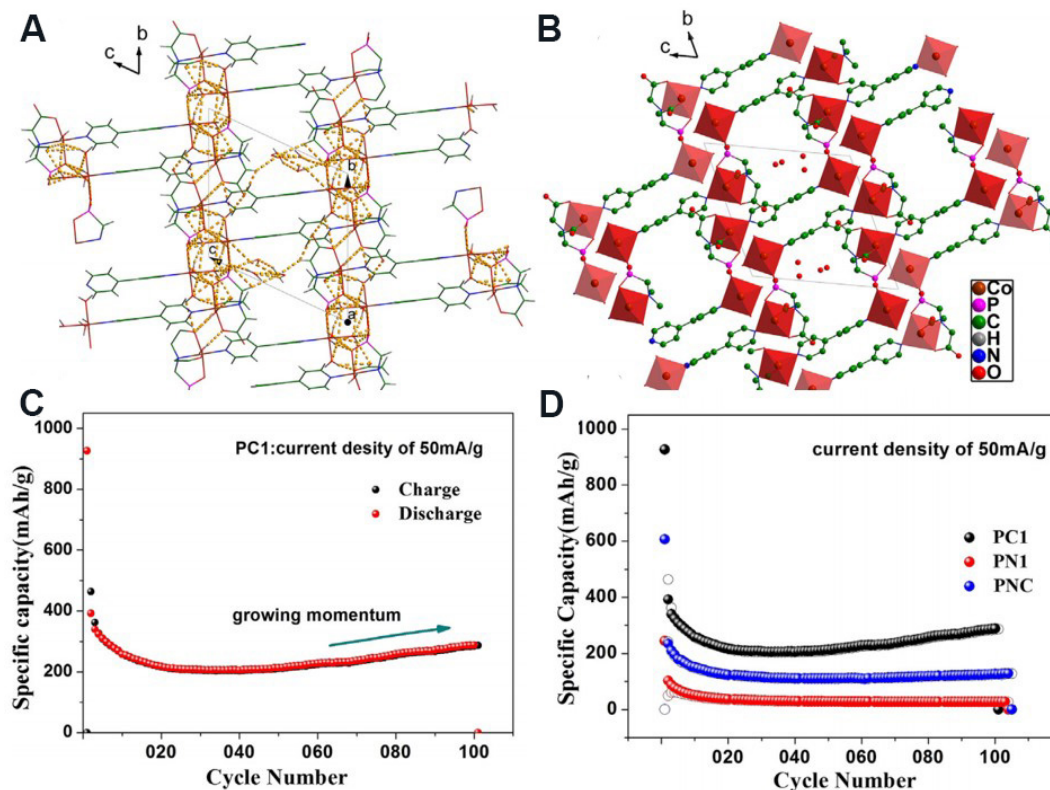


Figure 14. (A) Wireframe view of unit cell structure of cobalt phosphonate (PC1) along an axis, with dotted lines showing H-bonding among the chains (B). Polyhedron view of unit cell of PC1, with hydrogen atoms omitted for clarity and the red dots showing free water molecules. (C) Cycling stability diagram of PC1. (D) Comparison of cycling stability of $C_{15}H_{32}N_3Ni_2O_{16}P$ (PN1), $C_{15}H_{32}Co_2N_3O_{16}P$ (PC1) and $C_{30}H_{50}N_6Ni_{2.67}Co_{1.33}O_{27}P_2$ (PNC). Reproduced with permission from Ref.^[194] (Copyright 2019, Electrochimica Acta, Elsevier).

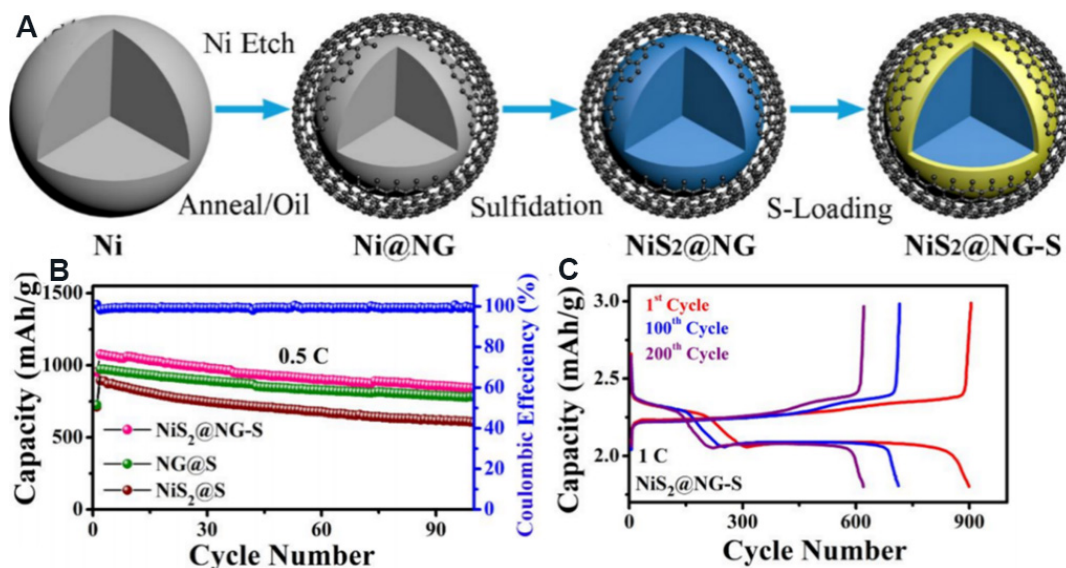


Figure 15. (A) Schematic representation of the synthesis of S-loaded $NiS_2/NG-S$ yolk-shells. (B) Long-term cycling stability of NiS_2/S , NG/S and $NiS_2/NG-S$ electrodes at 0.5 C. (C) Corresponding charge/discharge curves of $NiS_2/NG-S$ cathode after first, 100th and 200th cycles at 1 C. Reproduced with permission from Ref.^[195] (Copyright 2020, American Chemical Society).

the NiS₂ nanoshell in the NiS₂/NG-S yolk-shell structure limits the chemical adsorption of lithium polysulfide (LiPS). However, the free space of the NiS₂/NG yolk-shell and the NG/S nanoshell is conducive to a change in volume during the charge/discharge process and plays an important catalytic role in the LiPS transformation, resulting in excellent electrochemical performance for lithium-sulfur batteries. In the process of NG/S cathode cycling, Ni-based nanostructures are formed due to the presence of nickel residues (left during etching), which may play a vital role in the electrochemical performance of comparable batteries. In contrast, the slow redox reaction and poor conductivity of the bare NiS₂/S cathode result in poor electrochemical performance^[195].

The first battery was invented in 1799 using only Zn and Cu. Cu, being more malleable and ductile than silicon, acts as an adhesive that combines the electrode material and prohibits the electronic separation of the particles of silicon upon charge/discharge cycling, thereby reducing capacity fade. A thin-film electrode (porous copper-coated silicon) synthesized by magnetron sputtering were evaluated for cycling efficiency, and rate capability in lithium-ion coin-cells, and compared to equivalent uncoated silicon thin-film electrodes. The layer of Cu between the electrolyte and electrochemically active material enhances the cycling efficiency and rate capability of the Si electrode and decreases capacity loss due to pulverization. The rate capability and energy decrease considerably if the thickness of Cu is higher because the active material of silicon will not be accessed. Therefore, to increase the rate capability and capacity retention in LIBs, it is recommended that the porosity and thickness of the Cu coating are optimized^[196].

The easily scalable synthesis of the Cu-based metal-organic framework [Cu₂(C₈H₄O₄)₄]_n is a promising candidate for LIBs due to the porosity of crystalline materials that can store Li⁺. The terephthalate network responds reversibly with Li and retains 84% of its energy retention after 50 cycles. In the initial cycle, the theoretical capacity is ~95%, i.e., 227 mAh g⁻¹ at 24 mA g⁻¹^[197]. Unfortunately, most of the metal phosphides reported have an irregular particle size ranging from hundreds of nanometers to micrometers, thus providing limited cycling stability. The majority of metal phosphides have a limited number of charge/discharge cycles (30-150); however, Cu₃P nanowires without additives grow directly on the Cu collector as anode materials. After phosphidation treatment, it has a stable cycling capacity and the retention rate was ~70% over the 260th cycle^[198].

The electrochemical properties of yttrium-rich Li materials were studied by constant current charge/discharge experiments and EIS. The results show that a Y³⁺-doped lithium-rich electrode material has a capacity of 184.5 mAh g⁻¹ over 40 cycles at 1 C and a high capacity retention rate of 240.7 mAh g⁻¹ over 40 cycles at 0.1 C. It is demonstrated that an appropriate amount of Y³⁺ substituted for Mn⁴⁺ in Li_{1.2}Mn_{0.6-x}Ni_{0.2}Y_xO₂ results in high initial columbic efficiency, cycling capacity and rate capability. The electrochemical enhancement of Y³⁺-doped materials has been confirmed due to the “super-large” radius of Y³⁺, which can promote the fast transfer of Y³⁺ ions by spreading the layered structure. The strong Y-O bond can maintain the layered arrangement in the bulk and an extremely trace amount of Y₂O₃ is produced after excessive doping, which can protect the particles from the erosion of electrolytes and maintain Li⁺ and oxygen vacancies. This material leads to advanced LIBs that could possibly resolve renewable energy storage and electric transport requirements^[199].

A high-performance composite (Nafion-ZrNT) membrane consisting of perfluoro-sulfonic acid (Nafion) and ZrO₂ nanotubes (ZrNTs) was fabricated for vanadium redox flow batteries (VRBs). The VRB with a composite membrane enhances the selectivity of ions and presents a low rate of self-discharge, high energy efficiency and high discharge capacity compared to a commercial Nafion-117 membrane. The incorporation of the Nafion matrix with ZrNTs shows high oxidative stability (99.9%) and proton conductivity

(95.2 mS cm⁻¹). Compared with the Nafion-117 membrane (280 mAh g⁻¹), the Nafion-ZrNT composite membrane has higher ion selectivity (2.95×10^7 s min cm⁻³), lower V⁺ permeability (3.2×10^{-9} cm² min⁻¹) and higher discharge capacity (987 mAh g⁻¹) over 100 cycles. Compared with the original membrane, the self-discharge rate of the Nafion-ZrNT composite membrane is lower, upholding an open circuit voltage of 1.3 V for 330 h, which is lower than that of the original membrane (29 h). These superior properties resulted in a higher voltage and CEs compared to the VRB with the Nafion-117 membrane at a current density of 40 mA cm⁻²[200]. Pristine zirconium- and nickel-modified Li₂MnO₃ samples were also studied, with the Ni-modified material having a high discharge capacity and the Zr-modified electrode material showing less irreversible loss[201].

Lubimstsev *et al.*[202] showed that the origin of the high rate performance of Nb₂O₅ is due to the open channels between the sheets of NbO_x, which effectively facilitate local charge transfer and reduce the energy barrier. The charge storage of Nb₂O₅ is not restricted by semi-infinite diffusion because of its low conductivity ($\sim 10^{-6}$ S cm⁻¹). Nb₂O₅/graphene, Nb₂O₅/CNT and Nb₂O₅/carbon core-shell composites are examples of nanostructured Nb₂O₅/carbon materials used to enhance the conductivity of Nb₂O₅. Nb₂O₅ shows a high power capability and specific energy related to rapid Li⁺ intercalation within the (001) or (110) planes, which depend on the phase of the crystals[203]. A comparative study of TT-Nb₂O₅, T-Nb₂O₅ and M-Nb₂O₅ showed that T-Nb₂O₅ has excellent power treatment performance because of its rapid 2D Li⁺ transport in the crystal structure and no phase transition occurs through the electrochemical reaction. Polymer-bound electrodes have been mostly synthesized by mixing Nb₂O₅ nanoparticles, fibers and nanosheets with conductive additives. An extremely thin electrode without conductive additives was prepared by directly injecting Nb₂O₅ nanoparticles on thin mesoporous films used as a current collector. However, this approach remains limited due to scalability[204]. T-Nb₂O₅/C hybrid nanofiber mats were synthesized by treating NbC with CO₂ gas, resulting in a capacity of 156 mAh g⁻¹ from the high graphitization of the structure of carbon and the outstanding charge propagation in the nanofiber network[204]. To explain the intercalation and diffusion energy barriers in materials, first-principles calculations can be applied, which provide new awareness of the phenomena of ion transport and electrochemical performance. For example, Monte Carlo simulations have been used to explain the origin of the high rate of monoclinic Nb₂O₅ and show that the open channel system of quasi-2D NbO_x efficiently reduces the energy barrier of Li⁺ from one site to another[202].

Molybdenum disulfide (MoS₂) is like graphite in structure and consists of three atomic layers. The molybdenum layer is sandwiched between two sulfur layers. The large interlayer space and high surface area of MoS₂ make it an ideal host for ion intercalation/deintercalation. Bulk MoS₂ is used as an electrode material in LIBs. However, in the process of ion intercalation, the large volume expansion often leads to structural instability[205]. The electrochemical performance and stability of mesoporous MoS₂ are the same as that of mesoporous MoSe₂. The key difference between MoSe₂ and MoS₂ lies in the well-defined redox system of MoSe₂, which is characterized by a flat platform on the galvanostatic profile and a well-shaped peak pair in its cyclic voltammogram. Wang *et al.*[206] prepared core-shell MoSe₂/C nanocomposites by modifying hollow carbon nanofibers with small-sized and ultra-thin MoSe₂ nanosheets as an anode material for LIBs and they retain 100% of their initial capacity and specific capacity of 658 mAh g⁻¹ over 100 cycles at a current density of 0.5 mA g⁻¹. MoSe₂ has a large interlayer spacing (compared to MoS₂) and is thus suitable for providing accommodation for large metal cations, like Na, and has better performance than MoS₂. Morales *et al.*[207] suggested that Li_xMoSe₂ is subjected to structural change by the x value but the d spacing is almost the same during the process of intercalation/deintercalation. MoS₂ undergoes a structural change at 1.1 V vs. Li/Li⁺ with Li intercalation/deintercalation because of conversion from 2H-MoS₂ to 2T-Li_xMoS₂. This phase transformation is characterized by the cathodic peak at 1 V in CV. A similar performance is also

observed for MoSe_2 ^[168]. The results show that the theoretical adsorption capacity of 335 mAh g^{-1} can be attained by a double-sided Na^+ adsorption method for monolayer MoS_2 . A comparative study shows that the activation barrier of monolayer MoS_2 is 0.11 eV , while the interlayer migration barrier of bulk MoS_2 is 0.70 eV , confirming that Na^+ diffusion in monolayer MoS_2 is faster than in bulk MoS_2 . CNT/ MoS_2 was fabricated and showed outstanding electrochemical properties with a specific capacity of 1298 mAh g^{-1} ^[208].

The structure of intercalated ions (Mo_2CrC_2) and three highly symmetric positions in the Brillouin region are given in Figure 16A-D. The calculation of binding energy is determined by the Mo atom, C atom and metal ion at the top of the Cr atom on both sides of the MXene. Therefore, considering the dispersion interaction, Li^+ , Na^+ , K^+ and Mg^{2+} ions were considered. To test the energy stability of metal ions on the monolayer Mo_2CrC_2 MXene, the average calculated adsorption energy of Li^+ , Na^+ , K^+ and Mg^{2+} in different states has similar adsorption sites, as shown in Figure 16E. Using the PBE functional, the binding energies of these metal ions are calculated. When metal ions are adsorbed on the top of the Mo site, they move spontaneously to the top of the Cr site. After the adsorption of Li^+ , Na^+ , K^+ and Mg^{2+} , the adsorption energy is negative. This shows that these ions can be adsorbed by MXenes (Mo_2CrC_2). K^+ has better adsorption energy than the other ions, which may be related to its strong interaction with the MXene surface^[209].

Ag-Ca alloy batteries are a subtype of lead-acid batteries that are used instead of novel lead-calcium or traditional lead-antimony alloys. They are known for their resistance to the destructive effects of high temperatures and corrosion. The high energy density characteristics of silver oxide batteries are used in the aerospace industry and the military. They can also withstand high energy flow. Thin metallic coatings, such as Ag, have been shown to increase the cycling stability and capacity of Si materials. Ag/ TiO_2 -NTS composites can be easily prepared by a classical silver mirror reaction. Ag as an additive has high conductivity. At a high charge/discharge rate, the cycling stability and reversible capacity of TiO_2 nanotubes are enhanced and their cell polarization is reduced^[210]. MXene/Ag composite material consisting of layered MXene films and nanosized Ag particles was synthesized directly by reducing AgNO_3 on the surface of a $\text{Ti}_3\text{C}_2(\text{OH})_{0.8}\text{F}_{1.2}$ MXene. The composite has an initial specific capacity of $\sim 550 \text{ mAh g}^{-1}$ and reversible capacities of 310 mAh g^{-1} (1 C) and 150 mAh g^{-1} (50 C). The composite can withstand almost decaying capacity at different current densities, even above 5000 cycles^[211]. The main reason is the reduced interfacial resistance and the reduction of Ti(III) to Ti(II) through charge/discharge for long cycling with extremely high capacity.

Ag/1D- TiO_2 and Au/1D- TiO_2 , fabricated through a simple one-step electrospinning method, can enhance the electrochemical properties of 1D TiO_2 . The electronic configurations were maintained and the particle size of the TiO_2 consisting of the 1D nanostructure was decreased after the doping of Au or Ag nanoparticles into 1D TiO_2 . The inserted Au or Ag nanoparticles not only reduce the charge transport of TiO_2 nanoparticles but also act as conductive agents. For Li^+ storage performance, the storage capacity was increased by 20% or more compared to pristine 1D TiO_2 . The better charge transfer and smaller particle size contributed to the improved cycling stability and electrochemical properties of Au/1D- TiO_2 and Ag/1D- TiO_2 . In contrast, due to the poor crystalline nature, Ag/1D- TiO_2 shows less considerable changes than Au/1D- TiO_2 after the incorporation of Ag^[212]. Ag-doped vanadium oxide ($\text{Ag}/\text{V}_2\text{O}_5$) thin films exhibit higher discharge capacities due to the higher diffusion of Li^+ compared to non-doped V_2O_5 film cathodes. V_2O_5 films show a poor discharge capacity than $\text{Ag}/\text{V}_2\text{O}_5$, which appears to be due to a cauliflower-like structure. All the thin-film batteries show outstanding reversibility over 200 cycles^[213]. A $\text{Li}_4\text{Ti}_5\text{O}_{12}$ (LTO)/Ag composite was prepared by a simple chemical deposition process. In the voltage range of $1.0\text{-}2.5 \text{ V}$ (vs. Li^+/Li), after 120 charge/discharge cycles at 30 C, the high power capacity of the material reaches 131 mAh g^{-1} , maintaining more than 98% of the initial capacity. Nanosized Ag particles ($< 10 \text{ nm}$) were anchored on the

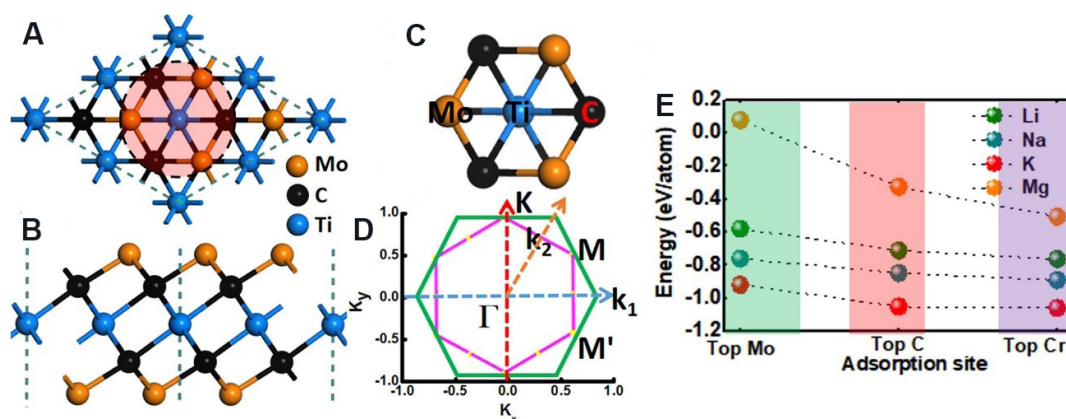


Figure 16. Structures of Mo_2CrC_2 supercell ($2 \times 2 \times 1$): (A) top view; (B) side view; (C) considered adsorption sites on the surface of Mo_2CrC_2 monolayer (top view). (D) Schematic diagram of top-view Mo_2CrC_2 with three high-symmetry sites. (E) Adsorption energy of metal ions in the first layer is located at Mo, Cr and C atom sites on both sides for Mo_2CrC_2 monolayer surface. (E) To test the energy stability of metal ions on the monolayer Mo_2CrC_2 MXene, the average calculated adsorption energy of Li^+ , Na^+ , K^+ and Mg^{2+} in different states has similar adsorption sites. Reproduced with permission from Ref.^[209] (Copyright 2020, Applied Surface Science, Elsevier).

surface of the nanocrystalline LTO (90 nm)^[214].

Tungsten (W), also known as wolfram, is a chemical element with atomic number 74. Kumagai *et al.*^[215] showed that monoclinic WO_3 particles synthesized by the moderate heating of H_2WO_4 show better cycling efficiency. Because the electrode materials interact with Li via the mechanism of intercalation, Li^+ diffusion in the host lattice plays a significant role. Therefore, it is attractive to find a structure of WO_3 that facilitates the diffusion of Li^+ and it is generally believed that by reducing the size of the material down to the nanometer scale, a significant enhancement in their properties is observed. The performance of hexagonal WO_3 nanorods as anode materials of LIBs has also been studied. The first cycle discharge capacity was 215 mAh g^{-1} . WO_3 hollow nanospheres have a high initial discharge capacity of more than 1054 mAh g^{-1} at a charge/discharge rate of 0.2 C. The electrode based on hollow particles maintains structural integrity even at a high current density of 2000 A g^{-1} ^[216].

ReS_2 nanosheets can be used as energy storage materials for LIBs. The growth of ReS_2 nanosheets was oriented vertically on the surface of the substrate. This achieves two significant goals. First, it greatly enhances the surface area of the nanosheet and second, it exposes the sharp edges of the ReS_2 nanosheets. The vertically grown ReS_2 nanosheets can be used as electrocatalysts and polysulfide immobilizers in the hydrogen evolution reaction and lithium-sulfur batteries. Over 300 charge/discharge cycles, the specific capacity of a Li-S battery with a vertical ReS_2 nanosheet catalyst was kept above 750 mAh g^{-1} and the capacity loss per cycle was only 0.063%, which is far better than the pristine one (i.e., without ReS_2). When it is tested under similar conditions, the capacity loss per cycle was 0.184%^[217].

The specific capacity of gold-coated porous Si is greater than 2500 mAh g^{-1} after 75 cycles and can attain 3000 mAh g^{-1} for over 50 cycles at $100 \mu\text{A cm}^{-2}$ with high CEs above 95%. In contrast, non-Au-coated porous Si had a capacity of 500 mAh g^{-1} at the very first cycle, which rapidly decreased to 76 mAh g^{-1} after the 10th cycle at a constant current rate of $50 \mu\text{A cm}^{-2}$, which is a considerable enhancement over Au-plated nonporous silicon. When the current is constant at $100 \mu\text{A cm}^{-2}$, the maximum capacity of Au-plated nonporous Si is 1 mAh g^{-1} and it faded over 10 cycles to 0.25 mAh g^{-1} , illustrating the importance of internal pores. The internal pores formed by the combination of porous Si and Au enhance the capacity and long-term cycling capacity of LIBs^[141]. $\text{NiCo}_2\text{O}_4/\text{Au}$ nanotube electrodes have an excellent capacity of

732.5 mAh g⁻¹ at a current density of 100 mA g⁻¹, even over 200 cycles with excellent cycling stability. Au nanoparticles can be inserted into the whole electrode to form 3D networks, which act as mechanical anchoring points or adhesion centers to firmly fix adjacent NiCo₂O₄ particles. Due to the stress or strain caused by the rapid ion/electron transfer during cycling, high volume expansion resistance occurs^[218]. An aniline [polyaniline (PANI)-1] and 4-*para*-phenylenediamine (PPDA) composite material was synthesized on the surface of the Au plate and used for LIBs. The maximum discharge capacity of the cathode material (PANI-PPDA/Au) is 103.2 mAh g⁻¹ and the decay rate is 0.147 mAh g⁻¹ at a charge/discharge rate of 0.4 mA g⁻¹^[219].

Magnesium-gallium (Mg-Ga) amalgam has been used as an anode material for a seawater activated battery. Under different current densities, the annealing sheets of Mg-4%Ga-2%Hg have the largest negative corrosion potential. The Mg-4%Ga-2% Hg alloy has a higher negative corrosion potential than AP65 and AZ31 alloys. EIS showed that the interface process of Mg-Ga-Hg alloy/seawater is determined by the activation control reaction. The electrochemical properties of the Mg-4%Ga-2%Hg alloy were improved by Mg₂Ga₅Hg₃ and Mg₃Hg phases. The prototype battery with CuCl as a cathode and Mg-4%Ga-2%Hg alloy used as an anode shows good discharge performance due to the microstructure and discharge characteristics of the alloy^[220].

F-block elements (lanthanides and actinides)

Heavier transition metals can also be used to replace LiMn₂O₄; however, they are far from ideal alternatives due to cost and size issues. In regards to this, only a very small amount of dopant can be applied, since this can increase the stability of the spinel due to stronger M-O bonds for transition metals^[221]. Furthermore, lanthanides are heavier than the first two rows of transition metals, thereby limiting the performance of electrodes in portable devices. Therefore, little attention has been given to lanthanide compounds in connection with LIB electrodes. The majority of research into lanthanides for energy storage is devoted to solid electrolytes based on fast lithium-ion conducting perovskites. This does suggest the potential of finding a suitable lanthanide series with an appropriate redox couple and conventionally occurring oxides. TMOs can alter their oxidation state in solution (e.g., Ce³⁺ to Ce⁴⁺), which is also an attractive phenomenon. Redox active electrolytes can compensate for the loss of energy density caused by the improvement of an open electrode structure, thus improving the accessibility of ions. A significant enhancement was noted in the electrochemical performance of numerous pseudocapacitive metal oxides, including Nb₂O₅ and CeO₂^[222].

Gd is a high neutron absorber, which makes it unsuitable for NPD experiments. Gd₂TiO₅ has a Ti₄₁/Ti₃₁ redox couple, comparable to the commercialized anode (Li₄Ti₅O₁₂) of LIBs. This Ti₄₁/Ti₃₁ redox couple creates a stable voltage of 1.55 V against Li, which deposits Li on the surface of the anode (dendrites), thereby enhancing the safety of LIBs. Thus, Li₄Ti₅O₁₂ anodes can provide safer and longer life to LIBs. Taking advantage of the comparable Ti₄₁/Ti₃₁ redox couple, Gd₂TiO₅ has a structure with comparatively large channels running beside the c axis, which may be feasible for Li or Na ion anode or insertion/extraction processes. Gd was initially selected as it is situated in the middle of the lanthanide series and is a good starting point to determine the effect of lanthanides on the electrochemical performance of electrodes. Gd₂TiO₅ has an interstitial-rich channel structure, which may be suitable for the insertion and extraction of Li⁺ during the charge/discharge process. The typical form of ion transport in electrodes tends to be intercalation or vacancies, whereas this material may provide the chance for ion transport through mobile interstitials. It was found that for LIBs, the capacity is 45 mAh g⁻¹ over 20 cycles at 4 mA g⁻¹^[223]. Na₂Ti₃O₇ (NTO) is an insertion-type anode material. The octahedral layer of TiO₆ can accommodate Na⁺ reversibly during cycling, with a theoretical capacity of 178 mAh g⁻¹. In addition, NTO also has an effective low charge/discharge platform of 0.3 V, which is the first reversible reaction between oxides and Na at such

a low voltage. Due to the above shortcomings, it is essential to enhance the intrinsic conductivity of NTO. It is found that the capacity and conductivity of the metal oxide electrode can be improved by the creation of lattice defects in the crystal. As dopants in the electrode of LIBs, lanthanides ions can considerably enhance both the rate performance and capacity of the electrode. Even a small amount of lanthanide leads to an improvement in the rate performance and specific capacity of LIBs. The discharge capacities of NTO and NTO:Yb are 44.9 and 89.4 mAh g⁻¹ at 30 C and 214.1 and 153.1 mAh g⁻¹ at 1 C, respectively [Figure 17A]. The discharge capacity of NTO is 43.9 mAh g⁻¹ and the retention capacity is 34.58%, while the discharge capacity of NTO:Yb remains at 71.6 mAh g⁻¹ with a capacity retention of ~46.02% over 1500 cycles at 5 C [Figure 17B]. The reversible capacity may be reduced and the capacity may fade after a few cycles at 5 C due to the enhancing polarization caused by a side reaction or the formation of an SEI layer^[224].

Doped samples of NTO show high electrochemical performance compared to pure NTO. Such a high-performance NTO anode was achieved without carbon coating and nanosizing. The insertion of lanthanides into the NTO structure causes a lattice distortion, resulting in the formation of oxygen vacancies, which considerably enhance faster charge storage kinetics and increase the donor density and electronic conductivity, thereby ensuring long-time cycling performance and superior rate performance^[225]. A uranium-doped LiMn₂O₄ cathode exhibited outstanding cyclability in comparison with a pristine LiMn₂O₄ cathode. The LiU_{0.01}Mn_{1.99}O₄ base cathode retains capacity at ~100% of its initial capacity over 100 cycles. Since the quantity of dopants is minimal, there is no cost issue and is thus suitable for commercialization. In contrast, since only a small amount of dopant is required, it does not decrease the theoretical capacity but does decrease the lattice constant^[226]. Finally, we summarize all the electrochemical performances of NTO:Ln samples in Figure 17C. The long-term cycling performance illustrates that Ln³⁺-doped samples have better electrochemical performance than that of pristine NTO^[225].

Hybrid materials

An approach to prepare electrochemical energy storage materials is to synthesize strongly coupled hybrids of inorganic and organic carbon nanomaterials, such as graphene, carbon nanotubes, chalcogenides, metal carbides and nitrides (MXenes)^[227]. Inorganic nanohybrid materials present a new route for preparing electrode materials with better electrochemical performance, synthesized by simple physical mixtures of conducting carbon materials and electrochemically active inorganic particles. Graphene, carbon nanotubes, metal carbides and nitrides, with various degrees of oxidation, offer novel substrates for the growth of nanoparticles. The interactions between the oxidized carbon substrates and inorganic precursors provide control over the structure, morphology and size of the inorganic nanoparticles. The conductivity of electrons and ions is very important to improve the rate performance of battery electrodes, especially when large and multivalent ions are applied in electrolytes. The theoretical values of the energy density of thin electrodes are much higher than the theoretical values of thick films.

A transition to 3D nanostructures (such as T-Nb₂O₅^[227] or MnO₂ spinel) is required to enhance the access of ions to the surface of electrochemically active materials and decrease both macroscopic electrode strain and diffusion limitations through the charge/discharge process. 3D architectures permit the use of thicker electrodes^[228]. 2D materials, like transition metal carbides, dichalcogenides, nitrides and oxides, can store larger metallic ions (Na⁺, K⁺, Mg²⁺ and Al³⁺) in between their layers. They are therefore recommended as promising anode materials for post-LIBs^[229], where the substrate material (MXene, graphene, and carbon nanotubes) acts as a conductive substrate for the active material and therefore gives mechanical strength and stability to the structure. In addition, they also increase the conductivity of the electrodes. Some “spacer reagents” can be incorporated between the layers to prevent from restacking and also enhance the electrochemical performance of the electrodes^[230]. A computational study showed that the functional groups in Li-S battery electrode materials are polar and therefore, due to the anchoring property on polysulfides,

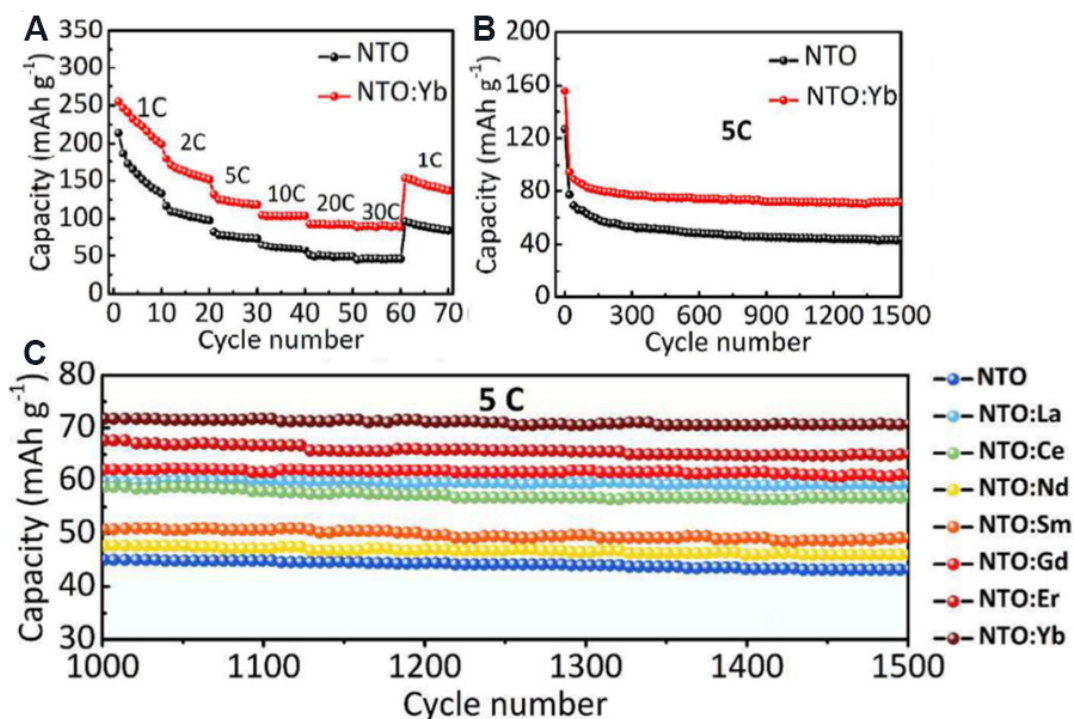


Figure 17. (A) Rate and (B) cycling performance of NTO and NTO:Yb in a half cell. (C) Cycling performance of NTO:Ln and NTO (Ln = La, Er, Gd, Sm, Ce, Nd or Yb) at a current rate of 5 C with a cycle number of 1000 to 1500. Reproduced with permission from Ref.^[224] (Copyright 2012, American Chemical Society). NTO: Na₂Ti₃O₇.

they can easily accommodate metal oxides^[231]. The properties of bulk transition metal dichalcogenides have different characteristics, such as metallic (NbS₂ and VS₂), semiconductors (MoS₂, WS₂, WTe₂ and TiSe₂), insulators (HfS₂) and low-temperature superconductors (TaS₂ and NbSe₂). These materials are converted into monolayers or few layers and also preserves their characteristics due to their confinement effects and gives additional characteristics^[232]. A liquid exfoliation process was employed to synthesize mono- and multilayer nanosheets of inorganic compounds, such as MoTe₂, WS₂, MoSe₂, NbSe₂, MoS₂, NiTe₂, TaSe₂, h-BN and Bi₂Te₃^[233].

MXenes

MXenes were first discovered by Naguib *et al.*^[234] in 2011 and they now represent the largest family of 2D materials. We can synthesize MXenes by the etching of selective atoms (A) from the MAX phase with the help of HF. The general formula of the MAX phase is Mn⁺AX_n, where A is a group A element, M is a transition metal, n can be 1, 2 or 3 and X is nitrogen and/or carbon. MAX has a large family (more than 60 phases) of ternary metal nitrides and carbides^[5]. Various MXenes have been experimentally fabricated to date, including Ti₃C₂, Ti₂C, Ti₃CN, V₂C, (V_{0.5}Cr_{0.5})₃C₂, Nb₂C (Ti_{0.5}Nb_{0.5})₂C and Ta₄C₃. Due to their high conductivity compared to graphene, MXenes have attracted significant consideration. Shein *et al.*^[235] examined the relative stability and structural features of MXenes (Tin⁺Nn and Tin⁺Cn). According to DFT calculations, by changing the surface terminators with a tunable bandgap, the conductivity of MXenes may be controlled. MXenes, where the surface of the sheet is terminated with surface terminators (i.e., -OH, -F and -O), are semiconductors but nonterminated MXenes have high conductivity and are metallic. The theoretical specific capacity of bare Ti₃C₂ is 320 mAh g⁻¹; however, the addition of a terminator group limits its storage capacity. The results show that the specific capacities of Ti₃C₂(OH)₂ and Ti₃C₂F₂ are 130 and 67 mAh g⁻¹, respectively^[236]. DFT calculations show that in Li-, Na-, K- and Ca-ion batteries, Ti₃C₂ can be

used as an electrode material. The atomic content of Li, Na and K has a linear relationship with the capacity. The theoretical capacities of Li, Na, Ca and K are 447.8, 351.8, 319.8 and 191.8 mAh g⁻¹, respectively^[237].

Kurtoglu *et al.*^[238] found that the elasticity of steel (400 GPa) is less than that of MXenes (> 500 GPa), which confirms that MXenes have comparatively high rigidity. It has been discovered that MXenes have a relatively similar capacity (372 mAh g⁻¹) as graphite electrodes for Li in LIBs; however, they have outstanding potential regarding cycling. For example, additive-free MXenes can retain a reversible capacity of 110 mAh g⁻¹ at a cycling rate of 36 C, while graphite cannot maintain this capacity at such a high cycling rate, which may be due to the smallest diffusion barrier for Li atoms in Ti₃C₂. With the help of DFT calculations, it has been determined that graphite and anatase TiO₂ (0.35-0.65 eV) have a greater diffusion barrier of Li atoms than Ti₃C₂ (0.07 eV)^[28]. MXenes can also be synthesized from a new layered ternary and quaternary compound {Mn[Al(Si)]₄ or C₃MnAl₃C₂}, which acts as a precursor for the preparation of MXenes. They synthesized Zr₃C₂T_x and Hf₃C₂T_x by eliminating the (AlC)_x units from Zr₃Al₃C₅ in the presence of a 50% concentrated solution of HF. The synthesized 2D MXene (Hf₃C₂T_z) material shows an excellent reversible volumetric capacity (1567 mAh cm⁻³) at 200 mA g⁻¹ over 200 cycles for LIBs^[239]. Li *et al.*^[240] used hydrogen peroxide (H₂O₂) to open the sheets and use it as an electrode material to give an excellent capacity of 389 mAh g⁻¹ over 50 cycles at 100 mA g⁻¹ and an excellent rate capability of 150 mAh g⁻¹ at 5 A g⁻¹.

In 2013, Mashtalir *et al.*^[241] synthesized a “paper” of Ti₃C₂ colloidal solution by reacting with DMSO, which gives the electrode a controlled capacity of 410 mAh g⁻¹ at 1 C and 110 mAh g⁻¹ at 36 C over 700 cycles. The enhancement of capacity may lead to the formation of an additional Li layer on the surface of the lithiated terminated MXene. The theoretical capacity of 320 mAh g⁻¹ was expected by Kurtoglu *et al.*^[238] for Li intercalation of bare Ti₃C₂. Zhou *et al.*^[242] proved the synthesis of a 2D Hf₃C₂T_z MXene by etching Hf₃[Al(Si)]₄C₆ in an aqueous solution of HF. For LIBs, this 2D Hf₃C₂T_z MXene material showed a better reversible volumetric capacity of 1567 mAh cm⁻³, over 200 cycles at 200 mA g⁻¹. To synthesize the multilayered Ti₃CNT_x MXene, Zhang *et al.*^[203] used environmentally-friendly LiF and HCl, unlike the directly HF etching etchant. In order to obtain the Ti₃CNT_x MXene with minimum restacking ability, they developed a freeze-dried method, which gives a specific discharge capacity of 300 mAh g⁻¹ over 1000 cycles at 0.5 A g⁻¹. The new 2D Nb₂C was examined for LIBs. At room temperature, the layered sample was successfully synthesized by etching of Al atoms from Nb₂AlC. A reversible capacity of 170 mAh g⁻¹ over 150 cycles was achieved for Nb₂C at 1 C, while a reversible capacity of 110 mAh g⁻¹ was attained at 10 C, respectively, with good cycling stability^[236].

Although the specific capacity of MXenes for LIBs (372 mAh g⁻¹) is analogous to the specific capacity of a commercial graphitic electrode, MXenes have excellent rate performance at high rates, whereas graphite cannot hold a high cycling rate. This may be due to the smaller diffusion barrier of the Li atoms on the surface of Ti₃C₂^[236]. For the charge/discharge process, the diffusion barrier is the key factor to determine the discharge rate of the battery. In good agreement with earlier reported values, the diffusion barrier for Li is 0.068 eV, for Na is 0.096 eV, for K is 0.103 eV, for Ca is 0.118 eV and for commercial graphite the diffusion barrier is 0.30 eV, which shows that Ti₃C₂ is the most promising high-rate electrode material. For improving the performance, having high capacity MXene with metal oxides is an alternative choice. The “conventional method” and “MXene bonding method” are used for the preparation of traditional polymer-bonded HC electrodes. Ahmed *et al.*^[243] proposed an atomic layer deposition technique to synthesize a SnO₂/Ti₃C₂T_x composite material for LIBs as anode materials. The SnO₂/MXene electrode coated with HfO₂ gives a discharge specific capacity of 843 mAh g⁻¹ at 500 mA g⁻¹ over 50 cycles. Zhang *et al.*^[244] also fabricated a Co₃O₄@Ti₃C₂T_x composite material successfully. A capacity of 999.3 mAh g⁻¹ at 500 mA g⁻¹ was achieved

after 900 cycles. An effective strategy was used by Lin *et al.*^[245] in 2015 to synthesize $\text{Ti}_3\text{C}_2\text{T}_x$ /carbon nanofibers, which are in a multi-stacked form.

Mashtalir *et al.*^[246] worked on the delaminated Nb_2CT_x /CNT composite material for LIBs in the same year. The free-standing CNT/MXene composite “paper” electrode, used as an anode material shows best cycling performances and recycling capacity of 400 mAh g^{-1} at 0.5 C. Ren *et al.*^[247] synthesized porous a 2D MXene ($\text{p-Ti}_3\text{C}_2\text{T}_x$) in aqueous solutions at room temperature. A flexible electrode was fabricated by the addition of CNTs ($\text{p-Ti}_3\text{C}_2\text{T}_x$ /CNT) and it exhibited a distinctly improved Li^+ storage capability of $\sim 500 \text{ mAh g}^{-1}$ at 0.5 C after 100 cycles and rate performance of 330 mAh g^{-1} at 10 C was achieved compared with pristine $\text{Ti}_3\text{C}_2\text{T}_x$. They also prepared porous V_2CT_x and Nb_2CT_x MXenes using the same method. Wu *et al.*^[248] synthesized $\text{MoS}_2\text{Ti}_3\text{C}_2$ -MXene/C nanocomposites by a simple carbon nanoplating method, where the reversible discharge capacity was 1750 mAh g^{-1} at 0.2 A g^{-1} and 1200 mAh g^{-1} over 700 cycles at 1 A g^{-1} . Rakhi *et al.*^[249] synthesized a MXene coated with whiskers of nanocrystalline $\epsilon\text{-MnO}_2$. The MXene/ $\epsilon\text{-MnO}_2$ showed outstanding cycling performance (88% retention) over 10,000 cycles.

Specifically, the MXene substrate with high conductivity can effectively remove the aggregation of MoSe_2 nanosheets and improve the electronic conductivity, while the carbon layer gives strength to the composite structure and further improve the overall conductivity of the hybrid nanosheets, as shown from the EIS results given in Figure 18. The strong chemical interaction at the interface of the MXene and MoSe_2 improves the durability of the structure and promotes the charge transfer dynamics. Therefore, MoSe_2 /MXene/C has a high rate performance of 183 mAh g^{-1} at 10 A g^{-1} and an outstanding reversible capacity of 355 mAh g^{-1} at 200 mA g^{-1} . The EIS measurements of MoSe_2 /MXene/C, MoSe_2 /MXene, MoSe_2 and MXene after several cycles show straight lines (low-frequency range) and semicircle depressions (middle- and high-frequency ranges), respectively, as given in Figure 18. The high-frequency semicircle is related to the surface contact resistance, while the low-frequency slope line represents the diffusion and phase transformation of ions in the electrode. This clearly shows that MoSe_2 /MXene/C has the smallest high-frequency concave semicircle and the smaller interfacial resistance. The proposed design strategy provides a broad prospect for the development of more useful PIBs electrode materials^[250].

Zou *et al.*^[211] produced a MXene/Ag composite material of layered MXene films and Ag nanoparticles. AgNO_3 is reduced in the presence of MXene [$\text{Ti}_3\text{C}_2(\text{OH})_{0.8}\text{F}_{1.2}$] and a MXene/Ag composite material is synthesized. The MXene/Ag composite material shows a better starting specific capacity of 550 mAh g^{-1} . Furthermore, this sample also shows reversible capacities of 150 mAh g^{-1} at 50 C and 310 mAh g^{-1} at 1 C even over 5000 cycles. This is due to the close connection of the conversion of Ti(III) to Ti(II) and the reduction of the interfacial resistance during the charge/discharge process. Sn^{4+} was successfully introduced inside the interlamination of an alkylated Ti_3C_2 . Because of the synergistic effect of the Sn^{4+} between the layers of alkyl- Ti_3C_2 matrix layers, it plays an important supporting role among the alk- Ti_3C_2 matrix layers and this process is known as the “pillar effect”. The nanocomposites show a capacity of 635 mAh g^{-1} and a better volumetric capacity of 1375 mAh cm^{-3} at a high current density of 216.5 mA cm^{-3} (100 mAh g^{-1}), which is considerably greater than the graphite electrode (550 mAh cm^{-3}) over 50 cycles. These nanocomposite materials hold a specific volumetric capacity of $504.5 \text{ mAh cm}^{-3}$ and a reversible charge capacity of 233 mAh g^{-1} even at an extremely high current density of 6495 mA cm^{-3} (3 A g^{-1})^[211].

Among the various MXenes, Ti_3C_2 and Ti_2C have been extensively studied. For example, Ti_3C_2 gives a capacity of 410 mAh g^{-1} for LIBs. Interestingly, by intercalation with different cations, such as NH_4^+ , Al^{3+} and Sn^{4+} , the capacity can be greatly increased to $\sim 800 \text{ mAh g}^{-1}$. As a comparison, V_2C MXene has a small molecular weight that can attain a higher theoretical LIB capacity of 940 mAh g^{-1} . Unfortunately, the

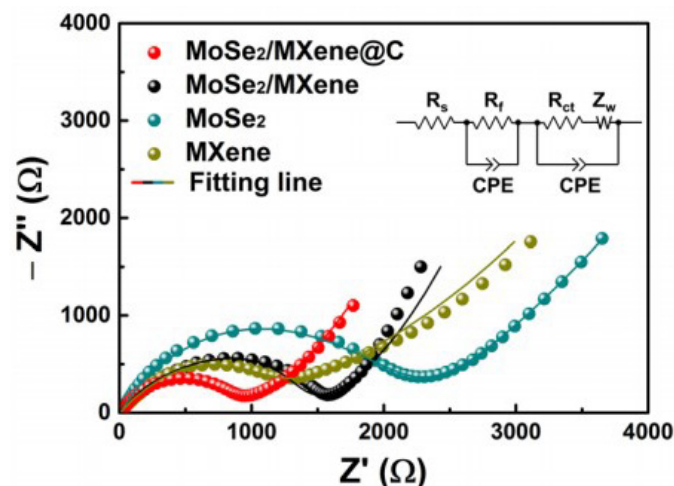


Figure 18. EIS results of MoSe₂/MXene/C, MoSe₂/MXene, MoSe₂ and MXene anodes after several cycles. The inset shows the corresponding equivalent circuits for data fitting, where R_{ct}, Z_w, R_f, CPE and R_s represent contact resistance, constant-phase element, electrolyte resistance, charge-transfer resistance and Warburg ion-diffusion resistance, respectively. Reproduced with permission from Ref.^[250] (Copyright 2019, American Chemical Society).

experimental V₂C MXene shows only 260 mAh g⁻¹ capacity at 1 C, which is significantly lower than the theoretical value. However, recently it has been noted that V₂C has excellent storage capacity (1100 mAh g⁻¹) for Li⁺ and good cycling stability after intercalation with Co^[179].

Graphene oxide

In 1958, Hummers synthesized GO using the most commonly used method today by treating oxidizing graphite with NaNO₃ and KMnO₄ in the presence of H₂SO₄^[251]. It is noteworthy that these processes release poisonous gases, such as NO₂, N₂O₄ and ClO₂, which may cause an explosion. Brodie was the first to synthesize GO in 1859 when a small amount of potassium chlorate (KClO₃) was reacted with graphite in the presence of fuming nitric acid^[252]. Graphene oxide is synthesized from monolayer films, like sheets of GO, which was planned more than a century ago. The properties of graphene oxide depend upon its extent of oxidation and special properties, like optical and electronic behavior. A large film of graphite can be synthesized from GO because it is water soluble and can be used as a component of the cathode and also as a binder in LIBs for carbon products. Moreover, its hydrophilicity allocates it on substrates uniformly, which is essential for applications in the field of electronics^[253]. The treatment of multiwalled carbon nanotubes with concentrated H₂SO₄, KMnO₄ and then phosphoric acid (H₃PO₄) gives graphene oxide nanoribbons in a scalable manner. This process is known as the “improved method” and can be used to synthesize improved GO. The basal plane of GO produced by the Hummers method is comparatively small^[2]. The majority of GO presented was fabricated based on Offerman’s process and the Hummers method, which offers little control over the degree of functionalization and is a time-consuming method.

Due to the very weak Van der Waals interaction, GO shows very low thermal stability^[254]. Anchoring of metal and non-metal oxides on sheets of graphene increases the cycling stability and electrochemical reversibility of the composite materials. Bismuth oxide (Bi₂O₃) has a high theoretical capacity of 690 mAh g⁻¹. A Bi₂O₃/rGO composite was synthesized by a hydrothermal process, which gives better cycling stability and electrochemical reversibility compared to bare Bi₂O₃ nanoparticles. Bi₂O₃/rGO used as an anodic material shows an outstanding initial capacity of 900 mAh g⁻¹ at 0.1 C and a rate capability of 270 mAh g⁻¹ at 10 C and 347.3 mAh g⁻¹ at 1 C, with a capacity retention rate over 79% after 100 cycles, which is much higher than for bare Bi₂O₃ nanocrystals^[159]. The strong interaction between the nanoparticles of

Co_3O_4 and graphene sheets is beneficial to control the volume expansion and the accumulation of Co_3O_4 NPs during the charge/discharge process, which gives a capacity of $\sim 935 \text{ mAh g}^{-1}$ over 30 cycles compared to bare graphene nanosheets and Co_3O_4 nanoparticles^[133,255]. An SnO_2 /graphene nanocomposite used as a LIB anode material have a reversible capacity of 432 and 638 mAh g^{-1} , respectively, over 100 and 150 cycles at 20 mA g^{-1} ^[256].

Alloys

In order to design better electrode materials with outstanding microstructures, corrosion resistance and hardness, the edifice of different elements can be applied. For this purpose, alloying is the best choice due to the potential for superior electrochemical properties and electronic conductivity. Alloys of Sb and Sn, such as Cu_6Sn_5 , SnSb , Mo_3Sb_7 and Cu_2Sb , have received particular attention because of their enhanced rate capability and long-term cycling performance. Such intermetallic candidates have outstanding properties compared to pure elemental electrodes since they are expected to show better capacity retention at very low temperatures (2.2 K) and low operating voltages (0.9 V) and possess excellent capacity retention vs. Li. One such candidate is Mo_3Sb_7 . This electrode material gives a reversible capacity of 494 mAh g^{-1} and its volumetric capacity (4273 mAh cm^{-3}) is comparatively close to pristine Sb (4422 mAh cm^{-3})^[155]. The alloys of lead and antimony are also applied in the assembly of lead-acid grid battery because of the soft nature of pure lead. It has been found that the introduction of small amounts of elements, like selenium and arsenic, to the alloys of lead-antimony, significantly enhances the electrochemical performance and mechanical properties of batteries^[192,208,211]. However, due to the dendrite structure of Pb-Sb alloys with Sb contents of 1.5-3.5 wt.%, they become very brittle, hard and easy to crack^[257].

Na can produce alloys with different elements like tin ($\text{Na}_{15}\text{Sn}_4$), bismuth (Na_3Sb), germanium (Na_3Ge) and lead ($\text{Na}_{15}\text{Pb}_4$). The thermodynamic potentials required for the alloying of Na is comparatively higher than that of Li atoms and make it potentially safer. An Sb/C nanocomposite shows a reversible capacity of 397 mAh g^{-1} for the initial 30 cycles. Afterward, the capacity fades rapidly to 100 mAh g^{-1} , while the Sn/C nanocomposite electrode shows poor recyclability and the initial capacity suddenly decreased to 80% after 13 cycles. The capacity decay in a single metal electrode is due to the expansion of volume during mechanical stress, which mainly occurred in the electrodes of Li alloys. The size of Li-Sn and Li-Sb alloys is less than the size of Na-Sn and Na-Sb alloys and this difference is further increased during the alloying process^[155]. The binary alloys of SnSb are more stable compared to the single metals, which may be due to the occurrence of an electrochemical reaction at a wide potential range of (0.0-0.9 V) and distinctive structural confinement through the charge/discharge process. Therefore, it is expected that the pristine Sb and Sn phases produced through the *in situ* charge/discharge process sustain the conductivity and integrity of the electrode material and fabricate a self-supporting network^[258].

CURRENT CHALLENGES FACING LIBS

The next generation of LIBs will be more capable, stable, durable, environmentally friendly and less expensive. However, we continue to confront some challenges. These challenges are as follows.

Overcharge and overdischarge

The major causes of safety incidents with LIBs are heat evolution and storage inside the batteries. Gas production is generally accompanied by heat generation and both are regulated by battery voltage and temperature. One of the most common reasons of heat evolution is overcharging. As a result, adopting precautions to avoid spontaneous overcharging within the battery will complement the exterior overcharge prevention methods. Thermal runaway occurs when a battery short circuit occurs due to separator breakdown and the heat generated locally cannot be dissipated efficiently. The development of temperature-

sensitive materials for limiting local temperature rises in the battery is a pivotal approach to avoid thermal runaway. Another possible technique for heat dissipation is to create an internal fast heat diffusion path (for example, by adding materials with high thermal conductivity). Finally, careful selection of active electrode materials and electrolytes is necessary to minimize heat and gas production, while also protecting the electrode interface^[259]. Furthermore, LIBs should not be charged at temperatures below 32 °F. Lithium coating results in the accumulation of Li atoms along the anode surface when charging at this temperature and the battery is more susceptible to harm, such as high-speed charging, which can lead to short circuit. Excessive discharge and overcharging of LIB packs must be avoided by those who use them. LIBs chemistry must have a voltage of at least 2 V. This problem might arise if the battery has been kept for an extended period of time or has been drained excessively. Both the cathode and the anode begin to break down when the voltage is less than 2 V. The anode collector will disintegrate when copper dissolves in the electrolyte. Cu ions begin to precipitate into metal Cu when the battery is charged over 2 V, resulting in a short circuit. Simultaneously, the cathode begins to release oxygen and the battery begins to lose capacity permanently after a few cycles.

Thermal runaway

The temperature difference between high-temperature operation and the battery will result in battery accelerated aging, out-of-control heating and other safety issues, posing a serious threat to vehicle safety. The breakdown of electrolyte and metal oxide cathode is caused by the pace at which the heat and pressure rise. The safety vent does not discharge the gas from the battery pack quickly enough and gas begins to build in the battery pack. Nothing can prevent this effect before the battery ignites or explodes and once one battery in the battery pack experiences thermal runaway, the next battery in the battery pack will begin to experience thermal runaway as well. Since it allows the system temperature to be managed, the well-designed built-in cooling system is a key component of LIB safety. A cooling system may be necessary if heat is created too late in the cycle to disperse. A cooling system is also necessary to manually regulate the overall temperature in the event of unequal temperature distribution. The operating temperature range for LIBs is 15-35 °C^[260]. As a result, an optimum cooling control system capable of maintaining this range is critical for safely extending battery life and lowering costs. The electrolyte is the most dangerous part of a LIB and the core is flammable. The exothermic reaction rate inside the battery increases when the battery temperature goes over 80 °C. These processes eventually cause LIBs to thermally runaway, causing the battery to burst and explode. The cause for this is that the high-temperature flammable gas in the battery interacts with the surrounding oxygen^[261].

Dendrite formation

One of the main causes of thermal runaway is the growth of Li dendrites, which can be mitigated by four different methods: (1) capping with additive molecules or ions; (2) redirecting dendrite growth away from the separator with Li friendly/hydrophobic coatings; (3) using a compartment/structured collector; and (4) inhibition using a solid electrolyte. Currently, the composite of a ceramic or glass electrolyte and polymer hybrid, as well as the insertion of an artificial interface stabilizing layer between Li and electrolyte, are the most prevalent and promising techniques among the aforementioned tactics. The dendrite development process in SES needs to be investigated and understood better in the future, so that a more practical and scalable method may be used to provide a new path to solve the dendrite problem^[262]. To assess dendritic inhibition, it is advised to utilize standard CE characterization, more powerful *in situ* characterization technology, restricted Li, early detection of “soft short circuit” and thinner electrolytes.

Safety issues caused by undesirable chemical reactions

Only Li⁺ shuttle occurs in the electrolyte during the insertion/extraction cycle of the cathode and anode in the typical voltage and temperature range. Electrochemical reactions grow more complicated at high

temperatures and pressures, with the breakdown of the SEI membrane, oxygen release on the cathode side and extra electrolyte/electrode side reactions occur^[263]. The temperature rises as a result of SEI membrane breakdown occurring, which increases the danger of oxygen leakage from active cathode materials. These processes eventually cause LIBs to thermally runaway, as described above^[261].

Short circuit

A separator is an important part of a LIB. Its purpose is to keep the positive and negative electrodes of the battery from making physical contact, to prevent internal short circuits, and to act as an electrolyte reservoir for ion transfer. The ideal separator should have a large electrolyte absorption capacity to lower the internal resistance, as well as an extremely thin thickness, high mechanical strength, electrochemical and structural stability, a highly porous structure and a large curvature to prevent tree-branched lithium dendrite formation. Industry and scientific research will require high-performance battery separators in the future as demand for high charge discharge efficiency and high energy density LIB growth. Experiments are now used to do research on separator materials and characteristics. Simultaneously, DFT simulations are a cost-effective and efficient method to design separators and battery systems. In order to provide safer and more powerful separators, it is very important to develop new LIBs or battery systems and optimize the manufacturing process. The following DFT research and development models are recommended for the future: (1) a novel thermal runaway model for LIB systems, which can combine a variety of battery separator materials with different mechanical and physical properties; and (2) a coupling multiscale simulation model to study all internal/external coupling phenomena.

FUTURE PROSPECTS OF LIBS

LIBs have come a long way since their introduction in 1991, with their specific energy content nearly tripling. Despite the necessity for complex control systems and battery energy reserves, LIBs have more than quadrupled their life, allowing them to fulfill most automotive calendar and cycle life requirements. While attaining significant performance gains, the cost of LIBs has been lowered by roughly two orders of magnitude and has been steadily declining in recent years. These LIB technological advancements have been made while retaining the high level of safety demanded by automotive goods.

1. The next generation of LIBs will be greater in capacity, have longer service lives, more environmentally friendly and less expensive, necessitating possible lightweight collectors with higher electrochemical stability and conductivity. Furthermore, in the future, a collector with a flexible construction will be required for the use of wearable devices.
2. A number of successful techniques are discovered based on an understanding of LIB structures and operating principles. The safety and performance stability of LIBs may be substantially enhanced by carefully selecting electrode materials, separators and electrolytes, as well as improving battery architecture. External methods, such as cooling and battery balance, can also significantly improve LIB safety performance under typical circumstances.
3. As the size of the real battery pack has grown in recent years, a new vehicle quick charging objective has emerged, resulting in a constant increase in the charging rate of the battery system. LIBs will be able to reach a total energy of 350 Wh/kg at the start of their life, based on current development and materials chemistry research results. Unfortunately, this energy content is insufficient to satisfy the vehicle energy objective if this performance is moved to the accessible end-of-life value of components^[264]. About a decade ago, numerous research initiatives beyond lithium ion were launched in response to this impending problem. The Li metal system has been the most advanced beyond lithium ion technology in the last

decade. The American Advanced Battery Alliance recently issued an automobile LIB objective that highlights the advancement and potential effect of LIBs.

4. New liquid electrolytes compatible with Li metal have recently made significant progress by enhancing the design of existing LIBs^[265]. The possibility of a Li metal solid-state battery has also been revised thanks to the discovery of many recently found solid Li superionic conductors (LMSSBs)^[266]. Traditional LIB cathodes and battery design characteristics are also used in most proposed LMSSB systems. Long-term LIBs development will need a deeper knowledge of Li mechanics^[267] and Li-electrolyte interactions, whether liquid or solid^[268]. Regardless of whether solid or liquid electrolyte systems are utilized, the basic architecture of these Li metal batteries will inherit the vast majority of the LIB system's technical and materials chemistry advancements.

5. The scientific community must still satisfy its standards in order for solid-state batteries to be commercialized in the future. The area specific resistance (ASR) of the interface between the solid-state ceramic electrolyte and the electrode (containing anode and cathode) is less than $25 \Omega \text{ cm}^{-2}$ (the total battery resistance of commercial LIBs is $22 \Omega \text{ cm}^{-2}$, which is utilized for liquid batteries). The ASR range of most solid ceramic electrolytes' ceramic Li metal interface is $37\text{-}20,000 \Omega \text{ cm}^{-2}$. The cathode is more powerful. Hitz *et al.*^[269] investigated the construction of a three-layer Li garnet electrolyte, which had a low interface impedance of $7 \Omega \text{ cm}^{-2}$ and a high current density of 10 mA/cm^2 . However, the production cost must be weighed against the existing technological level.

6. Environmental atmosphere is required for the stability of a sulfide-based Li-ion conductor ceramic electrolyte. The next class of most promising superionic Li-ion conductors ($\geq 10^{-4} \text{ S/cm}$) will be accurately identified using a combination of a computational prediction models of material selection and a density functional theory molecular dynamics calculation^[270]. Many potential possibilities have been found using machine learning calculation approaches, including $\text{Li}_5\text{B}_7\text{S}_{13}$, $\text{Li}_2\text{B}_2\text{S}_5$, Li_3ErCl_6 , LiSO_3F , Li_3InCl_6 , Li_2HfO , $\text{LiMgB}_3(\text{H}_9\text{N})_2$ and CsLi_2BS_3 . The Li-ion conductivity (74 mS/cm) of $\text{Li}_5\text{B}_7\text{S}_{13}$ is expected to be several times that of the fastest Li-ion conductor known today^[271].

7. To assess dendritic inhibition, it is advised to utilize standard CE characterization, restricted Li amount, early detection of "soft short circuit", more powerful *in situ* characterization technology and thinner electrolytes.

8. Coin cell batteries have been used to test the majority of existing Li-metal protection techniques. Testing the stability of Li metal in larger batteries is quite practical (such as pouch batteries). The artificial interface layer between SE and Li metal must be stable and functional.

9. Simulation is becoming increasingly essential in identifying novel electrolyte possibilities and assisting experimenters in gaining a better understanding and predicting performance. We have a fundamental knowledge of the design and interfacial stability of Li-metal anodes on different scales, notably the interface layer can guide Li-metal anode development and stabilization eventually commercialization of Li-metal anodes in ASLBs.

CONCLUSIONS

Emerging electrochemical energy storage devices will play a vital role in the future energy systems of the world. The innovation of electrode materials is a decisive factor for the improvement of new electrochemical energy storage devices. Nanotechnology opens up new properties and uses the advantage of

the best chemical properties of elements to bring them to a useful plane. The in-depth knowledge of elemental chemistry has been fully utilized, providing new applications for nanomaterials. The periodic table of elements is helpful to understand the chemical diversity of elements. It also helps us to find out the effective combination of elements to produce novel nanoenergy storage materials and assists us in making additional progress and innovation in the field of nanoscience and nanotechnology. The combination of periodic table knowledge with theoretical calculations and experimental procedures will pave the way for the development of novel materials with excellent electrochemical properties. The specific capacity, rate performance, energy density, cycling performance, long-term cycling stability and their mechanisms for LIBs of s-, p-, d- and f-block elements, transition and inner transition metals and hybrid materials (MXene, graphene oxide and alloys) were studied in detail, which provided appropriate treatment methods and creative remedial measures for the better performance of energy storage devices. We have also highlighted the challenges facing LIBs and their future prospects for the next generation.

DECLARATIONS

Authors' contributions

Conceptualization, methodology, writing -original draft: Bashir T

Writing - review and editing: Ismail SA

Literature survey - revision: Song Y, Zhou S

Literature survey - figures set up: Irfan RM

Validation, formal analysis; literature survey - revision: Yang S

Supervision, writing - review and editing: Zhao J, Gao L

Availability of data and materials

Not applicable.

Financial support and sponsorship

This work was supported by the National Natural Science Foundation of China (grant numbers 21703147 and U1401248); One of the authors (Bashir T) also acknowledges the support of China Scholarship Council (grant number 2018SLJ022487).

Conflicts of interest

All authors declared that there are no conflicts of interest.

Ethical approval and consent to participate

Not applicable.

Consent for publication

Not applicable.

Copyright

© The Author(s) 2021.

REFERENCES

1. Tomalia DA, Khanna SN. A systematic framework and nanoperiodic concept for unifying nanoscience: hard/soft nanoelements, superatoms, meta-atoms, new emerging properties, periodic property patterns, and predictive mendeleev-like nanoperiodic tables. *Chem Rev* 2016;116:2705-74. [DOI PubMed](#)
2. Marcano DC, Kosynkin DV, Berlin JM, et al. Improved synthesis of graphene oxide. *ACS Nano* 2010;4:4806-14. [DOI PubMed](#)
3. Naguib M, Gogotsi Y. Synthesis of two-dimensional materials by selective extraction. *Acc Chem Res* 2015;48:128-35. [DOI PubMed](#)
4. Naguib M, Mochalin VN, Barsoum MW, Gogotsi Y. 25th anniversary article: MXenes: a new family of two-dimensional materials. *Adv Mater* 2014;26:992-1005. [DOI PubMed](#)
5. Naguib M, Mashtalir O, Carle J, et al. Two-dimensional transition metal carbides. *ACS Nano* 2012;6:1322-31. [DOI PubMed](#)

6. Ong WJ, Tan LL, Ng YH, Yong ST, Chai SP. Graphitic carbon nitride (g-C₃N₄)-based photocatalysts for artificial photosynthesis and environmental remediation: are we a step closer to achieving sustainability? *Chem Rev* 2016;116:7159-329. DOI PubMed
7. Li W, Bashir T, Wang J, et al. Enhanced sodium-ion storage performance of a 2D MoS₂ anode material coated on carbon nanotubes. *ChemElectroChem* 2021;8:903-10. DOI
8. Yao L, Xi Y, Han H, Li W, Wang C, Feng Y. LiMn₂O₄ prepared from waste lithium ion batteries through sol-gel process. *J Alloys Compd* 2021;868:159222. DOI
9. Ozawa K. Lithium-ion rechargeable batteries with LiCoO₂ and carbon electrodes: the LiCoO₂/C system. *Solid State Ionics* 1994;69:212-21. DOI
10. Li L, Zhao R, Xu T, et al. Stabilizing a high-voltage LiNi_{0.5}Mn_{1.5}O₄ cathode towards all solid state batteries: a Li-Al-Ti-P-O solid electrolyte nano-shell with a host material. *Nanoscale* 2019;11:8967-77. DOI PubMed
11. Yang S, Yao J, Hu H, et al. Sonication-induced electrostatic assembly of an FeCO₃@Ti₃C₂ nanocomposite for robust lithium storage. *J Mater Chem A* 2020;8:23498-510. DOI
12. Gao X, Yang H. Multi-electron reaction materials for high energy density batteries. *Energy Environ Sci* 2010;3:174-89. DOI PubMed PMC
13. Chung SY, Bloking JT, Chiang YM. Electronically conductive phospho-olivines as lithium storage electrodes. *Nat Mater* 2002;1:123-8. DOI PubMed
14. Kim D, Kim J. Synthesis of LiFePO₄ nanoparticles in polyol medium and their electrochemical properties. *Electrochem Solid-State Lett* 2006;9:A439. DOI
15. Doeff MM, Ma Y, Visco SJ, De Jonghe LC. Electrochemical insertion of sodium into carbon. *J Electrochem Soc* 1993;140:L169-70. DOI
16. Alcántara R, Lavela P, Tirado JL, Stoyanova R, Kuzmanova E, Zhecheva E. Lithium-nickel citrate precursors for the preparation of LiNiO₂ insertion electrodes. *Chem Mater* 1997;9:2145-55. DOI
17. Wenzel S, Hara T, Janek J, Adelhelm P. Room-temperature sodium-ion batteries: improving the rate capability of carbon anode materials by templating strategies. *Energy Environ Sci* 2011;4:3342. DOI
18. Stevens DA, Dahn JR. High capacity anode materials for rechargeable sodium-ion batteries. *J Electrochem Soc* 2000;147:1271. DOI
19. Dominko R, Gaberscek M, Bele M, Mihailovic D, Jamnik J. Carbon nanocoatings on active materials for Li-ion batteries. *J Eur Ceram Soc* 2007;27:909-13. DOI
20. Gaberscek M, Dominko R, Bele M, Remskar M, Jamnik J. Mass and charge transport in hierarchically organized storage materials. Example: porous active materials with nanocoated walls of pores. *Solid State Ionics* 2006;177:3015-22. DOI
21. Kharbachi A, Zavorotynska O, Latroche M, Cuevas F, Yartys V, Fichtner M. Exploits, advances and challenges benefiting beyond Li-ion battery technologies. *J Alloys Compd* 2020;817:153261. DOI
22. Gogotsi Y, Simon P. Materials science. True performance metrics in electrochemical energy storage. *Science* 2011;334:917-8. DOI PubMed
23. Deng Z, Liu T, Chen T, et al. Enhanced electrochemical performances of Bi₂O₃/rGO nanocomposite via chemical bonding as anode materials for lithium ion batteries. *ACS Appl Mater Interfaces* 2017;9:12469-77. DOI PubMed
24. Ghodbane O, Pascal J, Favier F. Microstructural effects on charge storage properties in MnO₂ based electrochemical supercapacitors. *ECSS Trans* 2009;16:235-41. DOI PubMed
25. Lukatskaya MR, Mashtalir O, Ren CE, et al. Cation intercalation and high volumetric capacitance of two-dimensional titanium carbide. *Science* 2013;341:1502-5. DOI PubMed
26. Ali T, Wang X, Tang K, et al. SnS₂ quantum dots growth on MoS₂: atomic-level heterostructure for electrocatalytic hydrogen evolution. *Electrochim Acta* 2019;300:45-52. DOI
27. Pomerantseva E, Bonaccorso F, Feng X, Cui Y, Gogotsi Y. Energy storage: the future enabled by nanomaterials. *Science* 2019;366:eaan8285. DOI PubMed
28. Er D, Li J, Naguib M, Gogotsi Y, Shenoy VB. Ti₃C₂ MXene as a high capacity electrode material for metal (Li, Na, K, Ca) ion batteries. *ACS Appl Mater Interfaces* 2014;6:11173-9. DOI
29. Mills G, Jónsson H, Schenter GK. Reversible work transition state theory: application to dissociative adsorption of hydrogen. *Surf Sci* 1995;324:305-37. DOI
30. Tang Q, Zhou Z, Shen P. Are MXenes promising anode materials for Li ion batteries? *J Am Chem Soc* 2012;134:16909-16. DOI PubMed
31. Manthiram A, Fu Y, Chung SH, Zu C, Su YS. Rechargeable lithium-sulfur batteries. *Chem Rev* 2014;114:11751-87. DOI PubMed
32. Bruce PG, Freunberger SA, Hardwick LJ, Tarascon JM. Li-O₂ and Li-S batteries with high energy storage. *Nat Mater* 2011;11:19-29. DOI PubMed
33. Ye H, Li M, Liu T, Li Y, Lu J. Activating Li₂S as the lithium-containing cathode in lithium-sulfur Batteries. *ACS Energy Lett* 2020;5:2234-45. DOI
34. Liang X, Hart C, Pang Q, Garsuch A, Weiss T, Nazar LF. A highly efficient polysulfide mediator for lithium-sulfur batteries. *Nat Commun* 2015;6:5682. DOI PubMed
35. He X, Ren J, Wang L, Pu W, Jiang C, Wan C. Expansion and shrinkage of the sulfur composite electrode in rechargeable lithium batteries. *J Power Sources* 2009;190:154-6. DOI
36. Rauh R, Shuker F, Marston J, Brummer S. Formation of lithium polysulfides in aprotic media. *Journal of Inorganic and Nuclear Chemistry* 1977;39:1761-6. DOI
37. Yamin H, Gorenshstein A, Penciner J, Sternberg Y, Peled E. Lithium sulfur battery: oxidation/reduction mechanisms of polysulfides

- in THF solutions. *J Electrochem Soc* 1988;135:1045-8. DOI
38. Xiong S, Xie K, Diao Y, Hong X. Characterization of the solid electrolyte interphase on lithium anode for preventing the shuttle mechanism in lithium-sulfur batteries. *J Power Sources* 2014;246:840-5. DOI
39. Cañas NA, Fronczek DN, Wagner N, Latz A, Friedrich KA. Experimental and theoretical analysis of products and reaction intermediates of lithium-sulfur batteries. *J Phys Chem C* 2014;118:12106-14. DOI
40. Ali T, Yan C. 2D Materials for inhibiting the shuttle effect in advanced lithium-sulfur batteries. *ChemSusChem* 2020;13:1447-79. DOI PubMed
41. Luo C, Zhu H, Luo W, et al. Atomic-layer-deposition functionalized carbonized mesoporous wood fiber for high sulfur loading lithium sulfur batteries. *ACS Appl Mater Interfaces* 2017;9:14801-7. DOI PubMed
42. Abraham KM, Jiang Z. A polymer electrolyte-based rechargeable lithium/oxygen battery. *J Electrochem Soc* 1996;143:1-5. DOI
43. Ogasawara T, Débart A, Holzapfel M, Novák P, Bruce PG. Rechargeable Li_2O_2 electrode for lithium batteries. *J Am Chem Soc* 2006;128:1390-3. DOI PubMed
44. Peng Z, Freunberger SA, Chen Y, Bruce PG. A reversible and higher-rate Li-O_2 battery. *Science* 2012;337:563-6. DOI PubMed
45. Shao Y, Park S, Xiao J, Zhang J, Wang Y, Liu J. Electrocatalysts for nonaqueous lithium-air batteries: status, challenges, and perspective. *ACS Catal* 2012;2:844-57. DOI
46. Zhao G, Xu Z, Sun K. Hierarchical porous Co_3O_4 films as cathode catalysts of rechargeable Li-O_2 batteries. *J Mater Chem A* 2013;1:12862. DOI
47. Mourad E, Coustan L, Lannelongue P, et al. Biredox ionic liquids with solid-like redox density in the liquid state for high-energy supercapacitors. *Nat Mater* 2017;16:446-53. DOI PubMed
48. Mahne N, Fontaine O, Thotiyil MO, Wilkening M, Freunberger SA. Mechanism and performance of lithium-oxygen batteries - a perspective. *Chem Sci* 2017;8:6716-29. DOI PubMed PMC
49. Zhang T, Yang J, Zhu J, et al. A lithium-ion oxygen battery with a Si anode lithiated in situ by a Li_3N -containing cathode. *Chem Commun (Camb)* 2018;54:1069-72. DOI PubMed
50. Freunberger SA, Chen Y, Drewett NE, Hardwick LJ, Bardé F, Bruce PG. The lithium-oxygen battery with ether-based electrolytes. *Angew Chem Int Ed Engl* 2011;50:8609-13. DOI PubMed
51. Mirzaeian M, Hall PJ. Characterizing capacity loss of lithium oxygen batteries by impedance spectroscopy. *J Power Sources* 2010;195:6817-24. DOI
52. Burke CM, Pande V, Khetan A, Viswanathan V, McCloskey BD. Enhancing electrochemical intermediate solvation through electrolyte anion selection to increase nonaqueous Li-O_2 battery capacity. *Proc Natl Acad Sci U S A* 2015;112:9293-8. DOI PubMed PMC
53. Lee S, Kwon G, Ku K, et al. Recent progress in organic electrodes for Li and Na rechargeable batteries. *Adv Mater* 2018;30:e1704682. DOI PubMed
54. Liang Y, Tao Z, Chen J. Organic electrode materials for rechargeable lithium batteries. *Adv Energy Mater* 2012;2:742-69. DOI
55. Luo C, Ji X, Hou S, et al. Azo compounds derived from electrochemical reduction of nitro compounds for high performance Li-ion batteries. *Adv Mater* 2018;30:e1706498. DOI PubMed
56. Alt H, Binder H, Köhling A, Sandstede G. Investigation into the use of quinone compounds-for battery cathodes. *Electrochim Acta* 1972;17:873-87. DOI
57. Kim T, Song W, Son D, Ono LK, Qi Y. Lithium-ion batteries: outlook on present, future, and hybridized technologies. *J Mater Chem A* 2019;7:2942-64. DOI
58. Luo C, Huang R, Kevorkyants R, Pavanello M, He H, Wang C. Self-assembled organic nanowires for high power density lithium ion batteries. *Nano Lett* 2014;14:1596-602. DOI PubMed
59. Cariello M, Johnston B, Bhosale M, et al. Benzo-dipyridine derivatives as organic cathodes for Li- and Na-ion batteries. *ACS Appl Energy Mater* 2020;3:8302-8. DOI PubMed PMC
60. Lakraychi AE, Deunf E, Fahsi K, et al. An air-stable lithiated cathode material based on a 1,4-benzenedisulfonate backbone for organic Li-ion batteries. *J Mater Chem A* 2018;6:19182-9. DOI
61. Shea JJ, Luo C. Organic electrode materials for metal ion batteries. *ACS Appl Mater Interfaces* 2020;12:5361-80. DOI PubMed
62. Luo C, Borodin O, Ji X, et al. Azo compounds as a family of organic electrode materials for alkali-ion batteries. *Proc Natl Acad Sci U S A* 2018;115:2004-9. DOI PubMed PMC
63. Peng C, Ning G, Su J, et al. Reversible multi-electron redox chemistry of π -conjugated N-containing heteroaromatic molecule-based organic cathodes. *Nat Energy* 2017;2:17074. DOI
64. Lei Z, Chen X, Sun W, Zhang Y, Wang Y. Exfoliated triazine-based covalent organic nanosheets with multielectron redox for high-performance lithium organic batteries. *Adv Energy Mater* 2019;9:1801010. DOI
65. Thangadurai V, Kaack H, Weppner WJF. Novel fast lithium ion conduction in garnet-type $\text{Li}_3\text{La}_3\text{M}_2\text{O}_{12}$ ($\text{M} = \text{Nb}, \text{Ta}$). *J Am Ceram Soc* 2003;86:437-40. DOI
66. Manthiram A, Yu X, Wang S. Lithium battery chemistries enabled by solid-state electrolytes. *Nat Rev Mater* 2017;2:16103. DOI
67. Zhang M, Takahashi K, Imanishi N, et al. Preparation and electrochemical properties of $\text{Li}_{1-x}\text{Al}_x\text{Ge}_{2-x}(\text{PO}_4)_3$ synthesized by a sol-gel method. *J Electrochem Soc* 2012;159:A1114-9. DOI
68. Inaguma Y, Liqian C, Itoh M, et al. High ionic conductivity in lithium lanthanum titanate. *Solid State Commun* 1993;86:689-93. DOI
69. Chen R, Qu W, Guo X, Li L, Wu F. The pursuit of solid-state electrolytes for lithium batteries: from comprehensive insight to emerging horizons. *Mater Horiz* 2016;3:487-516. DOI

70. Sun C, Liu J, Gong Y, Wilkinson DP, Zhang J. Recent advances in all-solid-state rechargeable lithium batteries. *Nano Energy* 2017;33:363-86. DOI
71. Appetecchi G, Croce F, Scrosati B. Kinetics and stability of the lithium electrode in poly(methylmethacrylate)-based gel electrolytes. *Electrochim Acta* 1995;40:991-7. DOI
72. MacLashan GS, Andreev YG, Bruce PG. Structure of the polymer electrolyte poly(ethylene oxide)₆:LiAsF₆. *Nature* 1999;398:792-4. DOI
73. Abraham KM, Alamgir M. Li⁺-conductive solid polymer electrolytes with liquid-like conductivity. *J Electrochem Soc* 1990;137:1657-8. DOI
74. Choe H, Giaccai J, Alamgir M, Abraham K. Preparation and characterization of poly(vinyl sulfone)- and poly(vinylidene fluoride)-based electrolytes. *Electrochim Acta* 1995;40:2289-93. DOI
75. Kanehori K, Matsumoto K, Miyauchi K, Kudo T. Thin film solid electrolyte and its application to secondary lithium cell. *Solid State Ionics* 1983;9-10:1445-8. DOI
76. Chhowalla M, Teo KBK, Ducati C, et al. Growth process conditions of vertically aligned carbon nanotubes using plasma enhanced chemical vapor deposition. *J Appl Phys* 2001;90:5308-17. DOI
77. Bates J, Dudney N, Gruzalski G, et al. Fabrication and characterization of amorphous lithium electrolyte thin films and rechargeable thin-film batteries. *J Power Sources* 1993;43:103-10. DOI
78. Tabata H, Tanaka H, Kawai T. Formation of artificial BaTiO₃/SrTiO₃ superlattices using pulsed laser deposition and their dielectric properties. *Appl Phys Lett* 1994;65:1970-2. DOI
79. Han X, Gong Y, Fu KK, et al. Negating interfacial impedance in garnet-based solid-state Li metal batteries. *Nat Mater* 2017;16:572-9. DOI PubMed
80. Bates J. Electrical properties of amorphous lithium electrolyte thin films. *Solid State Ionics* 1992;53-56:647-54. DOI
81. Yu X, Bates JB, Jellison GE, Hart FX. A stable thin-film lithium electrolyte: lithium phosphorus oxynitride. *J Electrochem Soc* 1997;144:524-32. DOI
82. Larson RW, Day DE. Preparation and characterization of lithium phosphorus oxynitride glass. *J Non Cryst Solids* 1986;88:97-113. DOI
83. Li J, Ma C, Chi M, Liang C, Dudney NJ. Solid electrolyte: the key for high-voltage lithium batteries. *Adv Energy Mater* 2015;5:1401408. DOI
84. Haruyama J, Sodeyama K, Han L, Takada K, Tateyama Y. Space-charge layer effect at interface between oxide cathode and sulfide electrolyte in all-solid-state lithium-ion battery. *Chem Mater* 2014;26:4248-55. DOI
85. Ohta N, Takada K, Zhang L, Ma R, Osada M, Sasaki T. Enhancement of the high-rate capability of solid-state lithium batteries by nanoscale interfacial modification. *Adv Mater* 2006;18:2226-9. DOI
86. Yamaguchi Y, Takeuchi T, Sakaebe H, et al. Ab initio simulations of Li/pyrite-MS₂ (M=Fe, Ni) battery cells. *J Electrochem Soc* 2010;157:A630. DOI
87. Zhou W, Wang S, Li Y, Xin S, Manthiram A, Goodenough JB. Plating a dendrite-free lithium anode with a polymer/ceramic/polymer sandwich electrolyte. *J Am Chem Soc* 2016;138:9385-8. DOI PubMed
88. Wang L, Zhang X, Wang T, et al. Ameliorating the interfacial problems of cathode and solid-state electrolytes by interface modification of functional polymers. *Adv Energy Mater* 2018;8:1801528. DOI
89. Mehrer H. Diffusion in solids: fundamentals, methods, materials, diffusion-controlled processes. Springer Science & Business Media; 2007. p. 209-36.
90. Takechi K, Shiga T, Asaoka T. A Li-O₂/CO₂ battery. *Chem Commun (Camb)* 2011;47:3463-5. DOI PubMed
91. Lim HK, Lim HD, Park KY, et al. Toward a lithium-"air" battery: the effect of CO₂ on the chemistry of a lithium-oxygen cell. *J Am Chem Soc* 2013;135:9733-42. DOI PubMed
92. Xu S, Das SK, Archer LA. The Li-CO₂ battery: a novel method for CO₂ capture and utilization. *RSC Adv* 2013;3:6656. DOI
93. Liu Y, Wang R, Lyu Y, Li H, Chen L. Rechargeable Li/CO₂-O₂ (2:1) battery and Li/CO₂ battery. *Energy Environ Sci* 2014;7:677. DOI
94. Hou Y, Wang J, Liu L, et al. Mo₂C/CNT: an efficient catalyst for rechargeable Li-CO₂ batteries. *Adv Funct Mater* 2017;27:1700564. DOI
95. Németh K, Srajer G. CO₂/oxalate cathodes as safe and efficient alternatives in high energy density metal-air type rechargeable batteries. *RSC Adv* 2014;4:1879-85. DOI
96. Németh K, Srajer G. CO₂/oxalate cathodes as safe and efficient alternatives in high energy density metal-air type rechargeable batteries. *RSC Adv* 2014;4:1879-85. DOI
97. Ehteshami SMM, Chan S. The role of hydrogen and fuel cells to store renewable energy in the future energy network - potentials and challenges. *Energy Policy* 2014;73:103-9. DOI
98. Armand M, Tarascon JM. Building better batteries. *Nature* 2008;451:652-7. DOI PubMed
99. Dahn JR, Zheng T, Liu Y, Xue JS. Mechanisms for lithium insertion in carbonaceous materials. *Science* 1995;270:590-3. DOI
100. Claye AS, Fischer JE, Huffman CB, Rinzler AG, Smalley RE. Solid-state electrochemistry of the Li single wall carbon nanotube system. *J Electrochem Soc* 2000;147:2845. DOI
101. Xu M, Liang T, Shi M, Chen H. Graphene-like two-dimensional materials. *Chem Rev* 2013;113:3766-98. DOI PubMed
102. Liu M, Kutana A, Liu Y, Yakobson BI. First-principles studies of Li nucleation on graphene. *J Phys Chem Lett* 2014;5:1225-9. DOI PubMed
103. Seo MH, Choi SM, Lim EJ, et al. Toward new fuel cell support materials: a theoretical and experimental study of nitrogen-doped

- graphene. *ChemSusChem* 2014;7:2609-20. DOI PubMed
104. Kim D, Liu X, Yu B, et al. Amine-functionalized boron nitride nanosheets: a new functional additive for robust, flexible ion gel electrolyte with high lithium-ion transference number. *Adv Funct Mater* 2020;30:1910813. DOI
 105. Xiong J, Zhu W, Li H, et al. Few-layered graphene-like boron nitride induced a remarkable adsorption capacity for dibenzothiophene in fuels. *Green Chem* 2015;17:1647-56. DOI
 106. Wang X, Zeng Z, Ahn H, Wang G. First-principles study on the enhancement of lithium storage capacity in boron doped graphene. *Appl Phys Lett* 2009;95:183103. DOI
 107. Chou S, Wang J, Choucair M, Liu H, Stride JA, Dou S. Enhanced reversible lithium storage in a nanosize silicon/graphene composite. *Electrochem Commun* 2010;12:303-6. DOI
 108. Zhao N, Yang L, Zhang P, et al. Polycrystalline SnO₂ nanowires coated with amorphous carbon nanotube as anode material for lithium ion batteries. *Mater Lett* 2010;64:972-5. DOI
 109. Winter M, Besenhard JO. Electrochemical lithiation of tin and tin-based intermetallics and composites. *Electrochim Acta* 1999;45:31-50. DOI
 110. Julien C, Mauger A, Zaghbi K, Groult H. Comparative issues of cathode materials for Li-ion batteries. *Inorganics* 2014;2:132-54. DOI
 111. Ge M, Cao C, Biesold GM, et al. Recent advances in silicon-based electrodes: from fundamental research toward practical applications. *Adv Mater* 2021;33:e2004577. DOI PubMed
 112. Yang C, Zhang Y, Zhou J, et al. Hollow Si/SiO_x nanosphere/nitrogen-doped carbon superstructure with a double shell and void for high-rate and long-life lithium-ion storage. *J Mater Chem A* 2018;6:8039-46. DOI
 113. Zhou Y, Guo H, Wang Z, Li X, Zhou R, Peng W. Improved electrochemical performance of Si/C material based on the interface stability. *J Alloys Compd* 2017;725:1304-12. DOI
 114. Wang Z, Zhou L, Lou XW. Metal oxide hollow nanostructures for lithium-ion batteries. *Adv Mater* 2012;24:1903-11. DOI PubMed
 115. Adams BD, Radtke C, Black R, Trudeau ML, Zaghbi K, Nazar LF. Current density dependence of peroxide formation in the Li-O₂ battery and its effect on charge. *Energy Environ Sci* 2013;6:1772. DOI
 116. Seh ZW, Yu JH, Li W, et al. Two-dimensional layered transition metal disulphides for effective encapsulation of high-capacity lithium sulphide cathodes. *Nat Commun* 2014;5:5017. DOI PubMed
 117. Feng X, Ouyang M, Liu X, Lu L, Xia Y, He X. Thermal runaway mechanism of lithium ion battery for electric vehicles: a review. *Energy Stor Mater* 2018;10:246-67. DOI
 118. May GJ, Davidson A, Monahov B. Lead batteries for utility energy storage: a review. *J Energy Storage* 2018;15:145-57. DOI
 119. Neuville S. Differentiated carbon material for energy storage and conversion. *Mater Today Proc* 2018;5:13837-45. DOI
 120. Ullah S, Denis PA, Sato F. Beryllium doped graphene as an efficient anode material for lithium-ion batteries with significantly huge capacity: a DFT study. *Appl Mater Today* 2017;9:333-40. DOI
 121. Pei F, Fu A, Ye W, et al. Robust lithium metal anodes realized by lithiophilic 3D porous current collectors for constructing high-energy lithium-sulfur batteries. *ACS Nano* 2019;13:8337-46. DOI PubMed
 122. Zhou L, Hou ZF, Gao B, Frauenheim T. Doped graphenes as anodes with large capacity for lithium-ion batteries. *J Mater Chem A* 2016;4:13407-13. DOI
 123. Wu H, Chang S, Liu X, et al. Sr-doped Li₄Ti₅O₁₂ as the anode material for lithium-ion batteries. *Solid State Ionics* 2013;232:13-8. DOI
 124. Walz KA, Suyama AN, Suyama WE, et al. Characterization and performance of high power iron(VI) ferrate batteries. *J Power Sources* 2004;134:318-23. DOI
 125. Kao W, Haberer SL, Patel P. Barium metaplumbate for lead/acid batteries. *J Electrochem Soc* 1994;141:3300-5. DOI
 126. Hertzberg B, Sviridov L, Stach EA, Gupta T, Steingart D. A manganese-doped barium carbonate cathode for alkaline batteries. *J Electrochem Soc* 2014;161:A835-40. DOI
 127. Tanaka U, Sogabe T, Sakagoshi H, Ito M, Tojo T. Anode property of boron-doped graphite materials for rechargeable lithium-ion batteries. *Carbon* 2001;39:931-6. DOI
 128. Wang Y, Ai X, Cao Y, Yang H. Exceptional electrochemical activities of amorphous Fe-B and Co-B alloy powders used as high capacity anode materials. *Electrochem Commun* 2004;6:780-4. DOI
 129. Walter M, Kovalenko MV, Kravchyk KV. Challenges and benefits of post-lithium-ion batteries. *New J Chem* 2020;44:1677-83. DOI
 130. Shehzad K, Xu Y, Gao C, Duan X. Three-dimensional macro-structures of two-dimensional nanomaterials. *Chem Soc Rev* 2016;45:5541-88. DOI PubMed
 131. Qie L, Chen WM, Wang ZH, et al. Nitrogen-doped porous carbon nanofiber webs as anodes for lithium ion batteries with a superhigh capacity and rate capability. *Adv Mater* 2012;24:2047-50. DOI PubMed
 132. Dreyer DR, Park S, Bielawski CW, Ruoff RS. The chemistry of graphene oxide. *Chem Soc Rev* 2010;39:228-40. DOI PubMed
 133. Dong Y, Wu Z, Ren W, Cheng H, Bao X. Graphene: a promising 2D material for electrochemical energy storage. *Sci Bull* 2017;62:724-40. DOI
 134. Béguin F, Chevallier F, Vix-guterl C, et al. Correlation of the irreversible lithium capacity with the active surface area of modified carbons. *Carbon* 2005;43:2160-7. DOI
 135. Chen JS, Wang Z, Dong XC, Chen P, Lou XW. Graphene-wrapped TiO₂ hollow structures with enhanced lithium storage capabilities. *Nanoscale* 2011;3:2158-61. DOI PubMed
 136. Pumera M. Graphene-based nanomaterials for energy storage. *Energy Environ Sci* 2011;4:668-74. DOI
 137. Uthaisar C, Barone V, Peralta JE. Lithium adsorption on zigzag graphene nanoribbons. *J Appl Phys* 2009;106:113715. DOI

138. Liu Y, Wang X, Dong Y, Wang Z, Zhao Z, Qiu J. Nitrogen-doped graphene nanoribbons for high-performance lithium ion batteries. *J Mater Chem A* 2014;2:16832-5. DOI
139. Chan CK, Peng H, Liu G, et al. High-performance lithium battery anodes using silicon nanowires. *Nat Nanotechnol* 2008;3:31-5. DOI PubMed
140. Boukamp BA, Lesh GC, Huggins RA. All-solid lithium electrodes with mixed-conductor matrix. *J Electrochem Soc* 1981;128:725-9. DOI
141. Thakur M, Isaacson M, Sinsabaugh SL, Wong MS, Biswal SL. Gold-coated porous silicon films as anodes for lithium ion batteries. *J Power Sources* 2012;205:426-32. DOI
142. Obrovac MN, Christensen L, Le DB, Dahn JR. Alloy design for lithium-ion battery anodes. *J Electrochem Soc* 2007;154:A849. DOI
143. Lee S, Nam K, Jung H, Park C. Si-based composite interconnected by multiple matrices for high-performance Li-ion battery anodes. *Chem Eng J* 2020;381:122619. DOI
144. Xu H, Shi L, Wang Z, et al. Fluorine-doped tin oxide nanocrystal/reduced graphene oxide composites as lithium ion battery anode material with high capacity and cycling stability. *ACS Appl Mater Interfaces* 2015;7:27486-93. DOI PubMed
145. Share K, Cohn AP, Carter R, Rogers B, Pint CL. Role of nitrogen-doped graphene for improved high-capacity potassium ion battery anodes. *ACS Nano* 2016;10:9738-44. DOI PubMed
146. Ma Y, Yin G, Zuo P, Tan X, Gao Y, Shi P. A phosphorous additive for lithium-ion batteries. *Electrochem Solid-State Lett* 2008;11:A129. DOI
147. Chung K, Kim W, Choi Y. Lithium phosphorous oxynitride as a passive layer for anodes in lithium secondary batteries. *J. Electroanal Chem* 2004;566:263-7. DOI
148. Zhao C, Chen H, Liu H, et al. Quantifying the reaction mechanisms of a high-capacity CuP_2/C composite anode for potassium ion batteries. *J Mater Chem A* 2021;9:6274-83. DOI
149. Li W, Chou SL, Wang JZ, Kim JH, Liu HK, Dou SX. $\text{Sn}_{4+x}\text{P}_3$ @ amorphous Sn-P composites as anodes for sodium-ion batteries with low cost, high capacity, long life, and superior rate capability. *Adv Mater* 2014;26:4037-42. DOI PubMed
150. Lim YR, Shojaei F, Park K, et al. Arsenic for high-capacity lithium- and sodium-ion batteries. *Nanoscale* 2018;10:7047-57. DOI PubMed
151. Darwiche A, Marino C, Sougrati MT, Fraise B, Stievano L, Monconduit L. Better cycling performances of bulk Sb in Na-ion batteries compared to Li-ion systems: an unexpected electrochemical mechanism. *J Am Chem Soc* 2012;134:20805-11. DOI PubMed
152. Baggetto L, Allcorn E, Unocic RR, Manthiram A, Veith GM. Mo_3Sb_7 as a very fast anode material for lithium-ion and sodium-ion batteries. *J Mater Chem A* 2013;1:11163. DOI
153. Xiao L, Cao Y, Xiao J, et al. High capacity, reversible alloying reactions in SnSb/C nanocomposites for Na-ion battery applications. *Chem Commun (Camb)* 2012;48:3321-3. DOI PubMed
154. Yu DY, Prikhodchenko PV, Mason CW, et al. High-capacity antimony sulphide nanoparticle-decorated graphene composite as anode for sodium-ion batteries. *Nat Commun* 2013;4:2922. DOI PubMed
155. Zhang K, Wang Y, Liu P, Li W. Chemical fabrication and electrochemical performance of Bi_2S_3 -nanorods charged reduced graphene oxide. *Mater Lett* 2015;161:774-7. DOI
156. Yang W, Wang H, Liu T, Gao L. A Bi_2S_3 @CNT nanocomposite as anode material for sodium ion batteries. *Mater Lett* 2016;167:102-5. DOI
157. Li Y, Trujillo MA, Fu E, et al. Bismuth oxide: a new lithium-ion battery anode. *J Mater Chem A Mater* 2013;1. DOI PubMed PMC
158. Lu Y, Gasteiger HA, Parent MC, Chiloyan V, Shao-horn Y. The influence of catalysts on discharge and charge voltages of rechargeable Li-oxygen batteries. *Electrochem Solid-State Lett* 2010;13:A69. DOI
159. Chen JJ, Jia x, She QJ, et al. The preparation of nano-sulfur/MWCNTs and its electrochemical performance. *Electrochim Acta* 2010;55:8062-6. DOI
160. Ji X, Lee KT, Nazar LF. A highly ordered nanostructured carbon-sulphur cathode for lithium-sulphur batteries. *Nat Mater* 2009;8:500-6. DOI PubMed
161. Xiao J, Wang X, Yang X, et al. Electrochemically induced high capacity displacement reaction of $\text{PEO}/\text{MoS}_2/\text{graphene}$ nanocomposites with lithium. *Adv Funct Mater* 2011;21:2840-6. DOI
162. Fang X, Guo X, Mao Y, et al. Mechanism of lithium storage in MoS_2 and the feasibility of using $\text{Li}_2\text{S}/\text{Mo}$ nanocomposites as cathode materials for lithium-sulfur batteries. *Chem Asian J* 2012;7:1013-7. DOI PubMed
163. Lu ZW, Wang YH, Dai Z, et al. One-pot sulfur-containing ion assisted microwave synthesis of reduced graphene oxide@nano-sulfur fibrous hybrids for high-performance lithium-sulfur batteries. *Electrochim Acta* 2019;325:134920. DOI
164. Cui Y, Abouimrane A, Sun CJ, Ren Y, Amine K. Li-Se battery: absence of lithium polyselenides in carbonate based electrolyte. *Chem Commun (Camb)* 2014;50:5576-9. DOI PubMed
165. Yang CP, Xin S, Yin YX, Ye H, Zhang J, Guo YG. An advanced selenium-carbon cathode for rechargeable lithium-selenium batteries. *Angew Chem Int Ed Engl* 2013;52:8363-7. DOI PubMed
166. Zeng L, Zeng W, Jiang Y, et al. A flexible porous carbon nanofibers-selenium cathode with superior electrochemical performance for both Li-Se and Na-Se batteries. *Adv Energy Mater* 2015;5:1401377. DOI
167. Eftekhari A. The rise of lithium-selenium batteries. *Sustain Energy Fuels* 2017;1:14-29. DOI
168. Liu Y, Wang J, Xu Y, Zhu Y, Bigio D, Wang C. Lithium-tellurium batteries based on tellurium/porous carbon composite. *J Mater Chem A* 2014;2:12201-7. DOI
169. He J, Chen Y, Lv W, et al. Three-dimensional hierarchical reduced graphene oxide/tellurium nanowires: a high-performance

- freestanding cathode for Li-Te batteries. *ACS Nano* 2016;10:8837-42. DOI PubMed
170. Nakajima T. Fluorine compounds as energy conversion materials. *J Fluor Chem* 2013;149:104-11. DOI
171. Cui D, Zheng Z, Peng X, Li T, Sun T, Yuan L. Fluorine-doped SnO₂ nanoparticles anchored on reduced graphene oxide as a high-performance lithium ion battery anode. *J Power Sources* 2017;362:20-6. DOI
172. Zhang S, Zhang L, Wang W, Xue W. A Novel cathode material based on polyaniline used for lithium/sulfur secondary battery. *Synth Met* 2010;160:2041-4. DOI
173. Niessen RH, Notten PL. Hydrogen storage in thin film magnesium–scandium alloys. *J Alloys Compd* 2005;404-406:457-60. DOI
174. Amatucci G, Safari A, Shokoohi F, Wilkens B. Lithium scandium phosphate-based electrolytes for solid state lithium rechargeable microbatteries. *Solid State Ionics* 1993;60:357-65. DOI
175. Zheng P, Liu T, Su Y, Zhang L, Guo S. TiO₂ nanotubes wrapped with reduced graphene oxide as a high-performance anode material for lithium-ion batteries. *Sci Rep* 2016;6:36580. DOI PubMed PMC
176. Tao B, He J, Miao F. A hybrid sandwich structure of TiO₂/N-graphene/Ag supported by ordered silicon nanowires and its application as lithium-ion battery electrodes. *Mater Lett* 2020;262:127046. DOI
177. Ihsan M, Meng Q, Li L, et al. V₂O₅/mesoporous carbon composite as a cathode material for lithium-ion batteries. *Electrochim Acta* 2015;173:172-7. DOI
178. Poullikkas A. A comparative overview of large-scale battery systems for electricity storage. *Renew Sustain Energy Rev* 2013;27:778-88. DOI
179. Wang C, Chen S, Xie H, Wei S, Wu C, Song L. Atomic Sn⁴⁺ decorated into vanadium carbide MXene interlayers for superior lithium storage. *Adv Energy Mater* 2019;9:1802977. DOI
180. Yang F, Zhu Y, Xia Y, et al. Fast Zn²⁺ kinetics of vanadium oxide nanotubes in high-performance rechargeable zinc-ion batteries. *J Power Sources* 2020;451:227767. DOI
181. Zeng Y, Zhao T, An L, Zhou X, Wei L. A comparative study of all-vanadium and iron-chromium redox flow batteries for large-scale energy storage. *J Power Sources* 2015;300:438-43. DOI
182. Cao Y, Xiao L, Wang W, et al. Reversible sodium ion insertion in single crystalline manganese oxide nanowires with long cycle life. *Adv Mater* 2011;23:3155-60. DOI PubMed
183. Yensen N, Allen PB. Open source all-iron battery for renewable energy storage. *HardwareX* 2019;6:e00072. DOI
184. Wang Z, Liu C. Preparation and application of iron oxide/graphene based composites for electrochemical energy storage and energy conversion devices: Current status and perspective. *Nano Energy* 2015;11:277-93. DOI
185. Lv L, Peng M, Wu L, et al. Progress in iron oxides based nanostructures for applications in energy storage. *Nanoscale Res Lett* 2021;16:138. DOI PubMed PMC
186. Zhang L, Wu HB, Lou XWD. Iron-oxide-based advanced anode materials for lithium-ion batteries. *Adv Energy Mater* 2014;4:1300958. DOI
187. Jiang T, Bu F, Feng X, Shakir I, Hao G, Xu Y. Porous Fe₂O₃ nanoframeworks encapsulated within three-dimensional graphene as high-performance flexible anode for lithium-ion battery. *ACS Nano* 2017;11:5140-7. DOI PubMed
188. Zheng M, Qiu D, Zhao B, et al. Mesoporous iron oxide directly anchored on a graphene matrix for lithium-ion battery anodes with enhanced strain accommodation. *RSC Adv* 2013;3:699-703. DOI
189. Ma R, He L, Lu Z, Yang S, Xi L, Chung JCY. Large-scale fabrication of hierarchical α -Fe₂O₃ assemblies as high performance anode materials for lithium-ion batteries. *CrystEngComm* 2012;14:7882. DOI
190. Zhu S, Fan L, Lu Y. Highly uniform Fe₃O₄ nanoparticle-rGO composites as anode materials for high performance lithium-ion batteries. *RSC Adv* 2017;7:54939-46. DOI
191. Atar N, Eren T, Yola ML, Gerengi H, Wang S. Fe@Ag nanoparticles decorated reduced graphene oxide as ultrahigh capacity anode material for lithium-ion battery. *Ionics* 2015;21:3185-92. DOI
192. Qi S, Wu D, Dong Y, et al. Cobalt-based electrode materials for sodium-ion batteries. *Chem Eng J* 2019;370:185-207. DOI
193. Schipper F, Erickson EM, Erk C, Shin J, Chesneau FF, Aurbach D. Review - recent advances and remaining challenges for lithium ion battery cathodes: I. nickel-rich, LiNi_xCo_yMn_zO₂. *J Electrochem Soc* 2017;164:A6220-8. DOI
194. Chang H, Bai Y, Song X, et al. Hydrothermal synthesis, structural elucidation and electrochemical properties of three nickel and cobalt based phosphonates as anode materials for lithium ion batteries. *Electrochim Acta* 2019;321:134647. DOI
195. Asif M, Ali Z, Qiu H, Rashad M, Hou Y. Confined polysulfide shuttle by nickel disulfide nanoparticles encapsulated in graphene nanoshells synthesized by cooking oil. *ACS Appl Energy Mater* 2020;3:3541-52. DOI
196. Sethuraman VA, Kowolik K, Srinivasan V. Increased cycling efficiency and rate capability of copper-coated silicon anodes in lithium-ion batteries. *J Power Sources* 2011;196:393-8. DOI
197. Kumar R, Nithya C, Gopukumar S, Anbu Kulandainathan M. Diamondoid-structured Cu-dicarboxylate-based metal-organic frameworks as high-capacity anodes for lithium-ion storage. *Energy Technol* 2014;2:921-7. DOI
198. Fan M, Chen Y, Xie Y, et al. Half-cell and full-cell applications of highly stable and binder-free sodium ion batteries based on Cu₃P nanowire anodes. *Adv Funct Mater* 2016;26:5019-27. DOI
199. Li N, An R, Su Y, et al. The role of yttrium content in improving electrochemical performance of layered lithium-rich cathode materials for Li-ion batteries. *J Mater Chem A* 2013;1:9760. DOI
200. Aziz MA, Shanmugam S. Zirconium oxide nanotube-Nafion composite as high performance membrane for all vanadium redox flow battery. *J Power Sources* 2017;337:36-44. DOI
201. Li B, Wang Q, Zhang Y, Song Z, Yang D. Nickel-modified and zirconium-modified Li₂MnO₃ and applications in lithium-ion battery. *Int J Electrochem Sci* 2013;8:5396-406. DOI

202. Lubimtsev AA, Kent PRC, Sumpter BG, Ganesh P. Understanding the origin of high-rate intercalation pseudocapacitance in Nb₂O₅ crystals. *J Mater Chem A* 2013;1:14951. DOI
203. Zhang C, Beidaghi M, Naguib M, et al. Synthesis and charge storage properties of hierarchical niobium pentoxide/carbon/niobium carbide (MXene) hybrid materials. *Chem Mater* 2016;28:3937-43. DOI
204. Tolosa A, Krüner B, Fleischmann S, et al. Niobium carbide nanofibers as a versatile precursor for high power supercapacitor and high energy battery electrodes. *J Mater Chem A* 2016;4:16003-16. DOI
205. Chang K, Chen W. L-cysteine-assisted synthesis of layered MoS₂/graphene composites with excellent electrochemical performances for lithium ion batteries. *ACS Nano* 2011;5:4720-8. DOI
206. Wang H, Lan X, Jiang D, et al. Sodium storage and transport properties in pyrolysis synthesized MoSe₂ nanoplates for high performance sodium-ion batteries. *J Power Sources* 2015;283:187-94. DOI
207. Morales J. Electrochemical studies of lithium and sodium intercalation in MoSe₂. *Solid State Ionics* 1996;83:57-64. DOI
208. Luo Y, Zhang Y, Zhao Y, et al. Aligned carbon nanotube/molybdenum disulfide hybrids for effective fibrous supercapacitors and lithium ion batteries. *J Mater Chem A* 2015;3:17553-7. DOI
209. Xiao Y, Zhang W. Adsorption mechanisms of Mo₂CrC₂ MXenes as potential anode materials for metal-ion batteries: a first-principles investigation. *Appl Surf Sci* 2020;513:145883. DOI
210. He B, Dong B, Li H. Preparation and electrochemical properties of Ag-modified TiO₂ nanotube anode material for lithium-ion battery. *Electrochim Commun* 2007;9:425-30. DOI
211. Zou G, Zhang Z, Guo J, et al. Synthesis of MXene/Ag composites for extraordinary long cycle lifetime lithium storage at high rates. *ACS Appl Mater Interfaces* 2016;8:22280-6. DOI PubMed
212. Nam SH, Shim H, Kim Y, Dar MA, Kim JG, Kim WB. Ag or Au nanoparticle-embedded one-dimensional composite TiO₂ nanofibers prepared via electrospinning for use in lithium-ion batteries. *ACS Appl Mater Interfaces* 2010;2:2046-52. DOI
213. Hwang H, Oh S, Kim H, Cho W, Cho B, Lee D. Characterization of Ag-doped vanadium oxide (Ag_xV₂O₅) thin film for cathode of thin film battery. *Electrochim Acta* 2004;50:485-9. DOI
214. Liu Z, Zhang N, Wang Z, Sun K. Highly dispersed Ag nanoparticles (<10nm) deposited on nanocrystalline Li₄Ti₅O₁₂ demonstrating high-rate charge/discharge capability for lithium-ion battery. *J Power Sources* 2012;205:479-82. DOI
215. Kumagai N, Kumagai N, Tanno K. Electrochemical and structural characteristics of tungstic acids as cathode materials for lithium batteries. *Appl Phys A* 1989;49:83-9. DOI
216. Sasidharan M, Gunawardhana N, Yoshio M, Nakashima K. WO₃ hollow nanospheres for high-lithium storage capacity and good cyclability. *Nano Energy* 2012;1:503-8. DOI
217. Gao J, Li L, Tan J, et al. Vertically oriented arrays of ReS₂ nanosheets for electrochemical energy storage and electrocatalysis. *Nano Lett* 2016;16:3780-7. DOI PubMed
218. Zhu J, Xu Z, Lu B. Ultrafine Au nanoparticles decorated NiCo₂O₄ nanotubes as anode material for high-performance supercapacitor and lithium-ion battery applications. *Nano Energy* 2014;7:114-23. DOI
219. Lee M, Luo Y, Do J. Using PANI-PPDA/Au composite films as cathode of lithium secondary battery. *J Power Sources* 2005;146:340-4. DOI
220. Zhao J, Yu K, Hu Y, et al. Discharge behavior of Mg-4wt%Ga-2wt%Hg alloy as anode for seawater activated battery. *Electrochim Acta* 2011;56:8224-31. DOI
221. Eftekhari A, Moghaddam AB, Solati-hashjin M. Electrochemical properties of LiMn₂O₄ cathode material doped with an actinide. *J Alloys Compd* 2006;424:225-30. DOI
222. Rauda IE, Augustyn V, Dunn B, Tolbert SH. Enhancing pseudocapacitive charge storage in polymer templated mesoporous materials. *Acc Chem Res* 2013;46:1113-24. DOI PubMed
223. Pramudita JC, Aughterson R, Dose WM, Donne SW, Brand HEA, Sharma N. Using in situ synchrotron x-ray diffraction to study lithium- and sodium-ion batteries: A case study with an unconventional battery electrode (Gd₂TiO₅). *J Mater Res* 2015;30:381-9. DOI
224. Wu H, Zheng G, Liu N, Carney TJ, Yang Y, Cui Y. Engineering empty space between Si nanoparticles for lithium-ion battery anodes. *Nano Lett* 2012;12:904-9. DOI PubMed
225. Xia J, Zhao H, Pang WK, et al. Lanthanide doping induced electrochemical enhancement of Na₂Ti₃O₇ anodes for sodium-ion batteries. *Chem Sci* 2018;9:3421-5. DOI PubMed PMC
226. El-metwaly F, Abou-sekkina M, Saad F, Khedr A. Synthesis, effect of γ -ray and electrical conductivity of uranium doped nano LiMn₂O₄ spinels for applications as positive electrodes in Li-ion rechargeable batteries. *Mater Sci-Poland* 2014;32:571-7. DOI
227. Gogotsi Y. What nano can do for energy storage. *ACS Nano* 2014;8:5369-71. DOI PubMed
228. Augustyn V, Come J, Lowe MA, et al. High-rate electrochemical energy storage through Li⁺ intercalation pseudocapacitance. *Nat Mater* 2013;12:518-22. DOI PubMed
229. Xie Y, Dall'Agnese Y, Naguib M, et al. Prediction and characterization of MXene nanosheet anodes for non-lithium-ion batteries. *ACS Nano* 2014;8:9606-15. DOI PubMed
230. Chen J, Song W, Hou H, et al. Ti³⁺ self-doped dark rutile TiO₂ ultrafine nanorods with durable high-rate capability for lithium-ion batteries. *Adv Funct Mater* 2015;25:6793-801. DOI
231. Seh ZW, Yu JH, Li W, et al. Two-dimensional layered transition metal disulphides for effective encapsulation of high-capacity lithium sulphide cathodes. *Nat Commun* 2014;5:5017. DOI PubMed
232. Chhowalla M, Shin HS, Eda G, Li LJ, Loh KP, Zhang H. The chemistry of two-dimensional layered transition metal dichalcogenide nanosheets. *Nat Chem* 2013;5:263-75. DOI PubMed

233. Coleman JN, Lotya M, O'Neill A, et al. Two-dimensional nanosheets produced by liquid exfoliation of layered materials. *Science* 2011;331:568-71. DOI PubMed
234. Naguib M, Kurtoglu M, Presser V, et al. Two-dimensional nanocrystals produced by exfoliation of Ti₃AlC₂. *Adv Mater* 2011;23:4248-53. DOI PubMed
235. Shein IR, Ivanovskii AL. Graphene-like nanocarbitides and nanonitrides of d metals (MXenes): synthesis, properties and simulation. *Micro Nano Lett* 2013;8:59-62. DOI
236. Tang H, Hu Q, Zheng M, et al. MXene-2D layered electrode materials for energy storage. *Prog Nat Sci* 2018;28:133-47. DOI
237. Li J, Guo C, Li CM. Recent advances of two-dimensional (2D) MXenes and phosphorene for high-performance rechargeable batteries. *ChemSusChem* 2020;13:1047-70. DOI
238. Kurtoglu M, Naguib M, Gogotsi Y, Barsoum MW. First principles study of two-dimensional early transition metal carbides. *MRS Commun* 2012;2:133-7. DOI
239. Zhou J, Zha X, Chen FY, et al. A two-dimensional zirconium carbide by selective etching of Al₃C₃ from nanolaminated Zr₃Al₃C₅. *Angew Chem Int Ed Engl* 2016;55:5008-13. DOI PubMed
240. Li N, Jiang Y, Zhou C, et al. High-performance humidity sensor based on urchin-like composite of Ti₃C₂ MXene-derived TiO₂ nanowires. *ACS Appl Mater Interfaces* 2019;11:38116-25. DOI PubMed
241. Mashtalir O, Naguib M, Mochalin VN, et al. Intercalation and delamination of layered carbides and carbonitrides. *Nat Commun* 2013;4:1716. DOI PubMed
242. Zhou J, Zha X, Zhou X, et al. Synthesis and electrochemical properties of two-dimensional hafnium carbide. *ACS Nano* 2017;11:3841-50. DOI PubMed
243. Ahmed B, Anjum DH, Gogotsi Y, Alshareef HN. Atomic layer deposition of SnO₂ on MXene for Li-ion battery anodes. *Nano Energy* 2017;34:249-56. DOI
244. Zhang Z, Guo H, Li W, Liu G, Zhang Y, Wang Y. Sandwich-like Co₃O₄/MXene composites as high capacity electrodes for lithium-ion batteries. *New J Chem* 2020;44:5913-20. DOI
245. Lin Z, Sun D, Huang Q, Yang J, Barsoum MW, Yan X. Carbon nanofiber bridged two-dimensional titanium carbide as a superior anode for lithium-ion batteries. *J Mater Chem A* 2015;3:14096-100. DOI
246. Mashtalir O, Lukatskaya MR, Zhao MQ, Barsoum MW, Gogotsi Y. Amine-assisted delamination of Nb₂C MXene for Li-ion energy storage devices. *Adv Mater* 2015;27:3501-6. DOI PubMed
247. Ren CE, Zhao M, Makaryan T, et al. Porous two-dimensional transition metal carbide (MXene) flakes for high-performance Li-ion storage. *ChemElectroChem* 2016;3:689-93. DOI
248. Wu X, Wang Z, Yu M, Xiu L, Qiu J. Stabilizing the MXenes by carbon nanoplating for developing hierarchical nano hybrids with efficient lithium storage and hydrogen evolution capability. *Adv Mater* 2017;29:1607017. DOI PubMed
249. Rakhi RB, Ahmed B, Anjum D, Alshareef HN. Direct chemical synthesis of MnO₂ nanowhiskers on transition-metal carbide surfaces for supercapacitor applications. *ACS Appl Mater Interfaces* 2016;8:18806-14. DOI PubMed
250. Huang H, Cui J, Liu G, Bi R, Zhang L. Carbon-coated MoSe₂/MXene hybrid nanosheets for superior potassium storage. *ACS Nano* 2019;13:3448-56. DOI PubMed
251. Schedy A, Quarthal D, Oetken M. Graphene - exciting insights into the synthesis and chemistry of the miracle material of the 21st century and its implementation in chemistry lessons for the first time. *WJCE* 2018;6:43-53. DOI
252. Brodie BC. On the atomic weight of graphite. *Phil Trans R Soc* 1859;149:249-59. DOI PubMed
253. Andre Mkhoyan K, Contryman AW, Silcox J, et al. Atomic and electronic structure of graphene-oxide. *Nano Lett* 2009;9:1058-63. DOI PubMed
254. Yoo E, Kim J, Hosono E, Zhou HS, Kudo T, Honma I. Large reversible Li storage of graphene nanosheet families for use in rechargeable lithium ion batteries. *Nano Lett* 2008;8:2277-82. DOI PubMed
255. Li B, Cao H, Shao J, Li G, Qu M, Yin G. Co₃O₄@graphene composites as anode materials for high-performance lithium ion batteries. *Inorg Chem* 2011;50:1628-32. DOI PubMed
256. Su D, Ahn HJ, Wang G. SnO₂@graphene nanocomposites as anode materials for Na-ion batteries with superior electrochemical performance. *Chem Commun (Camb)* 2013;49:3131-3. DOI PubMed
257. Berchmans S, Bandodkar AJ, Jia W, Ramirez J, Meng YS, Wang J. An epidermal alkaline rechargeable Ag-Zn printable tattoo battery for wearable electronics. *J Mater Chem A* 2014;2:15788-95. DOI
258. Xia X, Obrovac MN, Dahn JR. Comparison of the reactivity of Na_xC₆ and Li_xC₆ with non-aqueous solvents and electrolytes. *Electrochem Solid-State Lett* 2011;14:A130. DOI
259. Chen Y, Kang Y, Zhao Y, et al. A review of lithium-ion battery safety concerns: The issues, strategies, and testing standards. *J Energy Chem* 2021;59:83-99. DOI
260. Wu W, Wang S, Wu W, Chen K, Hong S, Lai Y. A critical review of battery thermal performance and liquid based battery thermal management. *Energy Convers Manag* 2019;182:262-81. DOI
261. Finegan DP, Darst J, Walker W, et al. Modelling and experiments to identify high-risk failure scenarios for testing the safety of lithium-ion cells. *J Power Sources* 2019;417:29-41. DOI
262. Cao D, Sun X, Li Q, Natan A, Xiang P, Zhu H. Lithium dendrite in all-solid-state batteries: growth mechanisms, suppression strategies, and characterizations. *Matter* 2020;3:57-94. DOI
263. Maleki H, Deng G, Anani A, Howard J. Thermal stability studies of Li-ion cells and components. *J Electrochem Soc* 1999;146:3224-9. DOI
264. Masias A, Marcicki J, Paxton WA. Opportunities and challenges of lithium ion batteries in automotive applications. *ACS Energy Lett*

- 2021;6:621-30. [DOI](#)
265. Weber R, Genovese M, Louli AJ, et al. Long cycle life and dendrite-free lithium morphology in anode-free lithium pouch cells enabled by a dual-salt liquid electrolyte. *Nat Energy* 2019;4:683-9. [DOI](#)
266. Kamaya N, Homma K, Yamakawa Y, et al. A lithium superionic conductor. *Nat Mater* 2011;10:682-6. [DOI](#) [PubMed](#)
267. Masias A, Felten N, Sakamoto J. Characterizing the mechanical behavior of lithium in compression. *J Mater Res* 2021;36:729-39. [DOI](#)
268. Hatzell KB, Chen XC, Cobb CL, et al. Challenges in lithium metal anodes for solid-state batteries. *ACS Energy Lett* 2020;5:922-34. [DOI](#)
269. Hitz GT, Mcowen DW, Zhang L, et al. High-rate lithium cycling in a scalable trilayer Li-garnet-electrolyte architecture. *Mater Today* 2019;22:50-7. [DOI](#)
270. Ely T, Kamzabek D, Chakraborty D. Batteries safety: recent progress and current challenges. *Front Energy Res* 2019;7:71. [DOI](#)
271. Sendek AD, Cubuk ED, Antoniuk ER, Cheon G, Cui Y, Reed EJ. Machine learning-assisted discovery of solid Li-ion conducting materials. *Chem Mater* 2019;31:342-52. [DOI](#)